2016

Microfluidic Fiber Fabrication and its Application in Neural Tissue Engineering

Farrokh Sharifi
Iowa State University

Microfluidic fiber fabrication and its application in neural tissue engineering

by

Farrokh Sharifi

A dissertation submitted to the graduate faculty

in partial fulfillment of the requirements for the degree of

DOCTOR OF PHILOSOPHY

Major: Mechanical Engineering

Program of Study Committee:
Nastaran Hashemi, Major Professor
Xinwei Wang
Reza Montazami
Balaji Narasimhan
Iris Rivero

Iowa State University

Ames, Iowa

2016

DEDICATION

This dissertation is humbly dedicated to my beloved family:

My Parents:

Heshmatollah & Mansooreh Sharifi

My Brother:

Farshad Sharifi

My Grandmother:

Mohaddeseh Sharifi

for their unconditional love and permanent support.

TABLE OF CONTENTS

Page

TABLE OF FIGURES

Page

LIST OF TABLES

Page

ACKNOWLEDGMENTS

I would like to thank my committee chair, Dr. Nastaran Hashemi, and my committee members, Dr. Xinwei Wang, Dr. Reza Montazami, Dr. Balaji Narasimhan, and Dr. Iris Rivero, for their guidance and support throughout the course of this research.

I would like to appreciate Dr. Donald Sakaguchi and his students: Bhavika Patel, Adam Dziulko, and Daniel Stroud from Department of Genetics, Development and Cell Biology and Neuroscience for their assistance in cell culture part of this research.

I acknowledge the Office of Naval Research, Iowa State University Presidential Initiative for Interdisciplinary Research, Iowa State University Health Research Initiative (ISU-HRI), U.S. Department of Energy Office of Science under the Science Undergraduate Laboratory Internship (SULI) Program at Ames Laboratory, and William March Scholar for support of this work.

I would like to take the opportunity to express my appreciation to Zhenhua Bai, Payton Goodrich, Diamant Kurteshi, Mingchang Lu, Jeremy Caplin, Rui Ding, Michelle Grawe, and Ashley Christopherson for their assistance in this research. In addition, I would also like to thank my friends, colleagues, the department faculty and staff for making my time at Iowa State University a wonderful experience.

ABSTRACT

Microfibers are becoming increasingly important for biomedical applications such as tissue engineering, drug delivery, and cell encapsulation. In this study, a microfluidic approach was used to fabricate biocompatible and biodegradable polymeric fibers. Chapter one gives an overview of the common microfiber fabrication methods followed by their advantages and disadvantages. Then, it focuses on the microfluidic platform and provides more information about different solidification strategies applied to fabricate fibers in this method. This chapter reviews some studies, which were recently published in this area as well.

Chapter two discusses using the microfluidic approach to fabricate continuous Polyvinyl alcohol (PVA) microfibers. It was shown that the size and cross-section of the PVA fibers can be controlled by changing the PVA concentration and flow rate ratio between the core and sheath fluids. The PVA concentration was varied from 6% to 12%, and the sheath-to-core flow rate ratio used for this study was in the range of 500:5 μL/min to 500:20 μL/min, respectively. The ribbon-shaped PVA fibers were fabricated using our microfluidic approach. Additionally, we simulated the microfluidic fiber fabrication process and the results consisted well with the experimental results. The dissolution and mechanical properties of the PVA fibers fabricated with different characteristics were also studied.

Chapter three focuses on fabricating polycaprolactone (PCL) microfibers using the microfluidic approach. It was shown that through variations of the sheath fluid flow rate and PCL concentration in the core solution, the morphology of the fibers and their cross sections can be tuned. The fibers were made using PCL concentrations of 2%, 5%, and 8% in the core fluid with a wide range of sheath-to-core flow rate ratios from 120:5 μL/min to 10:5 μL/min, respectively. The results revealed that the mechanical properties of the PCL fibers made using microfluidic approach were significantly improved compared to the PCL fibers made by other fiber fabrication

methods. Additionally, the effects of flow rate ratio and PCL concentration on the mechanical properties of the PCL fibers were studied.

In chapter four, the PCL microfibers with different characteristics were used as fibrous scaffolds to get one step closer to the application of the polymeric fibers in tissue engineering. Adult Hippocampal Stem/Progenitor Cells (AHPCs) *in vitro* were chosen for this study. It was shown that the three-dimensional topography of the PCL substrates, along with chemical (extracellular matrix) guidance cues, supports the adhesion, survival, and differentiation of the AHPCs. Moreover, the PCL fibers with different sizes and shapes (straight and wavy) were used to quantitatively analyze cell adhesion, proliferation, and differentiation. Our first experiment showed that 5 μm had the most cell adhesion, 5 μm, straight 20 μm, and wavy 35 μm provided a significantly better condition for the glial differentiation compared to control. More cell proliferation was observed on the wavy 35 μm fibers than on straight 35 μm fibers, showing that fiber morphology may have an effect on cell proliferation. However, this study's goals were to perform two more experiments in order to have more reliable results.

In chapter five, we used a microfluidic approach and photopolymerization strategy to fabricate PEGDA spherical particles as well as bow tie-shaped fibers. In this work, we showed that with immiscible and miscible fluids, spherical microparticles and bow tie shaped fibers can be fabricated using PEGDA. The flow rate ratio between the core and sheath fluids is found an important parameter to accurately tune the diameter of the particles as well as cross-section and size of the fibers. Glucose, sucrose, collagen, gelatin, PEG, and PVA were incorporated into the PEGDA fibers to study the porosity of the resulting fibers. It was found that sucrose and PVA can create porosity on the surface of the fibers after soaking the fibers in water for 6 days at 37 °C. The tensile properties of the PEGDA fibers with different characteristics were tested. It was found

that when the core flow rate increases, the resulting fibers become more stiff and brittle, which might be due to the increase of the cross-linking density. The mechanical properties of the PEGDA/collagen drop due to the low strength of the collagen, which is a natural polymer. On the other hand, the incorporation of glucose could improve the tensile properties of PEGDA fibers. In addition, we encapsulated the AHPCs into the PEGDA fibers in order to create a cell-laden fiber. Propidium Iodide (PI) was used for the cell viability, and the results showed that the cells could not survive. We believe that another hydrogel or the same polymer with higher molecular weight needs to be used in order to increase the cell survival into the hydrogel network.

CHAPTER I

INTRODUCTION: MICROFIBER FABRICATION

1.1 Common Fiber Fabrications Methods

Fiber systems are becoming increasingly important for numerous biological applications, such as tissue engineering, since the fibers are able to guide cell growth, alignment, and migration [1, 2]. Additionally, the design of microfibers gives them the correct properties in order to perform drug delivery and drug release in the human body for medical purposes [3, 4]. The fibers have high surface area-to-volume and strength-to-weight ratios. Some of them are permeable and can be woven into textiles [5]. These properties allow microfibers to carry even delicate materials, such as water-soluble drugs, throughout a biological medium with good accuracy [6, 7]. This makes for safe insertion and transmittance of material used for treatment, demonstrating the effectiveness of microfibers in medicine. The method of generation of the microfibers plays a role in determining its viability in these types of applications.

Several approaches exist for the fabrication of microfibers from naturally derived or synthetic materials, such as: the microfluidic method, electrospinning, wetspinning, biospining, meltspinning, and rotary spinning [8]. **Figure 1.1** shows a schematic of the common fiber fabrication approaches. In electrospinning, the flow of a viscoelastic polymer subjected to an electric field between an injecting needle and a collector is applied to create fibers. This method is relatively simple and it is feasible to efficiently scale-up and control the involved parameters such as flow rate and voltage. However, there are some difficulties in the fabrication of thick, complex 3D scaffolds with this method [2, 9]. Additionally, electrospun microfibers are generally not easy to align and it requires extra care to ensure that the fibers are accurately aligned, especially because

the randomly aligned fibers are not desirable for applications like growing nerve cells [10]. Wetspinning, on the other hand, does not rely on electricity to solidify the fiber. A pre-polymer solution is injected into a coagulation bath that must be either a poor solvent or a non-solvent with respect to the polymer. Wetspinning is an efficient method for fabricating fibers with a wide range of diameters by changing the diameter of the needle(s). Nevertheless, long exposure to chemicals during the fabrication process is required, which can be harmful to cells [11].

The Biospinning method is a process in which silk fibers are fabricated by insects. Silk has high tensile strength and is biodegradable. In addition, after chemical processing, it is non-cytotoxic and non-inflammatory. The major challenges of using biospun fibers are the limitation of resources, which makes it difficult for the scale-up process, as well as the fact that the process of silk fiber fabrication is time consuming [12]. The meltspinning approach also creates a fiber that has high mechanical proberties, and various synthetic polymers can be used for fiber fabrication. However, the meltspinning process is in a high temperature range (150 - 300 ˚C) and requires using expensive equipment. Using high temperatures during the fiber fabrication process prevents the cell or protein from being loaded onto the fiber in order to deliver the bioactive molecules in biomedical applications [13]. Additionally, because the viscosity of the melted polymer is relatively high, a high pressure difference is needed to move the melted polymer through the spinneret [14, 15]. Pressure is also important in rotary spinning, since the solution is spun at the high speeds to increase the centrifugal force, which causes the solvent to evaporate, resulting in fibers [16].

Using microfluidics to fabricate fiber is a relatively new approach in which the fiber is created in a microchannel using coaxial flow of core (pre-polymer) and sheath fluids. The key benefits of using this method include versatility of size, continuity of the fiber fabrication process,

and simplicity of cell, protein or drug incorporation. This process is straightforward, cost-efficient, reproducible, and suitable for many biological applications since the fiber is created without using high temperature, high pressure, high voltages, or toxic materials.

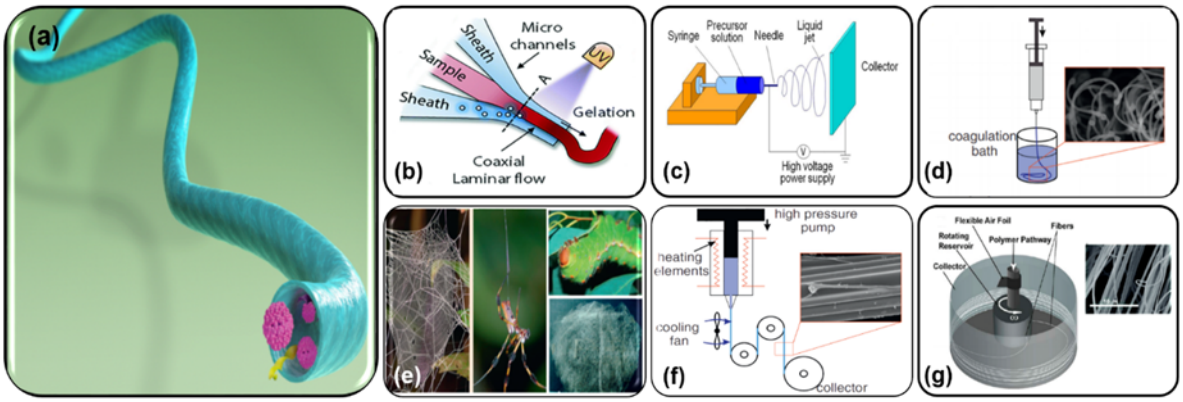

Figure 1.1 *Different methods used to fabricate polymeric fibers [17]. (a) Illustration depicting the encapsulation of macromolecules in a microfiber. (b) Schematic of the microfluidic fabrication of fibers. The manner in which the sheath and the core fluid flows are directed by micro channels to generate the fiber is depicted [18]. (c) For the electrospinning method, the viscoelastic polymer is subjected to an electric field [19]. (d) In the wet spinning process, the fibers are extruded to a coagulation bath [8]. (e) For the biospinning approach, the silk fibers are fabricated by insects [12]. (f) When meltspinning a microfiber, the polymer is heated to its melting point. Then, the melted polymer is extruded through a spinneret [13]. (g) In the rotary spinning method, the solution is spun at the high speeds at which the centrifugal force causes the solvent to evaporate, resulting in fibers [16].*

1.2 Fiber Solidification Strategies in Microfluidic Approach

There are physical and chemical methods used to solidify the prepolymer solution in a microchannel. Solvent extraction (casting) is the most common physical method, while the chemical solidification methods offer more variety of polymerization and cross-linking processes [20].

1.2.1 Solvent extraction (casting) method

The phase inversion process is the simplest solidification strategy since there is no need for a chemical reaction or cross-linking [2, 21, 22]. In this process, two fluids, i.e. core and sheath fluids, are introduced into the channel. After the two fluids merge in the channel, a coaxial flow is created. At the fluid/fluid interface, the exchange of polymer solvent and the sheath fluid occurs and the polymer is solidified in the outlet of the microchannel. This strategy has been used in many fiber fabrication studies [1, 2, 21-24]. **Figure 1.2** shows a schematic of the casting method as well as SEM images of some fibers fabricated by this approach.

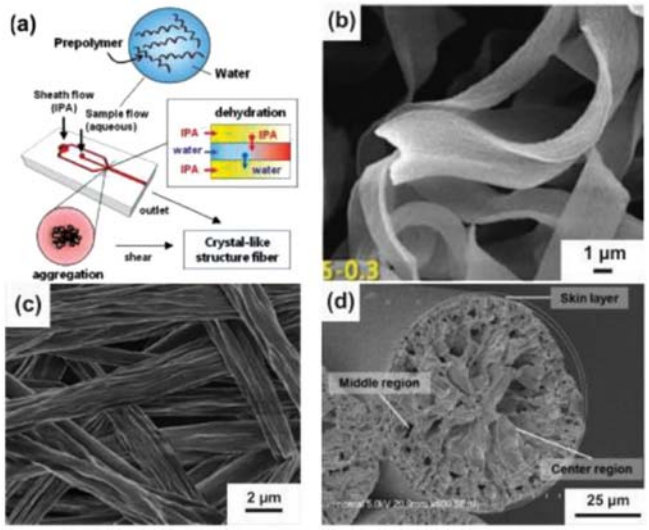

Figure 1.2 *Microfibers fabricated using solvent extraction strategy [20]. (a and b) Schematic of using the casting mechanism in microfluidic fiber fabrication and the resulting fiber [21]. (c) PMMA fiber fabrication. The wrinkling is due to evaporation gradient during the process [22]. (d) The cross section of PLGA microfibers. Three different areas are distinguishable because the rate of solvent extraction was not uniform [2].*

1.2.2 Chemical cross-linking method

In this strategy, small molecules or ions are used in order to facilitate the fiber solidification in the channel. The most common polymers used in this method are alginate [25-29], PLGA [2, 30, 31], and chitosan [32, 33]. Calcium chloride ($CaCl_2$) is one of the common cross-linking agents used in the sheath fluid to solidify the polymer at the outlet of the channel. **Figure 1.3** shows images of different fibers fabricated using the chemical cross-linking method.

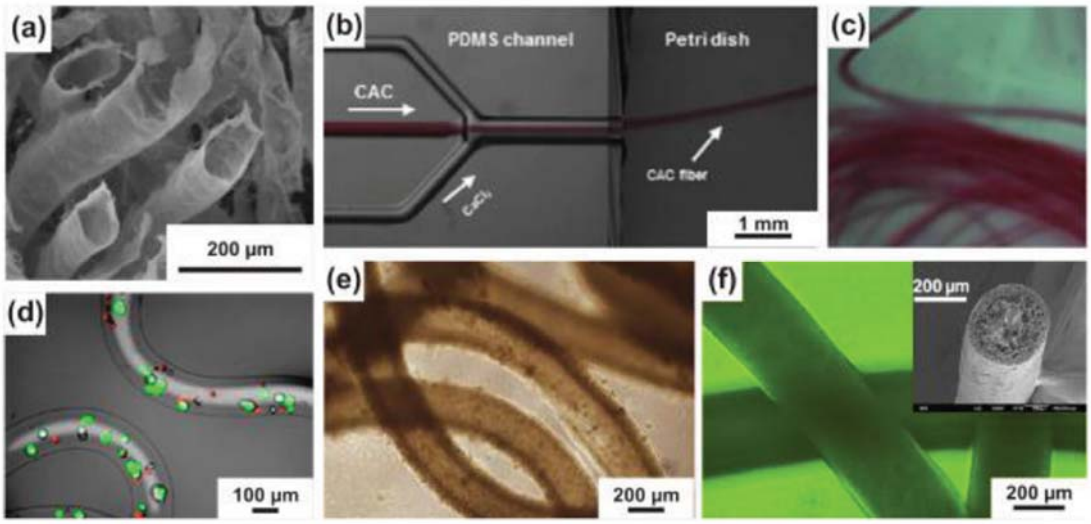

Figure 1.3 *Fibers made by using chemical cross-linking method [20]. (a) Hollow calcium alginate/poly(L-lysine) microtubes and cell-laden calcium alginate/poly(L-lysine) microfibers. (b and c) Fabrication of calcium alginate microfibers. (d) Encapsulation of viable (green) and dead (red) HepG2 cells inside Chitosan-alginate microfibers. (e) Gelatin-hydroxyphenylpropionic acid (Gel-HPA) microfibers cultured with Madlin-Darby canine kidney cells. (f) Alginate/Gel-HPA microfibers cross-linked by hydrogen peroxide.*

1.2.3 Photopolymerization method

In this method, free-radical polymerization reactions are used to solidify the prepolymer in the channel. The advantage of this method is the rapid solidification rate of the polymers in the channel. This method has been used to fabricate fibers with various materials and chemistries [34-38].

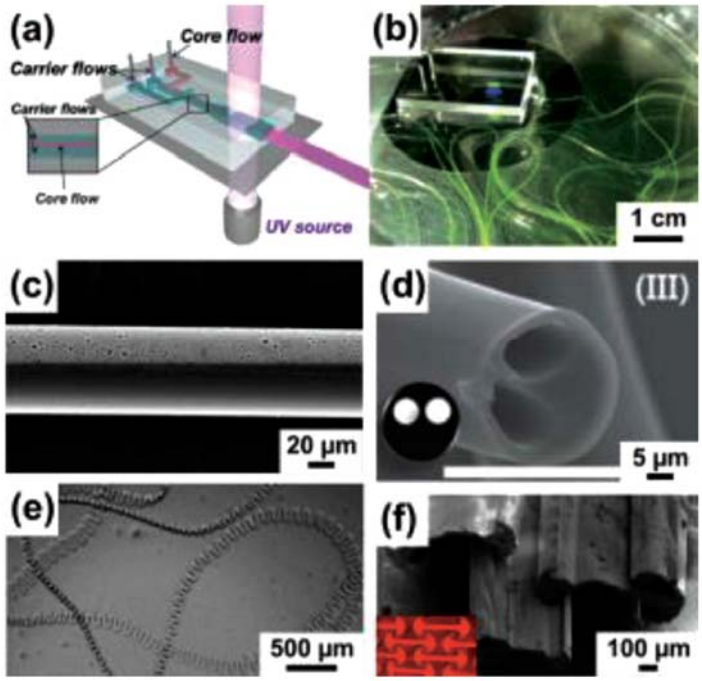

Figure 1.4 *Using photopolymerization strategy to fabricate microfluidic spun fibers [20]. (a and b) Schematic of photopolymerization process and the resulting continuous fibers [39]. (c) Fiber with anisotropic porosity [40]. (d) Hollow fiber with multiple core region [41]. (e) Crimpled microfibers [42]. (f) H-shape fibers [35].*

The common materials used in this method are methacrylates [34, 36], polyurethanes, immiscible combinations of hexadecane and polyethylene glycol diacrylate [43], and thiol-enes and thiolynes [5, 35]. Because the photopolymerization occurs in fraction of second, it is feasible

to fabricate fiber with noncircular cross-sections [5, 34, 35]. **Figure 1.4** displays a schematic of fiber fabrication using photopolymerization strategy and some of the resulting fibers.

Although casting and chemical cross-linking process have some limitations and difficulties associated with the rate of solidification and shape formation of the fiber, they are desirable for biomedical applications and most of the fibers are biocompatible and biodegradable.

REFERENCES

[1] Chung BG, Lee KH, Khademhosseini A, Lee SH. Microfluidic fabrication of microengineered hydrogels and their application in tissue engineering. Lab on a Chip. 2012;12:45-59.

[2] Hwang CM, Khademhosseini A, Park Y, Sun K, Lee S-H. Microfluidic Chip-Based Fabrication of PLGA Microfiber Scaffolds for Tissue Engineering. Langmuir. 2008;24:6845-51.

[3] Tiwari SK, Tzezana R, Zussman E, Venkatraman SS. Optimizing partition-controlled drug release from electrospun core-shell fibers. International Journal of Pharmaceutics. 2010;392:209-17.

[4] Caplin JD, Granados NG, James MR, Montazami R, Hashemi N. Microfluidic Organ-on-a-Chip Technology for Advancement of Drug Development and Toxicology. Advanced Healthcare Materials. 2015;4:1426-50.

[5] Boyd DA, Shields AR, Naciri J, Ligler FS. Hydrodynamic Shaping, Polymerization, and Subsequent Modification of Thiol Click Fibers. ACS Applied Materials & Interfaces. 2013;5:114-9.

[6] Kraitzer A, Ofek L, Schreiber R, Zilberman M. Long-term in vitro study of paclitaxel-eluting bioresorbable core/shell fiber structures. Journal of Controlled Release. 2008;126:139-48.

[7] Saraf A, Baggett LS, Raphael RM, Kasper FK, Mikos AG. Regulated non-viral gene delivery from coaxial electrospun fiber mesh scaffolds. Journal of Controlled Release. 2010;143:95-103.

[8] Tamayol A, Akbari M, Annabi N, Paul A, Khademhosseini A, Juncker D. Fiber-based tissue engineering: Progress, challenges, and opportunities. Biotechnol Adv. 2013;31:669-87.

[9] Deng M, James R, Laurencin CT, Kumbar SG. Nanostructured Polymeric Scaffolds for Orthopaedic Regenerative Engineering. IEEE Trans Nanobiosci. 2012;11:3-14.

[10] Jung J-H, Choi C-H, Chung S, Chung Y-M, Lee C-S. Microfluidic synthesis of a cell adhesive Janus polyurethane microfiber. Lab Chip. 2009;9:2596-602.

[11] Enea D, Henson F, Kew S, Wardale J, Getgood A, Brooks R, et al. Extruded collagen fibres for tissue engineering applications: effect of crosslinking method on mechanical and biological properties. Journal of Materials Science-Materials in Medicine. 2011;22:1569-78.

[12] Reddy N, Yang YQ. Structure and properties of cocoons and silk fibers produced by Hyalophora cecropia. Journal of Materials Science. 2010;45:4414-21.

[13] Ella V, Annala T, Lansman S, Nurminen M, Kellomaki M. Knitted polylactide 96/4 L/D structures and scaffolds for tissue engineering: shelf life, in vitro and in vivo studies. Biomatter. 2011;1:102-13.

[14] Akbari M, Sinton D, Bahrami M. Viscous flow in variable cross-section microchannels of arbitrary shapes. International Journal of Heat and Mass Transfer. 2011;54:3970-8.

[15] Yim EKF, Wan ACA, Le Visage C, Liao IC, Leong KW. Proliferation and differentiation of human mesenchymal stem cell encapsulated in polyelectrolyte complexation fibrous scaffold. Biomaterials. 2006;27:6111-22.

[16] Badrossamay MR, McIlwee HA, Goss JA, Parker KK. Nanofiber Assembly by Rotary Jet-Spinning. Nano Letters. 2010;10:2257-61.

[17] Sharifi F, Sooriyarachchi AC, Altural H, Rylander MN, Hashemi N. Fiber-Based Approaches for Drug Delivery and Regenerative Medicine Applications 2016 (submitted).

[18] Jun Y, Kang E, Chae S, Lee S-H. Microfluidic spinning of micro- and nano-scale fibers for tissue engineering. Lab on a Chip. 2014;14:2145-60.

[19] Jun-Seo P. Electrospinning and its applications. Advances in Natural Sciences: Nanoscience and Nanotechnology. 2010;1:043002.

[20] Daniele MA, Boyd DA, Adams AA, Ligler FS. Microfluidic Strategies for Design and Assembly of Microfibers and Nanofibers with Tissue Engineering and Regenerative Medicine Applications. Advanced Healthcare Materials. 2015;4:11-28.

[21] Chae S-K, Kang E, Khademhosseini A, Lee S-H. Micro/Nanometer-Scale Fiber with Highly Ordered Structures by Mimicking the Spinning Process of Silkworm. Advanced Materials. 2013;25:3071-8.

[22] Thangawng AL, Howell PB, Richards JJ, Erickson JS, Ligler FS. A simple sheath-flow microfluidic device for micro/nanomanufacturing: fabrication of hydrodynamically shaped polymer fibers. Lab on a Chip. 2009;9:3126-30.

[23] Sharifi F, Kurteshi D, Hashemi N. Microfluidic Fabrication of Highly Structured Polycaprolactone (PCL) Fibers. 2016 (submitted).

[24] Sharifi F, Patel BB, Dzuilko AK, Sakaguchi DS, Montazami R, Hashemi N. Microfluidic Spun Poly (ε-caprolactone) (PCL) Microfibrous Scaffolds to Navigate Neural Stem Cells for Regenerative Biomedical Applications. 2016 (submitted).

[25] Sugiura S, Oda T, Aoyagi Y, Satake M, Ohkohchi N, Nakajima M. Tubular gel fabrication and cell encapsulation in laminar flow stream formed by microfabricated nozzle array. Lab on a Chip. 2008;8:1255-7.

[26] Lee BR, Lee KH, Kang E, Kim DS, Lee SH. Microfluidic wet spinning of chitosan-alginate microfibers and encapsulation of HepG2 cells in fibers. Biomicrofluidics. 2011;5.

[27] Hammer J, Han LH, Tong XM, Yang F. A Facile Method to Fabricate Hydrogels with Microchannel-Like Porosity for Tissue Engineering. Tissue Engineering Part C-Methods. 2014;20:169-76.

[28] Lin YS, Huang KS, Yang CH, Wang CY, Yang YS, Hsu HC, et al. Microfluidic Synthesis of Microfibers for Magnetic-Responsive Controlled Drug Release and Cell Culture. Plos One. 2012;7:8.

[29] Onoe H, Okitsu T, Itou A, Kato-Negishi M, Gojo R, Kiriya D, et al. Metre-long cell-laden microfibres exhibit tissue morphologies and functions. Nature Materials. 2013;12:584-90.

[30] Hwang CM, Park Y, Park JY, Lee K, Sun K, Khademhosseini A, et al. Controlled cellular orientation on PLGA microfibers with defined diameters. Biomedical Microdevices. 2009;11:739-46.

[31] Wen X, Tresco PA. Fabrication and characterization of permeable degradable poly(dl-lactide-co-glycolide) (PLGA) hollow fiber phase inversion membranes for use as nerve tract guidance channels. Biomaterials. 2006;27:3800-9.

[32] Oh J, Kim K, Won SW, Cha C, Gaharwar A, Selimović Š, et al. Microfluidic Fabrication of Cell Adhesive Chitosan Microtubes. Biomedical Microdevices. 2013;15:10.1007/s10544-013-9746-z.

[33] Lee KH, Shin SJ, Kim C-B, Kim JK, Cho YW, Chung BG, et al. Microfluidic synthesis of pure chitosan microfibers for bio-artificial liver chip. Lab on a Chip. 2010;10:1328-34.

[34] Thangawng AL, Howell JPB, Spillmann CM, Naciri J, Ligler FS. UV polymerization of hydrodynamically shaped fibers. Lab on a Chip. 2011;11:1157-60.

[35] Boyd DA, Shields AR, Howell PB, Ligler FS. Design and fabrication of uniquely shaped thiol-ene microfibers using a two-stage hydrodynamic focusing design. Lab on a Chip. 2013;13:3105-10.

[36] Shields AR, Spillmann CM, Naciri J, Howell PB, Thangawng AL, Ligler FS. Hydrodynamically directed multiscale assembly of shaped polymer fibers. Soft Matter. 2012;8:6656-60.

[37] Daniele MA, North SH, Naciri J, Howell PB, Foulger SH, Ligler FS, et al. Rapid and Continuous Hydrodynamically Controlled Fabrication of Biohybrid Microfibers. Advanced Functional Materials. 2013;23:698-704.

[38] Daniele MA, Radom K, Ligler FS, Adams AA. Microfluidic fabrication of multiaxial microvessels via hydrodynamic shaping. RSC Advances. 2014;4:23440-6.
[39] Cho S, Shim TS, Yang SM. High-throughput optofluidic platforms for mosaicked microfibers toward multiplex analysis of biomolecules. Lab on a Chip. 2012;12:3676-9.

[40] Jung JH, Choi CH, Chung S, Chung YM, Lee CS. Microfluidic synthesis of a cell adhesive Janus polyurethane microfiber. Lab on a Chip. 2009;9:2596-602.

[41] Choi CH, Yi H, Hwang S, Weitz DA, Lee CS. Microfluidic fabrication of complex-shaped microfibers by liquid template-aided multiphase microflow. Lab on a Chip. 2011;11:1477-83.

[42] Nunes JK, Constantin H, Stone HA. Microfluidic tailoring of the two-dimensional morphology of crimped microfibers. Soft Matter. 2013;9:4227-35.

[43] Duboin A, Middleton R, Malloggi F, Monti F, Tabeling P. Cusps, spouts and microfiber synthesis with microfluidics. Soft Matter. 2013;9:3041-9.

CHAPTER 2

MECHANICAL AND PHYSICAL PROPERTIES OF DEGRADABLE POLY(VINYL ALCOHOL) MICROFIBERS FABRICATED BY MICROFLUIDIC APPROACH [1]

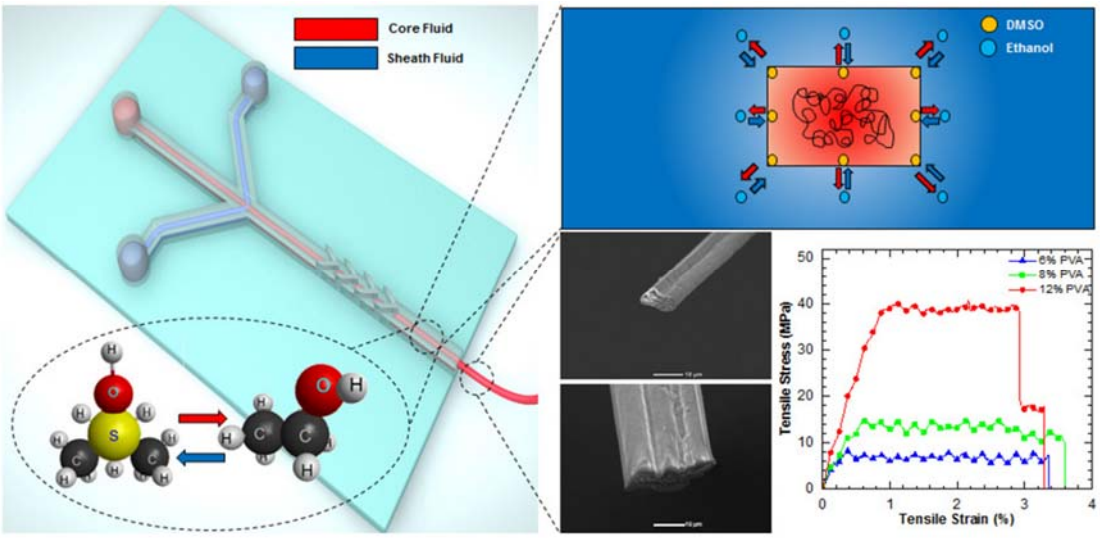

ABSTRACT

A microfluidic platform was used to fabricate continuous and non-rounded polyvinyl alcohol (PVA) microfibers. We showed that the size and cross-section of the PVA fibers can be controlled by changing the PVA concentration in dimethyl sulfoxide (DMSO) and flow rate ratio between the core and sheath fluids. The PVA concentration was varied from 6% to 12%, and the sheath-to-core flow rate ratio used for this study was in the range of 500 : 5 to 500 : 20. The aspect ratio of the fibers became larger when the PVA concentration increased and the flow rate ratio decreased. Additionally, we simulated the microfluidic fiber fabrication process and the results were consistent with the experimental results. The dissolution of the PVA fibers fabricated with different characteristics was also studied. It was shown that increasing the PVA concentration and decreasing the flow rate ratio increased the dissolution time of the fibers in DI water. A tensile test

[1] **F. Sharifi**, Z. Bai, R. Montazami, and N. Hashemi, "Mechanical and Physical Properties of Poly(vinyl alcohol) Microfibers Fabricated by Microfluidic Approach" *RSC Advances*, 6, 55343-55353 (2016).

was conducted to obtain the stress–strain curves for different types of fibers. The results showed that a wide range of mechanical properties can be achieved by changing the PVA concentration and the flow rate ratio. The increase of PVA concentration from 6% to 12% enhanced the tensile stress at break and Young's modulus by a factor of 4.9 and 2.02, respectively. The mechanical strength of the fibers was shown to drop when the flow rate ratio decreased.

2.1 Introduction

Nowadays, polymeric fibers are attracting more and more attention due to their remarkable characteristics such as extremely large surface area to volume ratio, flexibility in surface functionalities, and superior mechanical performance (*e.g.*, stiffness and tensile strength) compared with any other known form of the material [1-4]. These outstanding properties make the polymer fibers optimal candidates for many important applications such as tissue engineering, cell encapsulation, wound dressings, and drug release [5-9].

Several different fiber fabrication approaches exist such as microfluidic, electrospinning, and wet spinning [10, 11]. Microfluidics is an emerging approach that uses small amount of samples for a wide range of applications from biomedical systems to energy devices [12-15]. The microfluidic method is a simple, rapid, and low-cost method for producing fibers, which depends on a number of experimental parameters. Additionally, this approach does not need high temperature, voltage, or pressure, which can damage the living systems in the biomedical applications [16-18]. The shape of the resulting fiber is a function of the flow rates and the types and numbers of shaping elements in the channel walls such as various chevron grooves [19-21]. Presently, great efforts have been devoted to expand the variety of materials that can be applied to fabricate various types of structures using microfluidics. For instance, Thangawng *et al.* produced

round PMMA fibers with diameters down to 300 nm by varying the ratio between the sheath and core flow rates using a 5-diagonal groove device. Ribbon-shaped fibers with submicron thickness were also fabricated using a 7-chevron/5-diagonal groove combination device [22]. Recently, our group successfully fabricated uniform polycaprolactone (PCL) and gelatin microfibers *via* phase inversion solidification process [16]. We showed that various morphologies and cross-sections (round, square and ribbon) can be obtained by varying the PCL and gelatin concentrations in the core solution and the sheath-to-core flow rate ratio. It is expected that this strategy can be applied to fabricate various fibers.

Poly(vinyl alcohol) (PVA) is a nontoxic, biocompatible, hydrophilic synthetic polymer with good chemical, thermal, and mechanical stability. It also possesses a wide range of crystallinity. Recently, it was found that PVA can be used for transient electronics and bioelectronics [23, 24]. Previously, PVA microfibers were fabricated using an electrospinning approach [25-27]. However, using electrospinning method to fabricate fibers has some disadvantages. The electro-spun fibers are fabricated with only round cross-sections due to the surface tension between the polymer and air during formation. It is also hard to accurately align the electro-spun fibers. The fiber characteristics, such as diameter and surface properties, do not vary widely. The current PVA fibers, on the other hand, are not necessarily rounded. They can be fabricated with different aspect ratios by simply changing different parameters such as the flow rate ratio between two fluids. We showed that the non-rounded fibers results in variations in mechanical properties and increasing the surface area-to-volume ratio of the fibers which is important in applications such as tissue engineering and biosensors. Moreover, the microfluidic platform can be considered as an alternative approach to precisely control the fiber alignment. In fact, this alignment is not limited to the position of one fiber with respect to others. The

microfluidic approach makes it feasible to align the polymer chain of each fiber due to the shear force exerted on the pre-polymer solution from the sheath fluid in the flow direction. The aligned fibrous scaffold can significantly guide the growth direction of the cells, which is useful in regenerating nerve tissues, blood vessels, tendons, and muscle tissue. We demonstrated that the size and surface properties of microfluidic-spun PVA fibers can be easily tuned by simply changing the 3D hydrodynamic focusing force exerted on the core fluid. In addition, the current PVA fibers made in this study can be used to encapsulate cells for some biomedical applications such as cell delivery, whereas high voltage used in electrospinning method could be harmful for the cells. Despite its advantages, the production rate in microfluidic approach is slower than that of the electrospinning. This is a result of advances in the electrospinning technique brought about during several decades of industrial use. Microfluidic approach, on the other hand, is a new method that has shown promising potential for various biomedical applications, but it may take more time for this method to be fully understood and more well-known [16, 28-32].

PVA has been used in microfluidic fiber fabrication process before by Jeong *et al.* [33] However, in that study, fiber was made of 4-hydroxybutyl acrylate (4HBA), and PVA solution (PVA in DI water) was applied as a non-polymerizable fluid (sheath fluid) to adjust the shape of the fiber. In the present work, we fabricated PVA fibers using a microfluidic approach for the first time. We showed that the size, shape, dissolution, and mechanical properties of PVA microfluidic-spun fibers can be tuned by changing the PVA concentration and flow rate between the core and sheath fluids. In addition, the microfluidic fiber fabrication process was simulated using COMSOL Multiphysics to study the effect of flow rate ratio on the shape of the resulting fiber.

2.2 Experimental Section

2.2.1 Chemicals and materials

Poly(vinyl alcohol) (PVA) (M_w: 61 000 g mol^{-1}, 98.0–98.8 mol% hydrolysis) and absolute ethanol were purchased from Sigma-Aldrich. Dimethyl sulfoxide (DMSO) was purchased from Fisher Scientific. The Sylgard 184 Elastomer Base and Curing Agents were purchased from Dow Corning Corporation, Midland, MI.

2.2.2 Microfluidic channel device design

A poly(methyl methacrylate) (PDMS) channel was used in this study, which is a transparent and biocompatible elastomer. In order to make the channel, the Sylgard 184 Elastomer Base and Curing Agents (PDMS pre-polymers) in a 10 : 1 ratio were stirred and poured onto two molds made of a SU8 photoresist-patterned silicon wafer, and cured at 80 °C for 20 min. Then the PDMS layers were peeled off and one of them was punched to create a connection between the inlet of the channel and the syringes which include the core and sheath solutions. Finally, the plasma treatment was applied to bond the two PDMS layers together. The microchannel is symmetric with one inlet for the core fluid, two inlets for the sheath fluid, and four chevron grooves. The dimensions of the channel are 130 μm × 390 μm (height × width). The height and width of the grooves are 100 μm and 65 μm, respectively, and their angle with respect to the main direction of the flow is 45 degrees.

2.2.3 PVA fiber fabrication

In order to prepare the core solution, 25 mL of DMSO was heated to 120 °C within 20 min, and then PVA powders were added into the DMSO under vigorous stirring. After stirring for

2 hours, the mixture was cooled to room temperature. This process was repeated to prepare the core solutions with the PVA concentration in the range of 6–12 wt%. Absolute ethanol was applied as sheath fluid in this study. The core and sheath fluids were introduced into the channel using the 3 mL and 60 mL plastic syringes (BD Biosciences) for the core and sheath fluids, respectively, through a double syringe pump (Cole-Parmer, Veron Hillss, IL). The flow rates of the core fluid were in the range of 5–50 μL min^{-1}, whereas the constant flow rate of 500 μL min^{-1} was used for the sheath fluid.

2.2.4 Computational model

The microfluidic fiber fabrication process was simulated using the COMSOL Multiphysics (COMSOL, Inc., Burlington, MA) software. The purpose of the simulation was to study the effect of various flow rate ratios between the core and sheath fluids on the fiber shape and compare the numerical and experimental results. It was assumed that the process is steady-state at room temperature, and the fluids are incompressible. The flow and diffusion modules were coupled in COMSOL in order to achieve the concentration distribution of the core and sheath fluids, and to estimate the cross-section of the resulting fibers at the outlet. First, the velocity and pressure distributions were found for the channel, and then, the results were used to obtain the concentration profile of the fluids along the channel as well as the outlet.

2.2.5 Characterization

The viscosities of core solutions with different PVA concentrations were measured using a digital viscometer (DV-E, Brookfield Engineering Laboratories, Inc., Middleboro, MA). The size, shape, and morphology of the PVA microfibers were studied using field emission scanning

electron microscopy (FE-SEM) (JSM-6700F) at an acceleration voltage of 5 kV. In order to obtain the cross-sectional SEM images, the fibers were cut with a sharp razor. The dissolution of fibers were measured using UV-Vis spectrometer (PerkinElmer Lambda 25). In this part, the non-fluorescent blue dye (105002 Standard Blue Powder, Bright Dyes) with the absorbance wavelength of 630 nm was used in the core fluid. After calibration, the dissolution rates of the fibers with different characteristics in DI water were calculated. The tensile test was performed with an Instron Universal Testing machine (Model 5569, Instron Engineering Corp., Canton, MA) at an extension rate of 50 mm min^{-1}using a 2 kN load cell. For each test, one single fiber was attached on a paper frame in order to be gripped tightly by the Instron machine. The samples were prepared such that the distance between the two clamps is 20 mm at the beginning. Before starting the test, the two sides of the frame were cut to obtain the stress–strain curve of the fibers without the effects of the paper frame. The Bluehill software was used to control the Instron machine and get the results of the test.

2.3 Results and Discussion

2.3.1 Microfluidic fiber fabrication

The fabrication method for PVA microfibers utilizing a microfluidic device is shown in **Figure 2.1** (a). Both of the fluids, *i.e.* the core and sheath fluids, are introduced into the channel using silicone tubing. The channel has three inlets, one for the core fluid at the center and two for the sheath fluid.

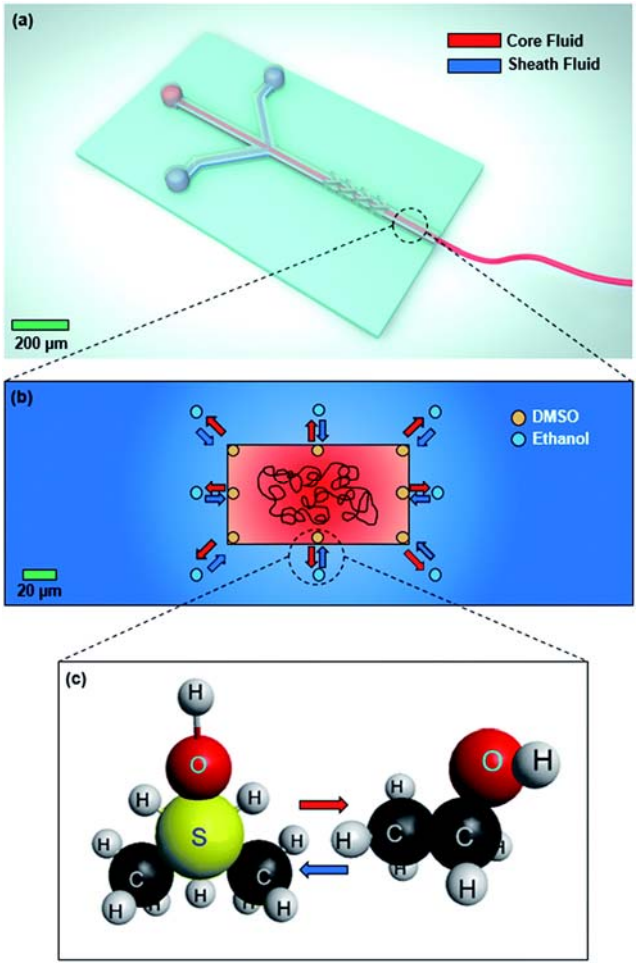

Figure 2.1 *(a) Schematic of the experimental setup used for microfluidic fiber fabrication. (b) Phase inversion solidification strategy applied to fabricate the microfluidic-spun PVA fibers. (c) Replacement of DMSO molecules with ethanol at the core/sheath interface, which results in aggregation and precipitation of PVA as a fiber.*

As shown in **Figure 2.1** (b), we employed the phase inversion process to solidify the poly(vinyl alcohol) (PVA). In this process, dimethyl sulfoxide (DMSO), the solvent of PVA, is replaced by the sheath fluid, *i.e.* ethanol, at the interface between the core and sheath fluids (**Figure 2.1** (c)).

The PVA solidifies because the ethanol is miscible with DMSO and it does not dissolve the PVA. In the microfluidic channel, the lateral hydrodynamic focusing force from the sheath

fluid compresses the core into a thin vertical strip, which results in increased height of the core fluid in the channel. At the same time, because of the laminar flow regime, diffusion takes place at the core/sheath fluid interface and the PVA stream rapidly solidifies as a result of the phase inversion process. Additionally, the channel consists of four chevron grooves at the downstream of the channel. Once the two fluids reach this area, the sheath fluid fills the chevron grooves due to the fact that the hydrodynamic resistance is inversely proportional to the flow rate. As a result, the sheath fluid compresses the core fluid perpendicular to the main flow direction [34, 35]. These vertical and lateral forces on the core fluid originate from the shear force between the core and sheath fluids due to the velocity difference at the fluid/fluid interface, which results in aligning the polymer chain in the direction of the flow.

2.3.2 Effect of PVA concentration

One of the important parameters which plays a significant role on the resulting fiber is the concentration of PVA in the core fluid. **Figure 2.2** shows the viscosity of the core solution as a function of PVA concentration. Based on this figure, when the PVA concentration increases from 6% to 12%, the viscosity of the core fluid rises from 78 to 297 cP. This shows the feasibility of microfluidic fiber fabrication in a wide range of viscosities.

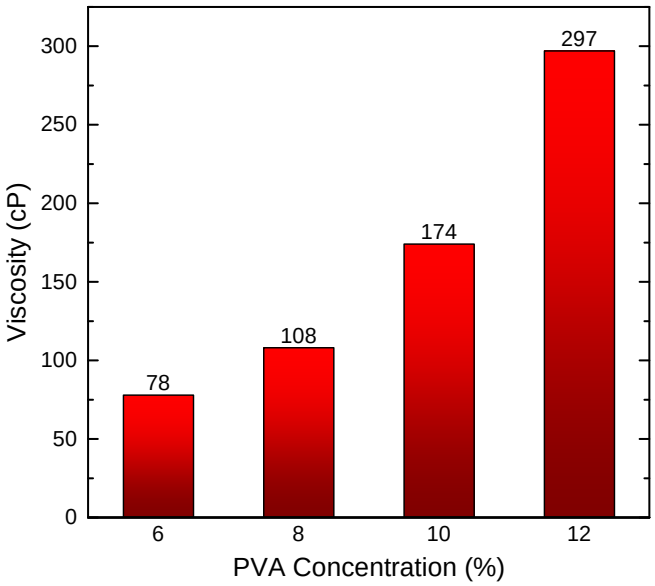

Figure 2.2 *Viscosity of core solution prepared by various PVA concentrations in DMSO.*

The scanning electron microscopic (SEM) images of the fibers fabricated using different PVA concentrations are shown in **Figure 2.3**. For this part, the flow rates of the core and sheath fluids were kept constant at 500 μL min^{-1} and 5 μL min^{-1}, respectively. **Figure 2.3** (a_1-c_1) demonstrates that the average diameter of the fibers increases with the increase of the PVA concentration in core fluid. That is because a fixed amount of core fluid will be in the microchannel in a steady state condition when the core flow rate is constant. Thus, a more concentrated core fluid results in a larger fiber being fabricated during the phase inversion process in the channel. However, due to the fact that the microchannel has a rectangular cross-section and the shape of the fiber varies based on the flow rate ratio between the core and sheath fluids, the resulting fibers will have different cross-sections.

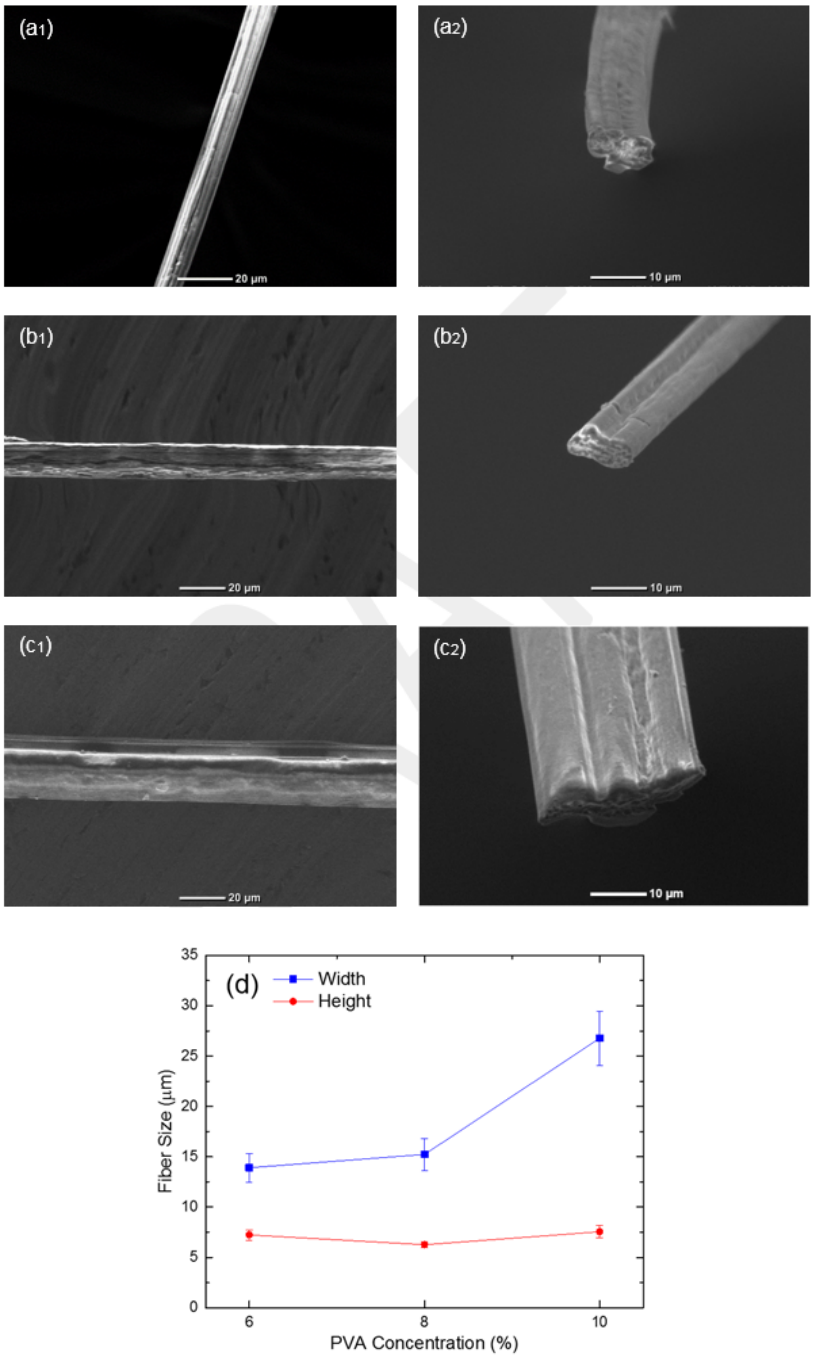

Figure 2.3 *Longitudinal (a_1–c_1) and cross-sectional (a_2–c_2) SEM images of PVA microfibers fabricated by PVA concentrations of (a) 6%, (b) 8%, and (c) 10% in DMSO solution. (d) Width and height of the fibers made by different PVA concentrations (%). The sheath and core flow rates were set as 500 μL min^{-1} and 5 μL min^{-1}, respectively.*

Therefore, it is more accurate to study the size and shape of the fibers using the cross-sectional images (**Figure 2.3** (a_2-c_2)). The results show that the ribbon shape PVA fibers can be fabricated through the hydrodynamic focusing process. The width and height of the PVA fibers made by 6%, 8%, and 10% PVA are summarized in **Figure 2.3** (d). These figures clearly illustrate the effects of both lateral and vertical forces exerted on the core fluid from the sheath fluid. Regarding the lateral force, when higher concentration of PVA is used, the core fluid covers more space of the channel due to the higher amount of PVA in DMSO. This leads to development of the fiber in a lateral direction from 13.9 μm to 26.8 μm. On the other hand, the magnitude of the vertical force is mostly dependent on the shape and height of the chevrons, which have not been changed during this study. As a result, the height of the PVA microfibers does not change significantly. When the PVA concentration increases from 6% to 8%, the width of the fiber rises, whereas its height decreases such that the aspect ratio increases by a factor of 1.84. This reveals the importance of the PVA concentration in the shape and size of the fiber.

2.3.3 Effect of flow-rate ratio between the sheath and core fluids

Using different flow rate ratios for the core and sheath fluids results in the changes of the shear force at the fluid/fluid interface. Therefore, the flow rate ratio between the core and sheath fluids plays a pivotal role in the shape and morphology of the resulting microfibers. In this section, we used the flow rate ratios in the range of 25–100. We could not use lower flow rate ratios because the resulting shear force from the sheath fluid would not be enough to hydrodynamically focus the core fluid in the vertical and lateral directions, which would result in clogging of the channel.

Figure 2.4 shows the SEM images of the fibers fabricated using the sheath-to-core flow rates of 500 : 5, 500 : 10, and 500 : 20, respectively. In the previous section, it was shown that by using the sheath-to-core flow rate of 500 : 5 and PVA concentration in the range of 6–10%, a

continuous and uniform fiber can be fabricated. However, it was observed that when the PVA concentration increases to 12% and the sheath-to-core flow rate ratio is kept at 500 : 5 μL min^{-1}, the large viscosity mismatch between the core and sheath fluid leads to the fabrication of a non-uniform fiber (**Figure 2.4** (a_1 and a_2)). However, **Figure 2.4** (a_1-c_1) demonstrates that the non-uniformity of the fibers at the PVA concentration of 12% can be improved by decreasing the sheath-to-core flow rate ratio from 500 : 5 to 500 : 10 and 500 : 20. The reason for this behavior is that when the PVA concentration increases to 12%, the viscosity contrast between the core and sheath fluids becomes larger. Therefore, the shear force between the core and sheath fluid exceeds the stable flow regime, which is the reason for the two viscous fluids to experience instability. To avoid this issue, we reduced the flow rate ratio between the two fluids in order to decrease the shear force at the core/sheath interface.

This reveals that the shape and morphology of the fibers are dependent on the flow rate ratio between the core and sheath fluids as well as the PVA concentration in the core solution. Furthermore, the cross-sectional SEM images of the fibers are shown in **Figure 2.4** (a_2 - c_2). The width and height of the PVA fibers fabricated by the PVA concentration of 12% and different sheath-to-core flow rates of 500 : 5, 500 : 10, and 500 : 20 are provided in **Figure 2.4** (d). The results demonstrate that the average width and height of the fiber at the sheath-to-core flow rate of 500 : 5 are 14.6 μm and 8.6 μm, respectively. The decrease of the flow rate ratio weakens the shear force of the sheath fluid on the core fluid because the relative velocity at the fluid/fluid interface reduces. Therefore, the core fluid develops in the microchannel such that the width of the resulting fiber increases by 45% at the flow rate ratio of 500 : 20, while the width of the channel negligibly varies.

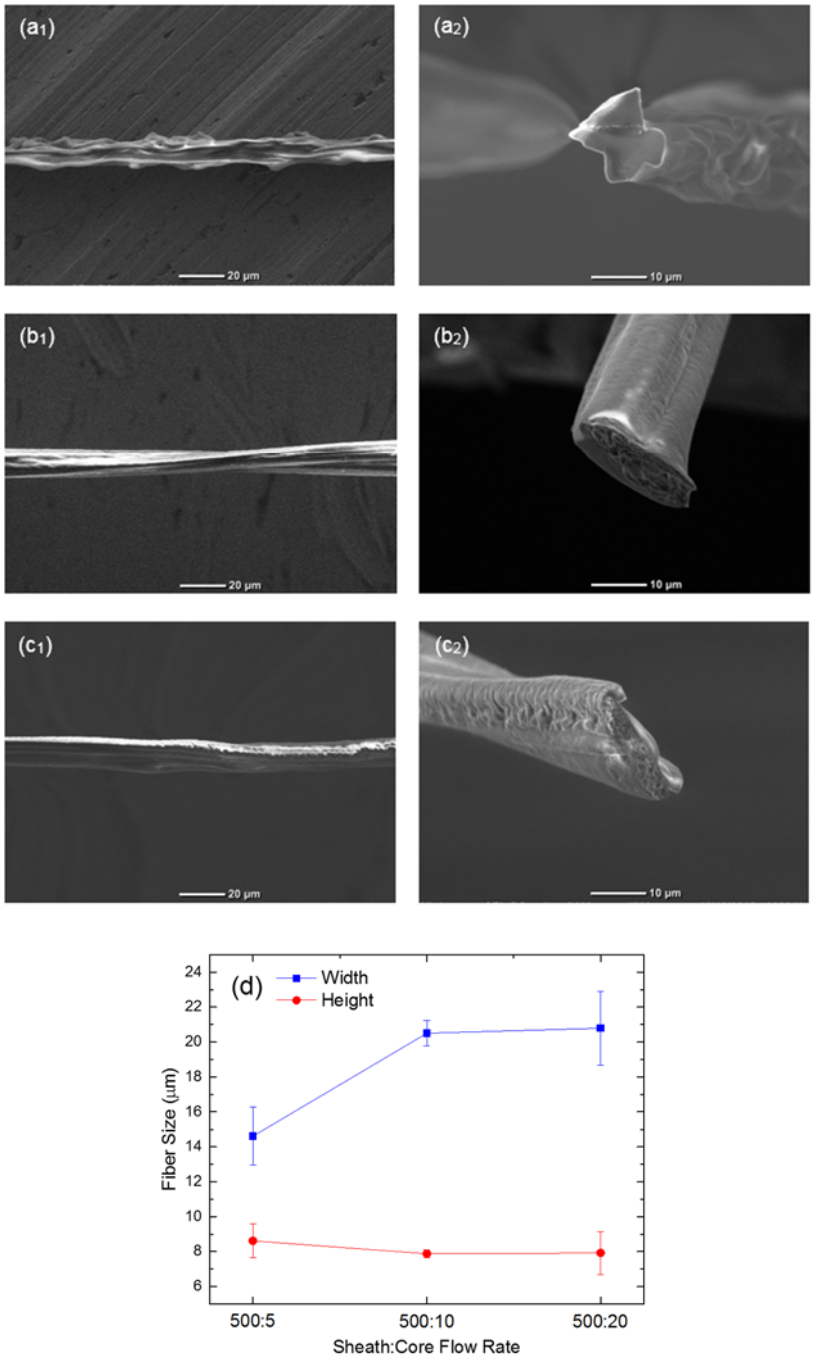

Figure 2.4 *Longitudinal (a_1–c_1) and cross-sectional (a_2–c_2) SEM images of PVA microfibers fabricated by the PVA concentration of 12% in DMSO and the sheath-to-core flow-rate ratios of (a) 500 : 5, (b) 500 : 10 and (c) 500 : 20. (d) Width and height of the fibers made by different flow rate ratios and 12% PVA concentration.*

Apart from the experimental work, the microfluidic fiber fabrication process was simulated using COMSOL multiphysics. For the simulation, one fourth of the microchannel was modeled due to the symmetric geometry of the channel and boundary conditions. The Navier Stokes and Fick equations were applied to find the velocity and concentration, respectively. **Figure 2.5** demonstrates the concentration distribution along the channel and at the outlet. The white and black colors represent the core and sheath fluids, respectively. **Figure 2.5** (a) clearly illustrates both of the lateral and vertical hydrodynamic focusing forces exerted by the sheath fluid on the core fluid. At the beginning of the channel, the velocity of the sheath fluid is considerably higher than that of the core fluid, and this velocity difference intensifies in the nozzle area. As a result, the core fluid is laterally focused, and it is changed to a vertical strip. After the nozzle region, the sequential chevron grooves play a significant role in creating the vertical force causing the shear force to wrap around the core fluid, such that the core fluid is placed at the center of the channel. In this area, the hydrodynamic resistance perpendicular to the flow direction decreases and the sheath fluid fills this area as the resistance is inversely proportional to the flow rate. Thus, the core fluid is vertically focused from top and bottom, which results in the fabrication of the ribbon-shaped fibers. Based on these explanations, it is obvious that the values of the core and sheath flow rates directly affect the size and aspect ratio of the resulting fibers. For example, **Figure 2.5** (b) and (c) shows the cross-section of the fibers at the outlet of the channel when the sheath-to-core flow rates are 500 : 10 and 500 : 20, respectively. As expected, the size and aspect ratio of the fiber increase when the flow rate ratio decreases. That is because the increase of the core flow rate reduces the relative velocity at the interface between the two fluids, which results in the decrease of the lateral shear force on the core fluid. However, the vertical force on the core fluid mostly depends on the height and number of the chevrons, which were kept constant in this study [35].

Therefore, the width of the fiber enlarges and the height of the fiber is not directly affected by changing the flow rate ratio, which results in fabrication of fibers with higher aspect ratios. This behavior was observed in experimental results (**Figure 2.4** (a_2 - c_2)), which shows a good agreement between the experimental and numerical results.

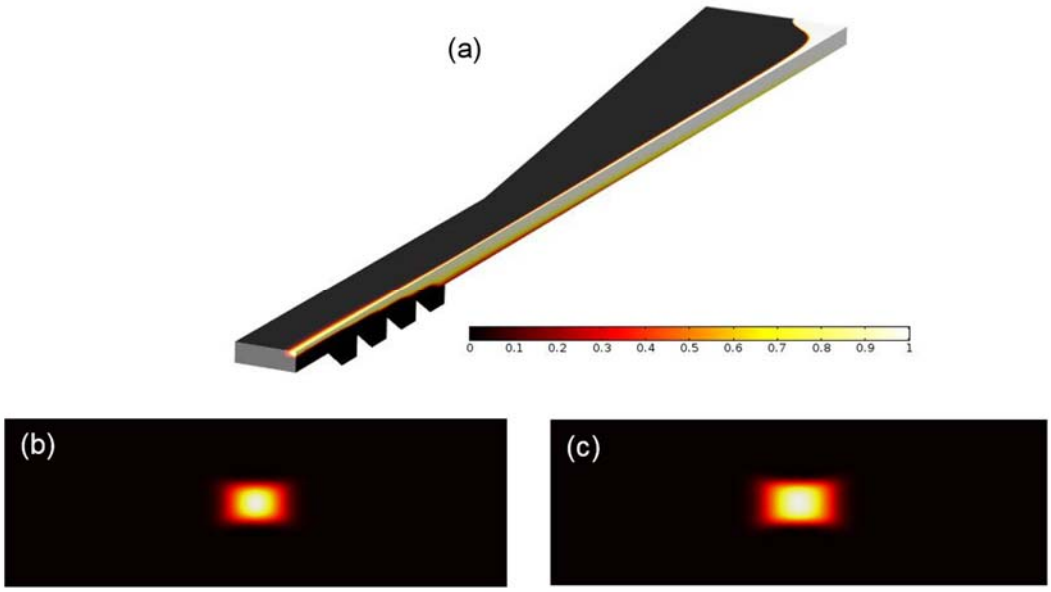

Figure 2.5 *The concentration (mol m^{-3}) profile of the sheath and core fluids (a) along the channel and (b and c) at the outlet with the sheath-to-core flow rates of 500 : 10 and 500 : 20, respectively. The white color represents the core fluid and the sheath fluid is black in this study.*

2.3.4 Characterization of the PVA fibers

The dissolution of the fibers with different characteristics was measured using UV-Vis spectroscopy and the results are shown in **Figure 2.6**. This method was selected because the weight of the fibers is very low and the dissolution of PVA is relatively fast. Therefore, the conventional methods, such as weighing the sample at different times, are not accurate for measuring the dissolution of the fibers. However, because PVA does not have any UV-Vis absorption band, we dyed the fibers with a blue color, which gives a peak at the wavelength of 630 nm. As an example,

the result of UV-Vis spectroscopy for the dissolution of the fiber fabricated using 12% PVA with the flow rate ratio of 500 : 5 is illustrated in **Figure 2.6** (a). The results show that the peak at the wavelength of 630 nm intensifies with time, which represents the dissolving of the PVA fiber in DI water. As expected, this figure demonstrates that the dissolution of the PVA fibers is fast. The speed of dissolution can be attributed to the fact that the hydroxyl groups in PVA create hydrogen-bonding with the molecules of highly polar solvents, such as water. This work was conducted for fibers fabricated with various PVA concentrations and flow rate ratios, and the results are provided in **Figure 2.6** (b).

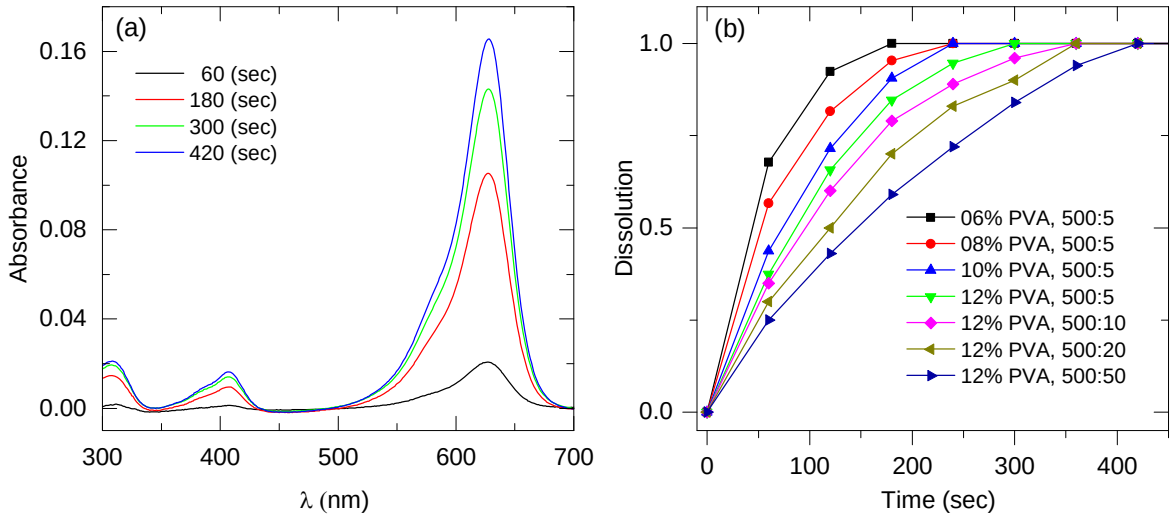

Figure 2.6 *Dissolution of the PVA fibers in DI water. (a) UV-Vis absorption spectra of dyed fiber with the PVA concentration of 12% in water at different times. (b) Dissolution of PVA microfibers fabricated by various PVA concentrations and flow-rates in water.*

Based on this figure, the increase of the PVA concentration increases the dissolution time of the PVA fibers. That is expected because when the core flow rate is set at 5 μL min^{-1}, the volume of the core fluid that occupies part of the channel is constant. Therefore, a more concentrated core solution gives a higher amount of PVA in the channel, which results in fabrication of larger fibers

that take a longer time to be dissolved in water. Additionally, the decrease of the flow rate ratio between the core and sheath fluids reduces the hydrodynamic focusing force, and the average size of the fiber becomes larger. This causes the PVA fiber to last longer in water.

The mechanical properties of biomaterials are important aspects in different biomedical applications such as tissue engineering. One of the goals of using scaffolds is to be able to mimic the mechanical properties of the tissue or organ. **Figure 2.7** shows the results of conducting a tensile test for the fibers created with different PVA concentrations and flow rate ratios. Additionally, the values of the tensile stress at break (MPa), tensile strain at break (%), and Young's modulus (MPa) are listed in **Table 2.1**. When the PVA concentration is 6% and the flow rate ratio between the sheath and core fluids is 500 : 5, the tensile stress at break, Young's modulus, and tensile strain at break (%) are 8.3 MPa, 2112.9 MPa, and 3.35, respectively. By increasing the PVA concentration to 12%, the tensile stress at break and Young's modulus are significantly enhanced by 390% and 102%, respectively. Similarly, the tensile strain at break (%) improves by increasing the PVA concentration to 10%. However, it reduces with further increase in the PVA concentration. All of the measurements were done at room temperature (below the glass transition temperature of the PVA at 85 °C), which results in low tensile strain at break for all types of the PVA fibers. In addition, when the flow rate ratio between the core and sheath fluids decreases from 500 : 5 to 500 : 20, the tensile stress at break, tensile strain at break, and Young's modulus drop by a factor of 1.76, 1.77, and 4.25, respectively. This can be due to the change of the cross-section of the fiber. As shown in **Figure 2.4**, when the flow rate ratio decreases, the aspect ratio of the fiber increases and the ribbon shape fiber is fabricated. In ribbon shape fibers, one side of the cross-section of the fiber is smaller than the other one. Therefore, when the fiber is under the tensile load and the cross-section of the sample decreases, the smaller side is weaker, which leads

to sample failure in lower loads and strains. This kind of behavior was observed for the thiol-ene and thiol-yne click fibers as well [28]. Nevertheless, the surface area of the ribbon shape fibers is larger than that of the square fibers, which is an important aspect for fibrous scaffolds to support the growth of more cells in tissue engineering.

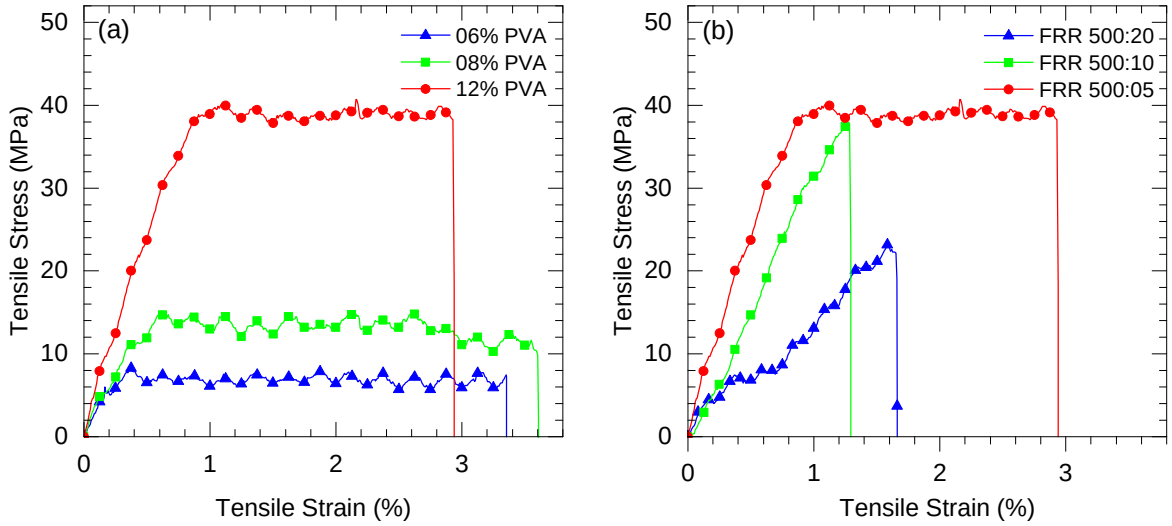

Figure 2.7 *Tensile properties of PVA fibers fabricated with (a) the flow rate ratio of 500 : 5 for the sheath:core fluids and various PVA concentrations in DMSO. (b) PVA concentration of 12% and different flow rate ratios.*

Table 2.1 *Mechanical properties of the fibers fabricated with various concentrations of PVA in DMSO and flow rate ratios between the core and sheath fluids.*

PVA Concentration (%)	Flow Rate Ratio (Sheath:Core)	Tensile Stress at Break (MPa)	Tensile Strain at Break (%)	Young's Modulus (MPa)
6	500:5	8.30	3.35	2112.9
8	500:5	14.83	3.61	2251.7
12	500:5	40.71	2.94	4265.1
12	500:10	37.81	1.29	3261.5
12	500:20	23.15	1.66	1003.4

There are some studies in which PVA fibers were fabricated using electrospinning method [36-39]. However, there is no report about the mechanical properties of single electrospun PVA fibers. In fact, it is common to measure the mechanical properties of the fibrous mats instead in this method. After comparing the results of this study with those reported for electrospun PVA mats, it was found that the microfluidic spun PVA fibers have a higher tensile stress at break and Young's modulus, but lower tensile strain at break. The reason for higher tensile stress might be due to the fact that the shear force exerted on the prepolymer solution align the polymer chain in the flow direction. It was expected to obtain lower strain (%) compared to the electrospun PVA mats because multiple fibers support each other and cause the mats to break at higher strain. In addition, higher strain of PVA mats can be due to the fact that the electrospun fibers are made randomly and most of them are not in the same direction as the tensile test. Consequently, they will break at higher strain.

Apart from fibrous mats, there are some reports that the mechanical properties of PVA films were measured [23, 40-47]. It was found that the values of tensile stress at break and Young's modulus are comparable with the ones reported in the literature for the PVA films. However, the tensile strain at break of the PVA films is larger. That might be related to the fabrication process. In this paper, the phase inversion solidification strategy was used to fabricate fiber. This strategy caused the molecules of DMSO and ethanol to be replaced which creates a porous fiber, whereas the PVA films made by different methods have lower porosity. Additionally, when a defect occurs in both PVA fiber and film, it propagates until the sample breaks. Because the average cross section area of the films is significantly larger than that of the fibers, the defect has to propagate more to completely break the sample, which results in higher strain at break (%) for the film.

2.4 Conclusions

The PVA microfiber was fabricated using a microfluidic approach. The effects of PVA concentration in the core fluid and flow rate ratio between the core and sheath fluid were investigated. The size, cross-section, dissolution of the fiber in DI water, as well as the mechanical properties of the fibers, were studied. It was found that when a higher PVA concentration is used, the size of the fiber increases, the dissolution of the fiber in water takes more time, and the mechanical properties are improved. When the PVA concentration increases from 6% to 12%, the tensile stress at break and Young's modulus are enhanced by 390% and 102%, respectively. On the other hand, when the flow rate ratio between the core and sheath fluids decreases, the size and aspect ratio of the fiber become larger, the fiber lasts longer in the water, and all of the tensile properties of the fiber drop. It was observed that the tensile stress at break, tensile strain at break, and Young's modulus can be enhanced by a factor of 1.76, 1.77, and 4.25 when the flow rate ratio increases from 25 to 100. Once again, it was proved that the microfluidic fiber fabrication is a promising platform to provide an accurate control on the size, shape, dissolution, and mechanical properties of the fibers, which could be useful in different biomedical applications.

REFERENCES

[1] Shi X, Ostrovidov S, Zhao Y, Liang X, Kasuya M, Kurihara K, et al. Microfluidic Spinning of Cell-Responsive Grooved Microfibers. Advanced Functional Materials. 2015;25:2250-9.

[2] Chae S-K, Kang E, Khademhosseini A, Lee S-H. Micro/Nanometer-Scale Fiber with Highly Ordered Structures by Mimicking the Spinning Process of Silkworm. Advanced Materials. 2013;25:3071-8.

[3] Daniele MA, Radom K, Ligler FS, Adams AA. Microfluidic fabrication of multiaxial microvessels via hydrodynamic shaping. Rsc Advances. 2014;4:23440-6.

[4] Daniele MA, Adams AA, Naciri J, North SH, Ligler FS. Interpenetrating networks based on gelatin methacrylamide and PEG formed using concurrent thiol click chemistries for hydrogel tissue engineering scaffolds. Biomaterials. 2014;35:1845-56.

[5] Daniele MA, Boyd DA, Adams AA, Ligler FS. Microfluidic Strategies for Design and Assembly of Microfibers and Nanofibers with Tissue Engineering and Regenerative Medicine Applications. Advanced Healthcare Materials. 2015;4.

[6] Jun Y, Kang E, Chae S, Lee SH. Microfluidic spinning of micro- and nano-scale fibers for tissue engineering. Lab on a Chip. 2014;14:2145-60.

[7] Ahn SY, Mun CH, Lee SH. Microfluidic spinning of fibrous alginate carrier having highly enhanced drug loading capability and delayed release profile. RSC Advances. 2015;5:15172-81.

[8] Kaufman JJ, Ottman R, Tao G, Shabahang S, Banaei E-H, Liang X, et al. In-fiber production of polymeric particles for biosensing and encapsulation. Proceedings of the National Academy of Sciences. 2013;110:15549-54.

[9] Lim D, Lee E, Kim H, Park S, Baek S, Yoon J. Multi stimuli-responsive hydrogel microfibers containing magnetite nanoparticles prepared using microcapillary devices. Soft Matter. 2015;11:1606-13.

[10] Tamayol A, Akbari M, Annabi N, Paul A, Khademhosseini A, Juncker D. Fiber-based tissue engineering: Progress, challenges, and opportunities. Biotechnology Advances. 2013;31:669-87.
[11] Akbari M, Tamayol A, Laforte V, Annabi N, Najafabadi AH, Khademhosseini A, et al. Composite Living Fibers for Creating Tissue Constructs Using Textile Techniques. Advanced Functional Materials. 2014;24:4060-7.

[12] Goodrich PJ, Sharifi F, Hashemi N. Rapid prototyping of microchannels with surface patterns for fabrication of polymer fibers. RSC Advances. 2015;5:71203-9.

[13] Sharifi F, Kurteshi D, Hashemi N. Microfluidic Fabrication of Highly Structured Polycaprolactone (PCL) Fibers. 2015.

[14] Kang E, Jeong GS, Choi YY, Lee KH, Khademhosseini A, Lee SH. Digitally tunable physicochemical coding of material composition and topography in continuous microfibres. Nature Materials. 2011;10:877-83.

[15] Daniele MA, North SH, Naciri J, Howell PB, Foulger SH, Ligler FS, et al. Rapid and Continuous Hydrodynamically Controlled Fabrication of Biohybrid Microfibers. Advanced Functional Materials. 2013;23:698-704.

[16] Bai ZH, Reyes JMM, Montazami R, Hashemi N. On-chip development of hydrogel microfibers from round to square/ribbon shape. Journal of Materials Chemistry A. 2014;2:4878-84.

[17] Boyd DA, Shields AR, Howell PB, Ligler FS. Design and fabrication of uniquely shaped thiol-ene microfibers using a two-stage hydrodynamic focusing design. Lab on a Chip. 2013;13:3105-10.

[18] Hu M, Deng R, Schumacher KM, Kurisawa M, Ye H, Purnamawati K, et al. Hydrodynamic spinning of hydrogel fibers. Biomaterials. 2010;31:863-9.

[19] Utech S, Prodanovic R, Mao AS, Ostafe R, Mooney DJ, Weitz DA. Microfluidic Generation of Monodisperse, Structurally Homogeneous Alginate Microgels for Cell Encapsulation and 3D Cell Culture. Advanced Healthcare Materials. 2015;4:1628-33.

[20] Caplin JD, Granados NG, James MR, Montazami R, Hashemi N. Microfluidic Organ-on-a-Chip Technology for Advancement of Drug Development and Toxicology. Advanced Healthcare Materials. 2015;4:1426-50.

[21] Mazutis L, Vasiliauskas R, Weitz DA. Microfluidic Production of Alginate Hydrogel Particles for Antibody Encapsulation and Release. Macromolecular Bioscience. 2015:n/a-n/a.

[22] Shields AR, Spillmann CM, Naciri J, Howell PB, Thangawng AL, Ligler FS. Hydrodynamically directed multiscale assembly of shaped polymer fibers. Soft Matter. 2012;8:6656-60.

[23] Acar H, Çınar S, Thunga M, Kessler MR, Hashemi N, Montazami R. Study of Physically Transient Insulating Materials as a Potential Platform for Transient Electronics and Bioelectronics. Advanced Functional Materials. 2014;24:4135-43.

[24] Jamshidi R, Çinar S, Chen Y, Hashemi N, Montazami R. Transient bioelectronics: Electronic properties of silver microparticle-based circuits on polymeric substrates subjected to mechanical load. Journal of Polymer Science Part B: Polymer Physics. 2015;53:1603-10.

[25] Mano F, Aroso IM, Barreiros S, Borges JP, Reis RL, Duarte ARC, et al. Production of Poly(vinyl alcohol) (PVA) Fibers with Encapsulated Natural Deep Eutectic Solvent (NADES) Using Electrospinning. ACS Sustainable Chemistry & Engineering. 2015;3:2504-9.

[26] Merkle VM, Tran PL, Hutchinson M, Ammann KR, DeCook K, Wu X, et al. Core–shell PVA/gelatin electrospun nanofibers promote human umbilical vein endothelial cell and smooth muscle cell proliferation and migration. Acta Biomaterialia.

[27] Sousa AMM, Souza HKS, Uknalis J, Liu S-C, Gonçalves MP, Liu L. Electrospinning of agar/PVA aqueous solutions and its relation with rheological properties. Carbohydrate Polymers. 2015;115:348-55.

[28] Boyd DA, Shields AR, Naciri J, Ligler FS. Hydrodynamic Shaping, Polymerization, and Subsequent Modification of Thiol Click Fibers. ACS Applied Materials & Interfaces. 2013;5:114-9.

[29] Sharifi F, Patel BB, Dzuilko AK, Sakaguchi DS, Montazami R, Hashemi N. Microfluidic Spun Poly (ε-caprolactone) (PCL) Microfibrous Scaffolds to Navigate Neural Stem Cells for Regenerative Biomedical Applications. 2015.

[30] Kang E, Choi YY, Chae S-K, Moon J-H, Chang J-Y, Lee S-H. Microfluidic Spinning of Flat Alginate Fibers with Grooves for Cell-Aligning Scaffolds. Advanced Materials. 2012;24:4271-7.

[31] Hwang CM, Khademhosseini A, Park Y, Sun K, Lee S-H. Microfluidic Chip-Based Fabrication of PLGA Microfiber Scaffolds for Tissue Engineering. Langmuir. 2008;24:6845-51.

[32] Reddy N, Yang Y. Microfluidic Spinning of Alginate Fibers. Innovative Biofibers from Renewable Resources: Springer Berlin Heidelberg; 2015. p. 151-4.

[33] Jeong W, Kim J, Kim S, Lee S, Mensing G, Beebe DJ. Hydrodynamic microfabrication via "on the fly" photopolymerization of microscale fibers and tubes. Lab on a Chip. 2004;4:576-80.

[34] Hashemi N, Howell JPB, Erickson JS, Golden JP, Ligler FS. Dynamic reversibility of hydrodynamic focusing for recycling sheath fluid. Lab on a Chip. 2010;10:1952-9.

[35] Howell Jr PB, Golden JP, Hilliard LR, Erickson JS, Mott DR, Ligler FS. Two simple and rugged designs for creating microfluidic sheath flow. Lab on a Chip. 2008;8:1097-103.

[36] Yao S, Li Y, Zhou Z, Yan H. Graphene oxide-assisted preparation of poly(vinyl alcohol)/carbon nanotube/reduced graphene oxide nanofibers with high carbon content by electrospinning technology. RSC Advances. 2015;5:91878-87.

[37] Ghobadi S, Sadighikia S, Papila M, Cebeci FC, Gursel SA. Graphene-reinforced poly(vinyl alcohol) electrospun fibers as building blocks for high performance nanocomposites. RSC Advances. 2015;5:85009-18.

[38] Yang D, Li Y, Nie J. Preparation of gelatin/PVA nanofibers and their potential application in controlled release of drugs. Carbohydrate Polymers. 2007;69:538-43.

[39] Jeong JS, Moon JS, Jeon SY, Park JH, Alegaonkar PS, Yoo JB. Mechanical properties of electrospun PVA/MWNTs composite nanofibers. Thin Solid Films. 2007;515:5136-41.

[40] Xu Y, Hong W, Bai H, Li C, Shi G. Strong and ductile poly(vinyl alcohol)/graphene oxide composite films with a layered structure. Carbon. 2009;47:3538-43.

[41] Sonker AK, Wagner HD, Bajpai R, Tenne R, Sui X. Effects of tungsten disulphide nanotubes and glutaric acid on the thermal and mechanical properties of polyvinyl alcohol. Composites Science and Technology. 2016;127:47-53.

[42] Ma H-L, Zhang L, Zhang Y, Wang S, Sun C, Yu H, et al. Radiation preparation of graphene/carbon nanotubes hybrid fillers for mechanical reinforcement of poly(vinyl alcohol) films. Radiation Physics and Chemistry. 2016;118:21-6.

[43] Liu H, Bandyopadhyay P, Kim NH, Moon B, Lee JH. Surface modified graphene oxide/poly(vinyl alcohol) composite for enhanced hydrogen gas barrier film. Polymer Testing. 2016;50:49-56.

[44] Yang X, Li L, Shang S, Tao X-m. Synthesis and characterization of layer-aligned poly(vinyl alcohol)/graphene nanocomposites. Polymer. 2010;51:3431-5.

[45] Liu L, Barber AH, Nuriel S, Wagner HD. Mechanical Properties of Functionalized Single-Walled Carbon-Nanotube/Poly(vinyl alcohol) Nanocomposites. Advanced Functional Materials. 2005;15:975-80.

[46] Shen B, Zhai W, Lu D, Wang J, Zheng W. Ultrasonication-assisted direct functionalization of graphene with macromolecules. RSC Advances. 2012;2:4713-9.

[47] May P, Khan U, O'Neill A, Coleman JN. Approaching the theoretical limit for reinforcing polymers with graphene. Journal of Materials Chemistry. 2012;22:1278-82.

CHAPTER 3

DESIGNING HIGHLY STRUCTURED POLYCAPROLACTONE FIBERS USING MICROFLUIDICS [1]

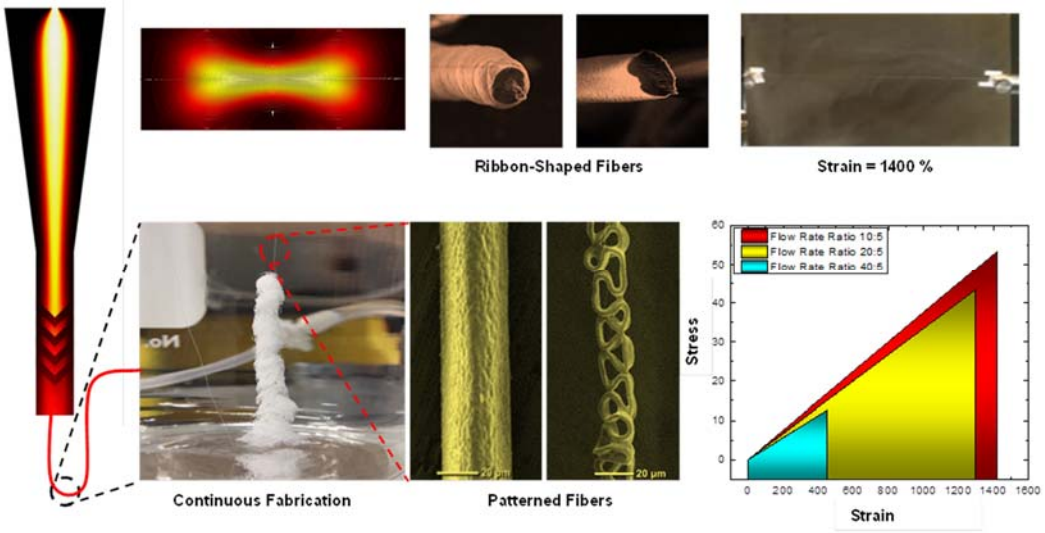

ABSTRACT

Microfibers are becoming increasingly important for biomedical applications such as regenerative medicine and tissue engineering. We have used a microfluidic approach to create polycaprolactone (PCL) microfibers in a controlled manner. Through the variations of the sheath fluid flow rate and PCL concentration in the core solution, the morphology of the microfibers and their cross-sections can be tuned. The microfibers were made using PCL concentrations of 2%, 5%, and 8% in the core fluid with a wide range of sheath-to-core flow rate ratios from 120:5 µL/min to 10:5 µL/min, respectively. The results revealed that the mechanical properties of the PCL microfibers made using microfluidic approach were significantly improved compared to the PCL microfibers made by other fiber fabrication methods. Additionally, it was demonstrated

[1] **F. Sharifi**, D. Kurteshi, and N. Hashemi, "Designing Highly Structured Polycaprolactone Fibers using Microfluidics", *Journal of the Mechanical Behavior of Biomedical Materials*, 61, 530-540 (2016).

that by decreasing the flow rate ratio and increasing the PCL concentration, the size of the microfiber could be increased. Varying the sheath-to-core flow rate ratios from 40:5 to 10:5, the tensile stress at break, the tensile strain at break, and the Young′s modulus were enhanced from 24.51 MPa to 77.07 MPa, 567% to 1420%, and 247.25 MPa to 539.70 MPa, respectively. The porosity and roughness of microfiber decreased when the PCL concentration increased from 2% to 8%, whereas changing the flow rate ratio did not have considerable impact on the microfiber roughness.

3.1 Introduction

Fiber systems are becoming increasingly important for numerous biological applications, such as tissue engineering, as the fibers are able to guide cell growth, alignment, and migration [1, 2]. Additionally, the design of microfibers gives them the correct properties in order to perform drug delivery and drug release in the human body for medical purposes [3, 4]. The fibers have high surface area-to-volume and strength-to-weight ratios. Some of them are permeable and can be woven into textiles [5]. These properties allow microfibers to carry even delicate materials, such as water-soluble drugs, throughout a biological medium with good accuracy [6, 7]. This makes for safe insertion and transmittance of material used for treatment, demonstrating the effectiveness of microfibers in medicine. The method of generation of the microfibers plays a role in determining its viability in these types of applications.

Several approaches exist for the fabrication of microfibers from naturally derived or synthetic materials such as electrospinning, wetspinning, biospining, meltspinning, and the microfluidic techniques [8]. Electrospinning is relatively a simple method and it is feasible to efficiently scale-up and control the involved parameters such as flow rate and voltage. However,

there are some difficulties in the fabrication of thick, complex 3D scaffolds with this method [2, 9]. Additionally, electrospun microfibers are generally not easy to align and it requires extra care to ensure that the fibers are accurately aligned, especially because the randomly aligned fibers are not desirable for applications like growing nerve cells [10]. Wetspinning is an efficient method for fabricating fibers with a wide range of diameters by changing the needle(s) diameter. Nevertheless, long exposure to chemicals during the fabrication process is required, which can be harmful to cells [11]. Biospinning method is the process of fabricating silk fibers by insects. Silk has high tensile strength and is biodegradable. In addition, after chemical processing, it is non-cytotoxic and non-inflammatory. The major challenges of using biospun fibers are the limitation of resources, which makes it difficult for the scale-up process, as well as the fact that the process of silk fiber fabrication is time consuming [12]. In the meltspinning approach, various synthetic polymers can be used for fiber fabrication with this method. Fibers created by meltspinning have high mechanical properties. However, the meltspinning process is in a high temperature range (150–300 °C) and requires using expensive equipment. Using high temperatures during the fiber fabrication process prevents the cell or protein from being loaded onto the fiber in order to deliver the bioactive molecules in biomedical applications [13]. Additionally, because the viscosity of the melted polymer is relatively high, a high pressure difference is needed to move the melted polymer through the spinneret [14, 15].

Using microfluidics to fabricate fiber is a relatively new approach in which the fiber is created in a microchannel using coaxial flow of core (pre-polymer) and sheath fluids. The key benefits of using this method include versatility of size, continuity of the fiber fabrication process, and simplicity of cell, protein or drug incorporation. This process is straightforward, cost-efficient, reproducible, and suitable for many biological applications since the fiber is created without using

high temperature, high pressure, high voltages, or toxic materials. By changing the flow rate and flow rate ratio, the fiber size and aspect ratio can be simply controlled [2, 16-18]. The microfluidic fiber fabrication can be employed to create fibers with various materials using different cross-linking mechanisms such as photopolymerization (e.g., polyethyleneglycol diacrylate, 4-hydroxybutyl acrylate) [19-22], ionic gelation (e.g., alginate) [23], and thermal phase transition (e.g., agar) [24, 25]. However, there are some studies which employ phase inversion process instead of cross linking method to solidify the polymer [2, 17]. used the solution of poly(lactic-co-glycolic acid) (PLGA) in dimethyl sulfoxide (DMSO) and mixture of glycerin and distilled water as the core and sheath fluids, respectively [2]. At the fluid–fluid interface in the channel, the DMSO in the core fluid is replaced by water in the sheath fluid and the polymer is solidified. Likewise, Bai *et al.* dissolved gelatin in DMSO and showed that by exchanging the DMSO in the core fluid and ethanol in the sheath fluid, the gelatin can be solidified [17].

This approach makes it feasible to fabricate fibers with different shapes of solid [16, 17, 26], tubular [27, 28], hybrid [10], and flat [29, 30] dimensions for divergent applications such as cell encapsulation, alignment, and immobilization. There are different physical and chemical methods for solidification of fibers including diffusion-limited solidification by solvent extraction, diffusion-limited solidification by chemical cross-linking, and photo polymerization [31]. The fibers fabricated by photopolymerization are not easily degraded and metabolized in biomedical applications. In addition, ultraviolet radiation (UV) has damaging effects on bioactive species [32]. It was demonstrated by Hwang *et al.* that the concentration of photo-initiator has adverse impacts on the cell viability [33]. The negative aspects of UV-light can be minimized by decreasing the exposure time and using less-harmful wavelengths than the standard one [34]. Due to these

limitations, photopolymerization is not the most desired approach for fabrication of fibers in cell encapsulation applications.

Although some thermoplastic polymers have been used in microfluidic fiber fabrication such as PLGA [2] and poly(methyl methacrylate) (PMMA) [35], there is no report on microfluidic fabrication of PCL fibers. PCL is a Food and Drug Administration (FDA) approved polymer which is widely used as a biomaterial due to its biocompatibility and biodegradability [36-38]. Due to slower degradation rate of this polymer, for instance compared to PLGA, it possesses no adverse impacts on cell viability and migration because it does not change the PH of the environment during the degradation sharply [39]. This polymer also has good mechanical properties, is not toxic, and its rate of degradation can be controlled. Furthermore, PCL does not trigger immune responses in the body [40].

In this paper, we have employed solvent extraction to fabricate biocompatible and biodegradable PCL microfibers in a microfluidic platform for the first time. PCL grants us the advantage of having a biocompatible and strong material from which to make fibers. Using microfluidics, we are able to avoid the constraints of other methods such as electrospinning [2]. We can produce fibers with different cross-sectional shapes while the fabrication is continuous and stops only when the core and sheath solutions stop flowing. By fabricating PCL using a microfluidic microchannel, we are benefitting from combining the properties of a proven biocompatible material and the unique properties of a microfluidic fabrication technique to create fibers for many biomedical applications such as tissue engineering and drug delivery. After solidification of PCL fibers, they exit the channel directly into a water bath where the sheath fluid is washed off. The fibers are then collected and characterized to understand their physical and

mechanical properties. We have also performed simulations using COMSOL multiphysics to compare with the experimental results.

3.2 Materials

Polycaprolactone (M_n=80,000) and polyethylene glycol (PEG) (M_n=20,000) were obtained from Sigma Aldrich (St. Louis, MO). The solvent for the core solution is 2,2,2-trifluoroethanol (TFE), which was purchased from Oakwood Chemical (West Columbia, SC). The material used for the microfluidic channel is polydimethylsiloxane (PDMS). The core solution was prepared by pouring PCL into the TFE at different concentrations by volume (2%, 5%, and 8% PCL). The sheath fluid was made using a PEG concentration of 5% into a mixture of water and ethanol with a volume ratio of 1:1. The solutions were prepared at room temperature. The syringes used to pump the fluids were obtained from BD Medical (Franklin Lakes, New Jersey). The syringe pumps used to introduce fluids to the microchannel were purchased from Cole Parmer (Vernon Hills, Illinois).

3.3 Microfluidic Approach

Using a dual-drive syringe pump, the core and sheath fluids are simultaneously introduced into the microchannel. The core fluid enters the channel through the central opening and the sheath flow enters on each of the sides. Additionally, our microchannel contains three inlets, one in the middle for introducing the core flow and two on the sides for running sheath flows (**Figure 3.1**).

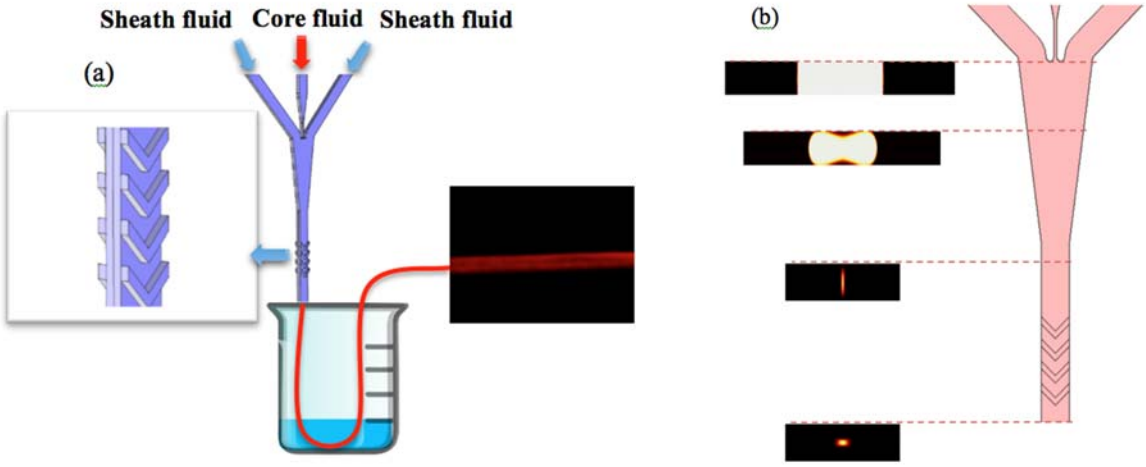

Figure 3.1 *(a) A schematic of microfluidic fiber fabrication method. (b) Concentration pattern of the core fluid at different sections of the channel; the flow rate ratio of 80:5 µL/min for the sheath and core fluids, respectively.*

The shear force between the core and sheath fluids focuses the core fluid in the center of the microchannel hydrodynamically [41-44] and fibers are formed from the core fluid employing solvent extraction solidification approach. The microfluidic method enables the fabrication of fibers with different sizes and cross sections. The dimensions of the fiber depend on the core and sheath flow rates [45]. Additionally, the shear force aligns the polymer chains along the flow direction in the final microfiber product. Therefore, we can control the microstructures of the fibers and their bulk mechanical properties. Here, the phase inversion process causes the TFE in the core fluid to be replaced by the sheath fluid. Because PCL does not dissolve in the sheath fluid, it becomes solidified as a microfiber further downstream the channel.

Figure 3.1 (a) illustrates a schematic of microfluidic fiber fabrication. The pattern of the core fluid at different sections of the channel is illustrated by **Figure 3.1** (b). In fact, the sheath fluid has a lateral hydrodynamic force on the core fluid in the nozzle area. After that, the cross section of the channel remains constant until two fluids meet the chevrons of the channel. In this

region, the hydrodynamic resistance in the direction parallel to the peaks and valleys is less than the direction of the channel. Consequently, the component of velocity which is perpendicular to the channel increases for both of the fluids. The hydrodynamic resistance is inversely proportional to the flow rate. Therefore, the sheath fluid will experience less resistance compared to the core fluid since the flow rate of the sheath fluid is considerably higher than the core fluid. Sheath fluid wraps around the core fluid and exerts vertical hydrodynamic force towards the center of the channel in the chevrons region. After passing through these chevrons, the core fluid will be focused at the center of the channel and there will not be any contact between the core fluid and the channel walls. Apart from exerting hydrodynamic force, the sheath fluid plays the role of a lubricant in the channel to facilitate fiber extrusion. Therefore, the viscosity of the sheath fluid should be matched to that of the core fluid. For this purpose, polyethylene glycol (PEG) is added to the sheath fluid in order to increase its viscosity. **Figure 3.2** shows the viscosity of core and sheath fluids at different concentrations of PCL and PEG (2–8%), respectively. While the range of viscosity varies from 19 cP to 500 cP for the core fluid, it is limited to 2–16 cP for the sheath fluid. In this study, we used 5% PEG in the sheath fluid and changed the concentration of the PCL in the core fluid from 2% to 8% in order to show the versatility of microfluidic approach in fabricating fiber using a wide range of core fluid viscosity.

While the core flow rate is kept constant at 5 μL/min, the sheath flow rate varies from 10 μL/min to 120 μL/min. Our microchannel contains three inlets, one in the middle for introducing the core flow and two on the sides for running sheath flows. The channel has four chevron grooves that create vertical hydrodynamic force. The magnitude of the hydrodynamic force is directly related to the flow rate ratio (velocity gradient between sheath and core fluid), which is an important parameter in determining the features of the fiber.

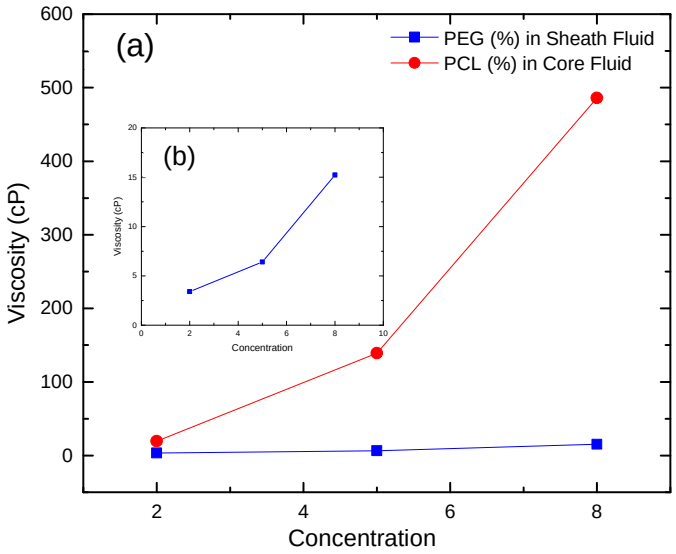

Figure 3.2 *Viscosity of (a) the core and sheath solutions using different concentrations of PCL and PEG, respectively; (b) enlarged view of sheath solution viscosity made by three different concentrations of PEG.*

Downstream from the microchannel entrance, the fluid comes into contact with the chevron grooves, which are engrained on the top and bottom surfaces of the channel. The grooves play an important role in focusing the core fluid vertically and determining the final cross-sectional shape of the fibers. The shear stress aligns the polymer chains in the core flow in the direction of the flows. The solidification of core flow occurs once it comes to contact with the sheath flows. During the whole process, the channel is positioned vertically and the resulting fibers exit directly into a water bath.

After the fibers were recovered, their characteristics were evaluated through several means. A scanning electron microscope (SEM) from Nikon (Tokyo, Japan) was used to determine the morphology of the fibers. The SEM was used to study the effects of changing the flow rate ratio of sheath and core fluids as well as the PCL concentration in the core solution on the morphology and cross section of the fabricated microfibers. In addition, the mechanical properties of the fibers

were measured to assess their strength. Finally, the microfluidic fiber fabrication was simulated using COMSOL multiphysics software in order to compare the experimental and numerical results.

3.4 Characterization

The morphology and cross section of the microfibers were studied using the field emission scanning electron microscopy (FE-SEM) (JSM-6700F at an acceleration voltage of 5 kV). The viscosities of the core and sheath solutions were measured using a digital viscometer (DV-E, Brookfield Engineering Laboratories, Inc., Middleboro, MA). For measuring the stress–strain behavior of the fibers, single fiber was tested using Instron Universal Testing machine (Model 5569, Instron Engineering Corp., Canton, MA). For each type of the fibers, 10 samples were tested and the average values for each type were reported. Since the PCL fibers have high ductility, we used a 10 N load cell to get enough resolution, and the extension rate was set to 20 mm/min. In this test, the samples were prepared by attaching them on a paper frame in order to be gripped properly by the Instron machine. After mounting the sample on the machine, we cut two sides of the frame to get the mechanical properties of PCL fiber. The length of the samples for this test was 15 mm. The results were found using Bluehill software. A video file is provided in supplementary materials, that shows high ductility of the fiber during the tensile test. The stress–strain curves were fitted with linear line for the elastic region. Second order polynomial equation was used for the plastic region because its coefficient of determination (R-Square) was better compared to the linear line for all of the data.

3.5 Results and Discussion

We fabricated microfibers using 2%, 5%, and 8% PCL and 5% PEG in TFE and water/ethanol (with the volume ratio of 1:1), respectively. Varying the sheath and core flow rates, it was found that the core flow rate of 5 μL/min and the sheath flow rate of 10–120 μL/min are appropriate flow rates in order to obtain continuous microfiber.

The versatility of the microfluidic fiber fabrication method can be highlighted by using various flow rates of sheath fluid and PCL concentrations in the core fluid. The results revealed that the flow rate ratio of the core and sheath fluids plays a significant role in the morphology of the fabricated fibers. Using a very low sheath flow rate does not allow for enough of both the vertical and horizontal hydrodynamic forces on the core fluid. As a result, the width of the core fluid increases. Also, the aggregation of the polymer becomes stronger than its elongation along the channel. This condition leads to occurrence of clogging in the microchannel. On the other hand, if the core fluid has a high flow rate, there is a possibility that the core fluid exit the channel and no solidification happens. **Figure 3.3** shows the SEM images of the representative microfibers obtained using different flow rate ratios. The concentrations of PCL and PEG were kept at a constant value of 5% in the core and sheath fluids, respectively.

This figure illustrates that the roughness of the surface is not significantly affected by changing the flow rate ratio between the fluids. However, at the higher flow rates of sheath fluid, the microfibers have wavy structures, and as the sheath flow rate decreases, the microfibers tend to be more uniform and straight. This means that the Kelvin–Helmholtz instability occurs at high flow rate ratios due to sharp difference of velocities at the core fluid/sheath fluid interface in the channel, and it leads to the creation of wavy shaped microfibers. Additionally, this figure demonstrates that the size of the microfibers increases when the sheath flow rate reduces.

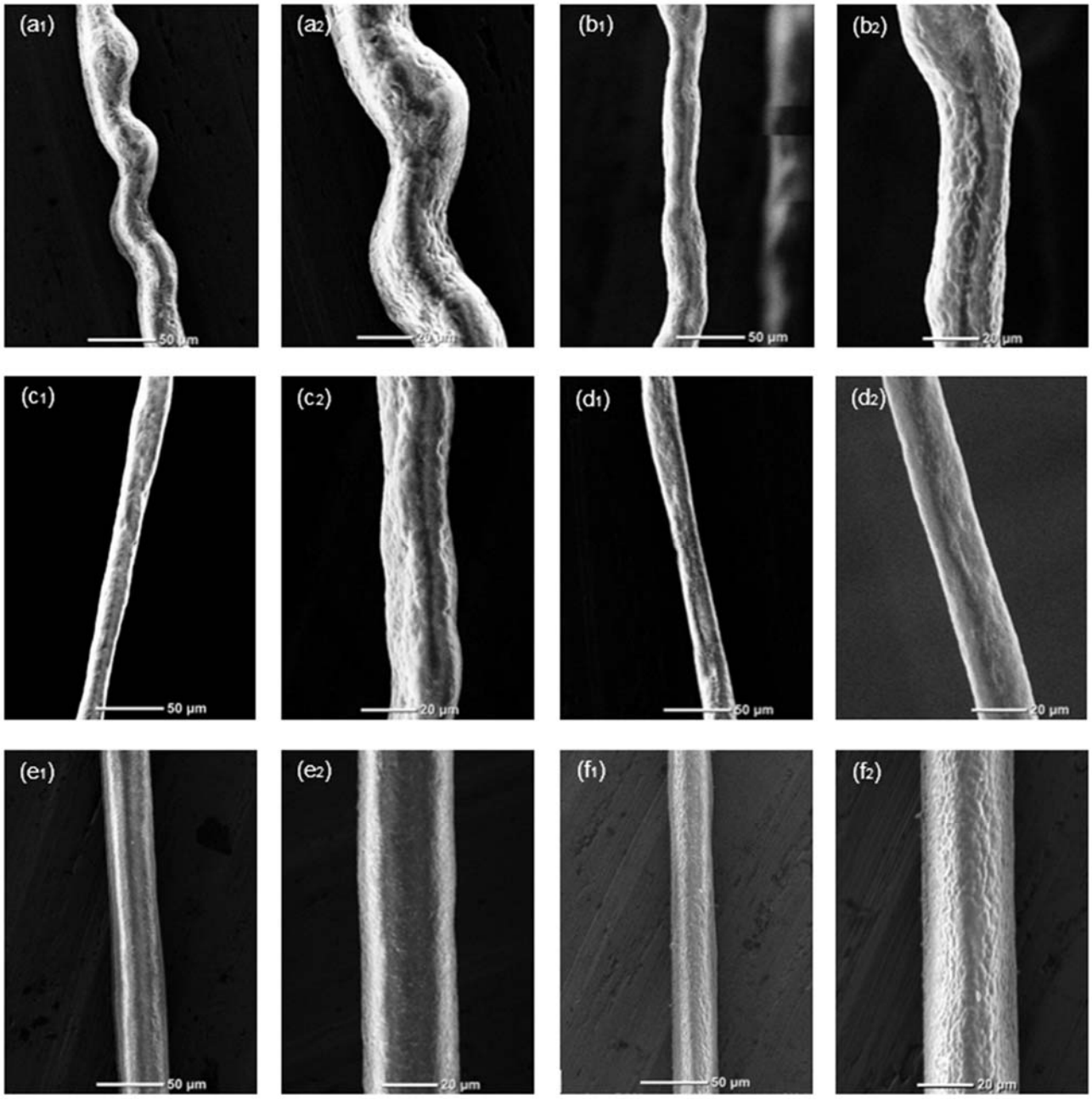

Figure 3.3 *SEM images of PCL microfibers with 5% PCL in TFE (core fluid) and 5% PEG in water and ethanol (sheath fluid) and different flow rates of (a) 120: 5 (b) 100: 5 (c) 80: 5 (d) 60: 5 (e) 20: 5, and (f) 10: 5 µL/min for the sheath and core fluids, respectively.*

This is expected, because when the difference of the velocities decreases, the hydrodynamic shear force exerted from the sheath fluid on the core fluid weakens. Consequently,

the core fluid expands in the channel and the average diameter of the fiber increases. In **Figure 3.4** (a-c), the cross-sectional SEM images of the microfibers fabricated with different flow rate ratios are provided. This figure shows that the cross-section of the fibers made by microfluidic approach can be tuned by simply changing the flow rate ratio between the sheath and core fluids. Additionally, the dimensions of the fibers (average±standard error) are shown in **Figure 3.4** (d).

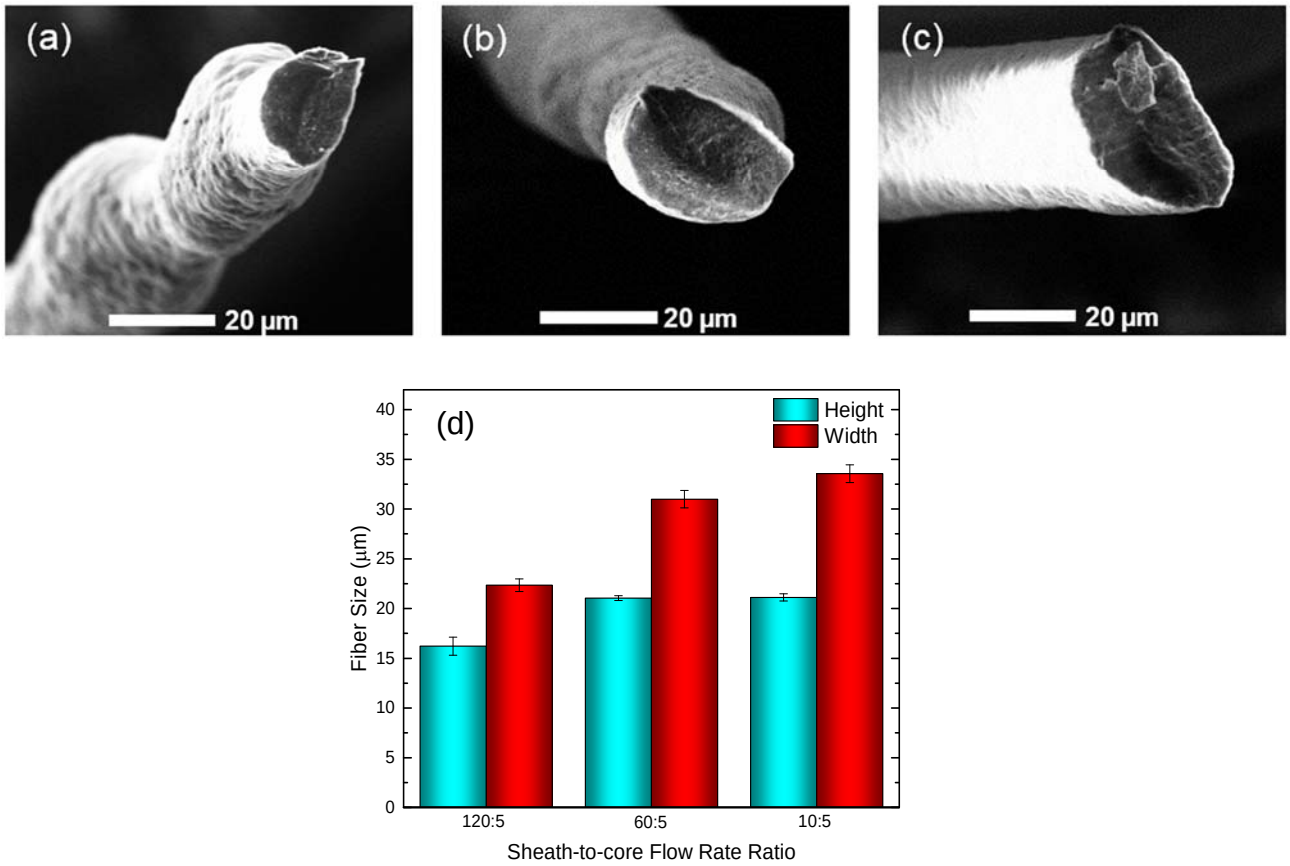

Figure 3.4 *Cross sectional SEM images of PCL microfibers with 5% PCL in TFE (core fluid) and 5% PEG in water and ethanol (sheath fluid) fabricated by sheath and core flow rates of (a) 120:5, (b) 60:5, and (c) 10:5 µL/min, respectively. (d) Dimensions of the PCL fibers fabricated using different sheath-to-core flow rate ratios.*

The width and height of the PCL fiber at the sheath-to-core flow rate ratio of 120:5 are 16.21 µm and 22.34 µm, respectively. The decrease of the flow rate ratio to 10:5 increases both the width and height of the fiber to 21.12 µm and 33.56 µm, respectively. Moreover, the aspect ratio of the fiber increases by a factor of 1.15 when the flow rate ratio reduces from 120:5 to 10:5. That was expected because when the flow rate ratio between two fluids diminishes, the lateral hydrodynamic force exerted to the core fluid by sheath fluid weakens. Consequently, the core fluid has more freedom to grow in the lateral direction. On the other hand, when the sheath flow rate increases, the shear force intensifies and the core fluid is stretched more due to the higher hydrodynamic force that leads to the fabrication of fibers with smaller size.

The microfluidic fiber fabrication was simulated using COMSOL multiphysics. The Navier–Stokes equation for incompressible flow at steady state was used to numerically solve the momentum balance. Because the inertial forces are negligible at low Reynolds number, the motion of the fluid can be approximately described by the reversible Stokes equation in which the nonlinear term can be neglected. We used Fick's law, $-\nabla.(-D.\nabla c) + u.\nabla c = 0$, In this equation, D is the diffusion coefficient and c represents the concentration. The Navier–Stokes equation was solved first and was then followed by the convection–diffusion relationships. Due to symmetry, one fourth of the channel was modeled. This figure illustrates that the velocity of two fluids increases by passing through the nozzle part of the channel. In the chevrons area, the component of velocity which is perpendicular to the channel, increases by passing the fluid through the chevrons.

Figure 3.5 (a) shows the concentration distribution along the channel. The bright and dark colors represent the situations of core and sheath fluids, respectively along the channel. Therefore, the effects of lateral and vertical hydrodynamic focusing forces of the sheath fluid on the core fluid

can be observed clearly by following the brighter color along the channel. Additionally, the bright color at the output of the microchannel represents the cross sectional pattern of the microfiber fabricated using a specific flow rate ratio. Based on **Figure 3.5** (a), the thickness of the core fluid reduces after the nozzle area, which reveals an increasing lateral force of the sheath fluid on the core fluid.

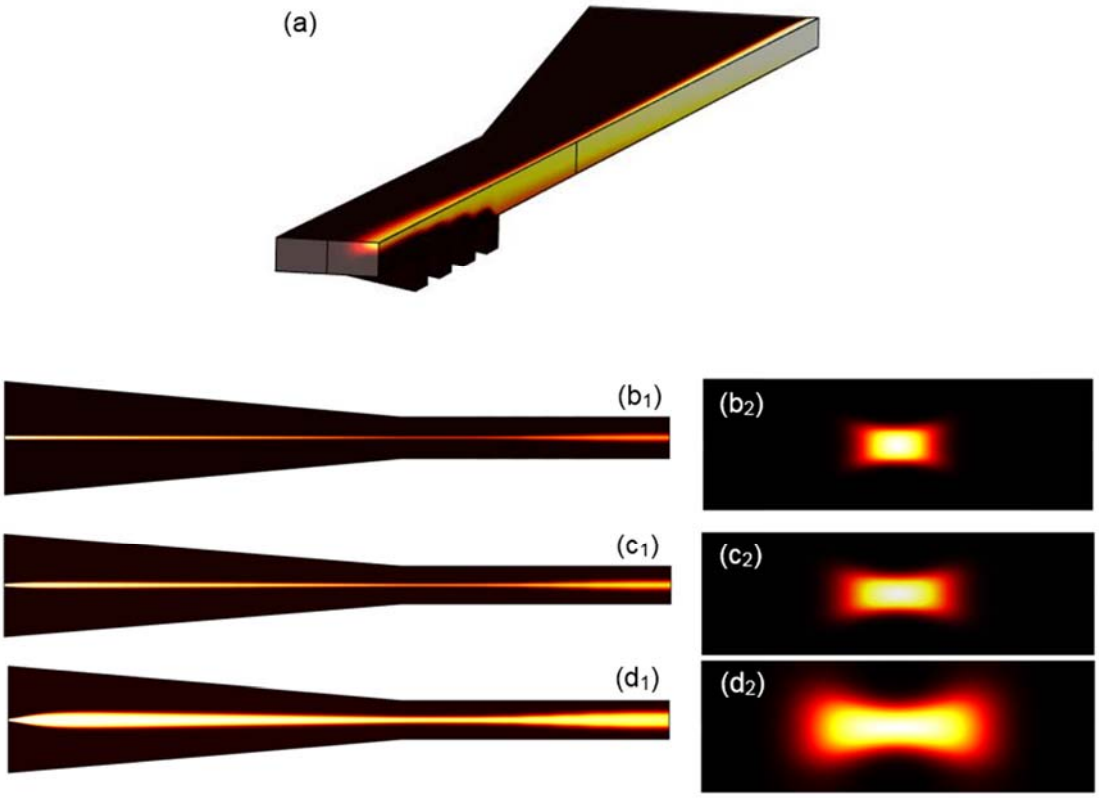

Figure 3.5 *(a) Three-dimensional concentration distribution of core fluid in sheath fluid along the channel; the flow rate ratio is 80:5 µL/min for the sheath and core fluids, respectively; Top view of the channel and the cross section of the fibers with sheath and core flow-rates of (b_1) and (b_2) 120:5, (c_1) and (c_2) 60:5, and (d_1) and (d_2) 10:5 µL/min, respectively.*

Downstream from the initial focusing region, the series of chevrons change the hydrodynamic resistance in the channel such that the resistance in the perpendicular direction

becomes smaller than the parallel one. **Figure 3.5** (a) displays that the vertical force in the chevrons region gradually focuses the core solution at the center of the channel. The concentration distribution of the core and sheath fluids are shown in **Figure 3.5** (b_1-d_1) for different values of sheath flow-rate and constant value of 5 µL/min for the core flow rate. This figure illustrates a weakening of the hydrodynamic lateral force of the sheath fluid on the core fluid due to decreasing the sheath flow-rate. Consequently, the width of the fabricated fiber becomes larger. The vertical hydrodynamic force, however, does not change significantly due to the fact that this force is originated from the number of the chevrons. Therefore, the combination of a decrease in lateral force and a constant value of the vertical force leads to the development of the ribbon-shape pattern. **Figure 3.5** (b_2-d_2) illustrates the trend in which the core cross section changes to a ribbon-shaped pattern. These results demonstrated consistency between the experimental and numerical results.

The concentration of the core fluid can be changed in microfluidic fiber fabrication as well as the flow rate and flow rate ratio between the sheath and core fluid in order to change the characteristics of microfibers. **Figure 3.6** illustrates the effects of different concentrations (2%, 5%, and 8%) of PCL in the core fluid on morphology of fibers. Increasing the PCL concentration results in fiber with smoother surface. Additionally, 2% PCL fibers show more porosity compared to the fibers made from higher PCL concentrations. When core fluid with low concentration of PCL is introduced into the channel, the total amount of PCL in core fluid is not enough to create a uniform fiber after solvent extraction and the resulting fibers become more porous. Moreover, the higher roughness and existence of porosity on the fiber at low concentrations of PCL is due to rapid exchange of TFE and sheath fluid compared to higher concentrations. While the uniform microfibers have higher mechanical properties, more porous microfibers can enhance cell adhesion

and cell proliferation, which are desirable in tissue engineering applications. Furthermore, tuning the porosity and microstructures of the fibers by changing the PCL concentration in the core fluid is another advantage of microfluidic approach.

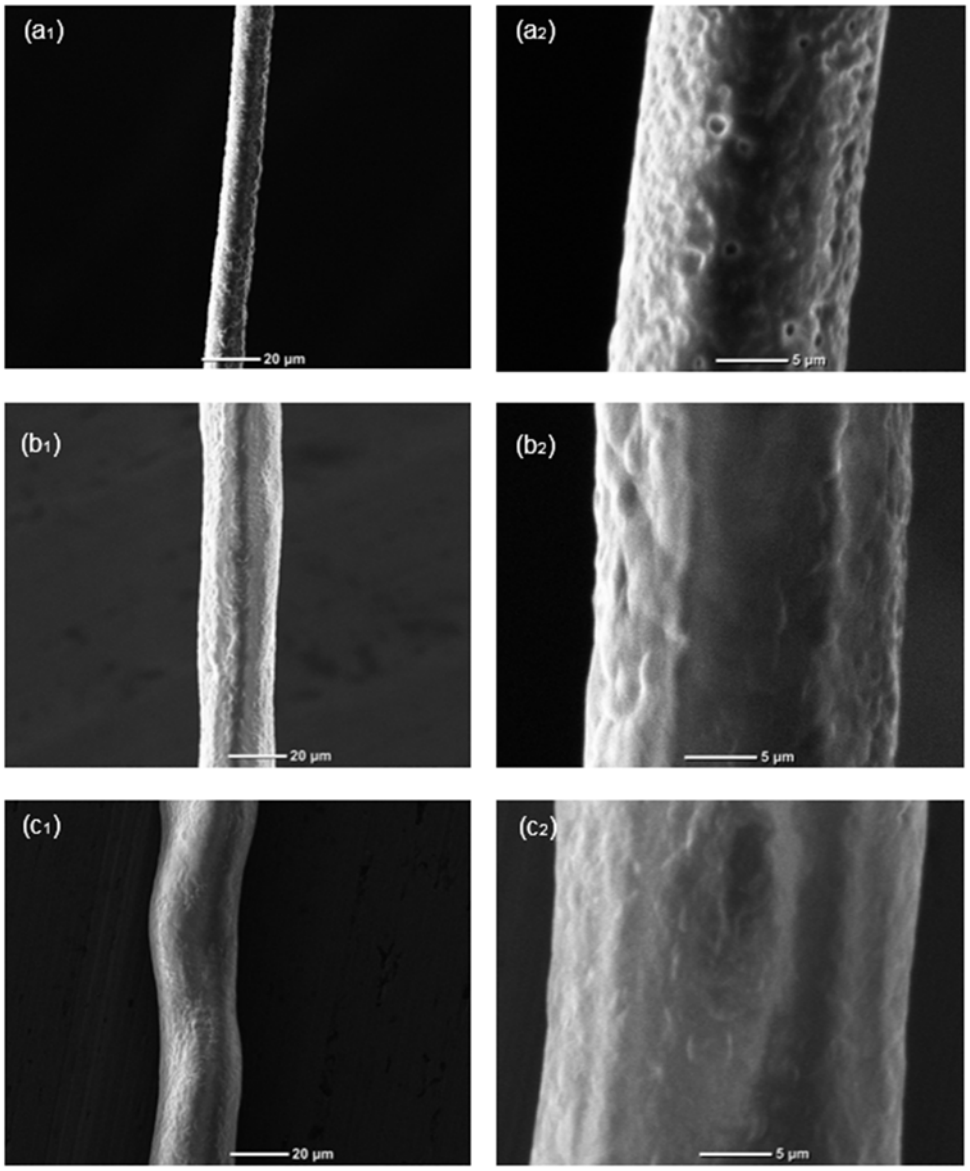

Figure 3.6 *SEM images of PCL microfibers with 5% PEG in the sheath fluid and the PCL concentrations of (a_1) and (a_2) 2%; (b_1) and (b_2) 5%; and (c_1) and (c_2) 8% in the core fluid. Sheath flow rate is 60 µL/min and core flow rate is 5 µL/min.*

The cross-sectional SEM images of PCL microfibers fabricated using different percentages of PCL in the core fluid are shown in **Figure 3.7** (a-c). This figure demonstrates that the PCL concentration can influence the size of the resulting fiber as well as the flow rate ratio between the two fluids. **Figure 3.7** (d) displays the dimensions of the fibers made by different PCL concentration in the core fluid.

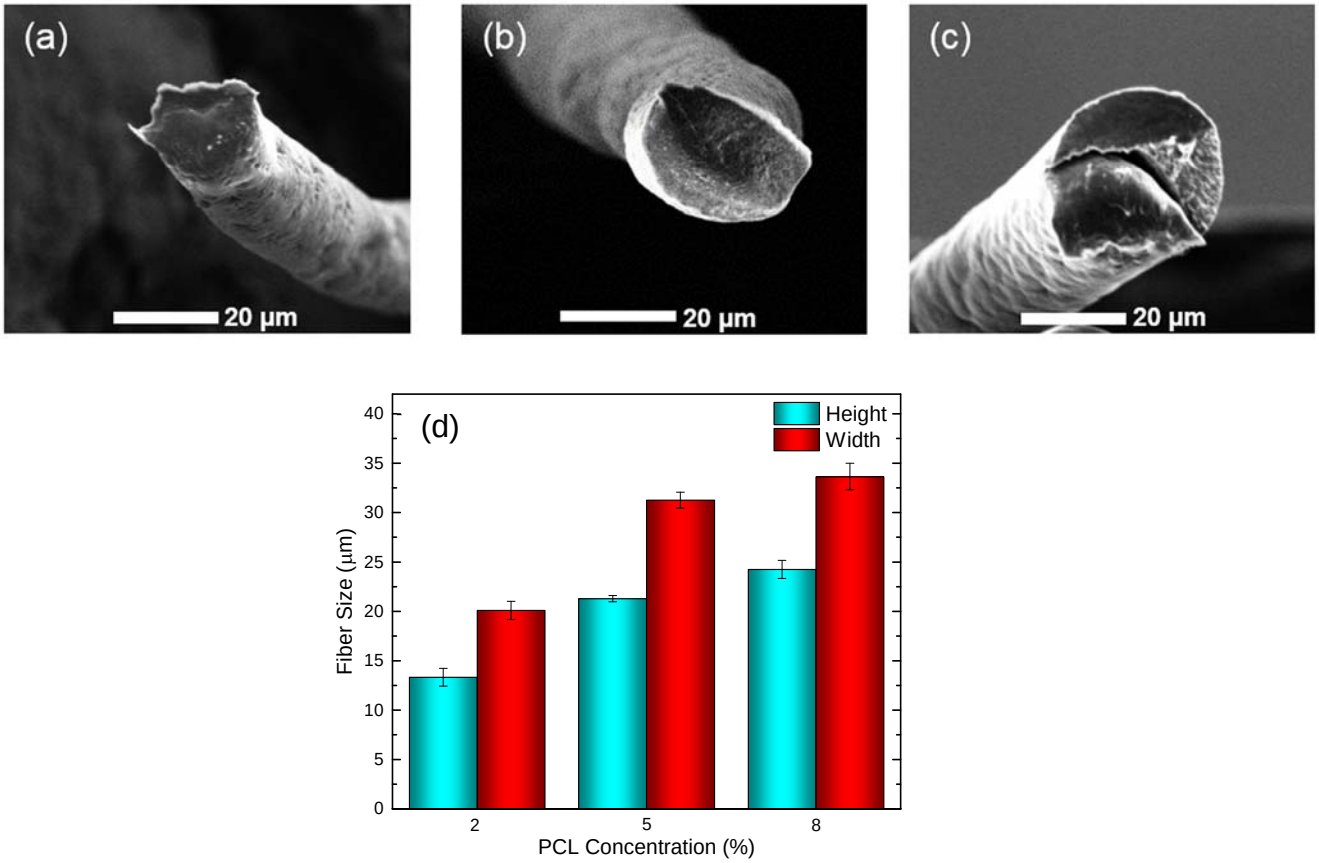

Figure 3.7 *Cross sectional SEM images of PCL microfibers with different concentrations of (a) 2%; (b) 5%; and (c) 8% PCL in the core fluid and 5% PEG in the sheath fluid with the flow rate of 60:5 µL/min for the sheath and core fluids, respectively. (d) Dimensions of the PCL fibers fabricated using different PCL concentrations in the core fluid.*

We observed that the dimension of the fiber (width×height) increases from 20.1 µm×13.3 µm to 33.65 µm×24.25 µm when the PCL concentration changes from 2% to 8%,

while the aspect ratio does not change significantly. That is because when lower amount of PCL in the core solution flows through the channel, the dimensions of PCL solidified as a fiber during the phase inversion process in the microchannel will be reduced.

The mechanical properties of the fibers made by different flow rate ratios were investigated. Stress–strain behavior of different fibers are shown in **Figure 3.8** (a). This figure demonstrates a wide range of mechanical properties that can be obtained using this microfluidic approach. As expected from a typical plastic material, the elastic region of the PCL stress–strain curve is in a small range, which is shown in **Figure 3.8** (b). The Young's Modulus of the fibers are shown in **Figure 3.8** (c). Additionally, yield strain (%), yield stress (MPa), Young′s modulus (MPa), strain at break (%), and stress at break (MPa) are listed in **Table 3.1** for different PCL microfibers.

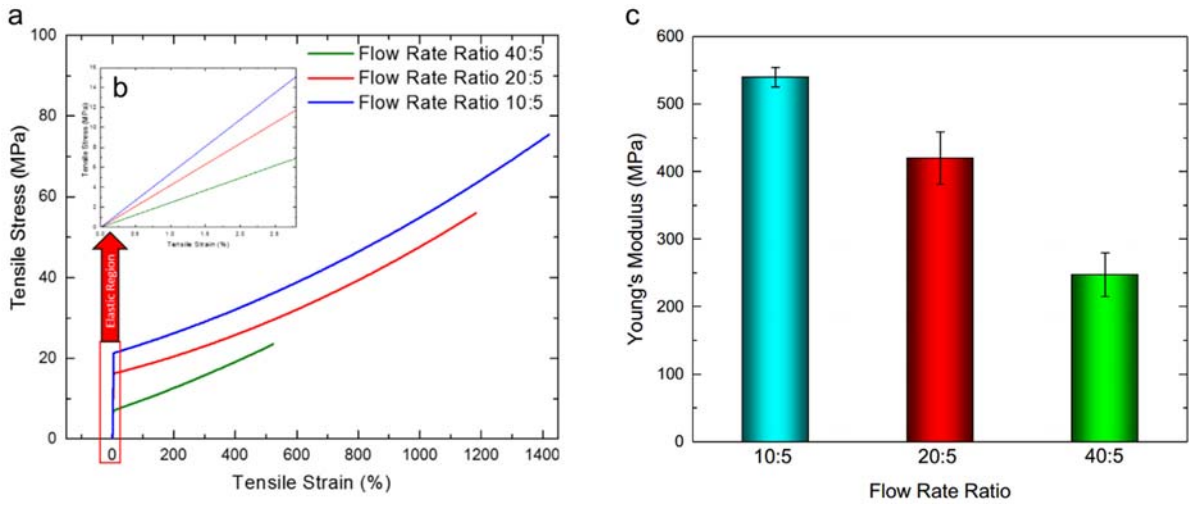

Figure 3.8 *(a) Tensile stress–strain behavior, (b) enlarged view of the elastic region of stress–strain curve, and (c) Young's modulus of PCL microfibers fabricated with different flow rate ratios with the PCL concentration of 5% in TFE.*

Table 3.1 *Mechanical properties of PCL fibers made by different sheath-to-core flow rate ratios.*

Flow rate ratio	Yield strain (%)	Yield stress (MPa)	Young's modulus (MPa)	Strain at break (%)	Stress at break (MPa)
40:5	2.70±0.65	6.02±1.02	247.25±32.08	567±61.24	24.51±3.11
20:5	3.78±0.24	15.78±1.50	420.03±38.89	1079.25±63.20	57.35±5.46
10:5	3.92±0.33	20.05±1.15	539.70±14.50	1420.4±79.47	77.07±5.64

The results show that the decrease of the flow rate ratio from 40:5 to 10:5, significantly improves the tensile stress at break, tensile strain at break, and the Young's modulus from 24.51 MPa to 77.07 MPa, 567% to 1420%, and 247.25 MPa to 539.70 MPa, respectively. The yield stress (MPa) and yield elongation (%) improve by a factor of 3.33 and 1.45 when the flow rate ratio decreases from 40:5 to 20:5.

Although the mechanical properties of electrospun PCL fibrous scaffold widely have been studied, there are few reports about the mechanical properties of PCL single fibers made by electrospinning method. It was found that the reported values of the tensile strain at break (%) for electrospun fibers are significantly lower than our results [46-49]. This could be due to the microstructure organization of the fibers as the shear stress plays a pivotal role in aligning the polymer chains in the direction of the flow and consequently creating highly structured fibers. However, the values of stress at break and Young's modulus obtained in this study are comparable with the ones reported for the electrospun PCL fibers. Also based on the SEM images of microfiber cross sections shown in **Figure 3.4**, decreasing the flow rate ratio leads to an increase in the size and aspect ratio of the fiber cross section such that the fiber cross section tends to have a ribbon shape. Consequently, this improvement in mechanical properties of microfibers can be due to the ribbon shape of the microfiber cross-section.

3.6 Conclusions

PCL microfibers with improved mechanical properties were fabricated using the microfluidic fiber fabrication. Employing microfluidic fiber fabrication approach, we created microfibers with the maximum strain of 1420%. We showed through SEM that the morphology and size of the fibers could be controlled by varying the PCL percentage in the core solution and the flow rate ratio of sheath to core fluids. While the smoothness of the fiber was improved by increasing the PCL concentration in the core solution from 2% to 8%, the flow rate ratio did not have a substantial influence on the roughness of the fiber. The aspect ratio of the fiber increases by diminishing the flow rate ratio because when the sheath flow rate decreases, the core fluid expands in the channel, which increases the width of the fiber. Numerical simulations were consistent with the experimental results. This development in size and cross section of the fiber enhanced the mechanical properties of the microfiber. These are the most improved properties compared to those of the previous reports about PCL fibers created using other fabrication methods. This improvement reveals unique capability of microfluidic platform to create fibers with a wide range of mechanical properties simply by changing the fabrication parameters such as flow rate ratio and viscosity.

REFERENCES

[1] Chung BG, Lee KH, Khademhosseini A, Lee SH. Microfluidic fabrication of microengineered hydrogels and their application in tissue engineering. Lab on a Chip. 2012;12:45-59.

[2] Hwang CM, Khademhosseini A, Park Y, Sun K, Lee S-H. Microfluidic Chip-Based Fabrication of PLGA Microfiber Scaffolds for Tissue Engineering. Langmuir. 2008;24:6845-51.

[3] Tiwari SK, Tzezana R, Zussman E, Venkatraman SS. Optimizing partition-controlled drug release from electrospun core-shell fibers. International Journal of Pharmaceutics. 2010;392:209-17.

[4] Caplin JD, Granados NG, James MR, Montazami R, Hashemi N. Microfluidic Organ-on-a-Chip Technology for Advancement of Drug Development and Toxicology. Advanced Healthcare Materials. 2015;4:1426-50.

[5] Boyd DA, Shields AR, Naciri J, Ligler FS. Hydrodynamic Shaping, Polymerization, and Subsequent Modification of Thiol Click Fibers. ACS Applied Materials & Interfaces. 2013;5:114-9.

[6] Kraitzer A, Ofek L, Schreiber R, Zilberman M. Long-term in vitro study of paclitaxel-eluting bioresorbable core/shell fiber structures. Journal of Controlled Release. 2008;126:139-48.

[7] Saraf A, Baggett LS, Raphael RM, Kasper FK, Mikos AG. Regulated non-viral gene delivery from coaxial electrospun fiber mesh scaffolds. Journal of Controlled Release. 2010;143:95-103.

[8] Tamayol A, Akbari M, Annabi N, Paul A, Khademhosseini A, Juncker D. Fiber-based tissue engineering: Progress, challenges, and opportunities. Biotechnol Adv. 2013;31:669-87.

[9] Deng M, James R, Laurencin CT, Kumbar SG. Nanostructured Polymeric Scaffolds for Orthopaedic Regenerative Engineering. IEEE Trans Nanobiosci. 2012;11:3-14.

[10] Jung J-H, Choi C-H, Chung S, Chung Y-M, Lee C-S. Microfluidic synthesis of a cell adhesive Janus polyurethane microfiber. Lab Chip. 2009;9:2596-602.

[11] Enea D, Henson F, Kew S, Wardale J, Getgood A, Brooks R, et al. Extruded collagen fibres for tissue engineering applications: effect of crosslinking method on mechanical and biological properties. Journal of Materials Science-Materials in Medicine. 2011;22:1569-78.

[12] Reddy N, Yang YQ. Structure and properties of cocoons and silk fibers produced by Hyalophora cecropia. Journal of Materials Science. 2010;45:4414-21.

[13] Ella V, Annala T, Lansman S, Nurminen M, Kellomaki M. Knitted polylactide 96/4 L/D structures and scaffolds for tissue engineering: shelf life, in vitro and in vivo studies. Biomatter. 2011;1:102-13.

[14] Akbari M, Sinton D, Bahrami M. Viscous flow in variable cross-section microchannels of arbitrary shapes. International Journal of Heat and Mass Transfer. 2011;54:3970-8.

[15] Yim EKF, Wan ACA, Le Visage C, Liao IC, Leong KW. Proliferation and differentiation of human mesenchymal stem cell encapsulated in polyelectrolyte complexation fibrous scaffold. Biomaterials. 2006;27:6111-22.

[16] Daniele MA, North SH, Naciri J, Howell PB, Foulger SH, Ligler FS, et al. Rapid and Continuous Hydrodynamically Controlled Fabrication of Biohybrid Microfibers. Advanced Functional Materials. 2013;23:698-704.

[17] Bai Z, Reyes JMM, Montazami R, Hashemi N. On-chip development of hydrogel microfibers from round to square/ribbon shape. Journal of Materials Chemistry A. 2014;2:4878-84.

[18] Goodrich PJ, Sharifi F, Hashemi N. Rapid prototyping of microchannels with surface patterns for fabrication of polymer fibers. RSC Advances. 2015;5:71203-9.

[19] Oh HJ, Kim SH, Baek JY, Seong GH, Lee SH. Hydrodynamic micro-encapsulation of aqueous fluids and cells via 'on the fly' photopolymerization. Journal of Micromechanics and Microengineering. 2006;16:285-91.

[20] Jeong W, Kim J, Kim S, Lee S, Mensing G, Beebe DJ. Hydrodynamic microfabrication via "on the fly" photopolymerization of microscale fibers and tubes. Lab on a Chip. 2004;4:576-80.

[21] Daniele MA, Radom K, Ligler FS, Adams AA. Microfluidic fabrication of multiaxial microvessels via hydrodynamic shaping. RSC Advances. 2014;4:23440-6.

[22] Daniele MA, Adams AA, Naciri J, North SH, Ligler FS. Interpenetrating networks based on gelatin methacrylamide and PEG formed using concurrent thiol click chemistries for hydrogel issue engineering scaffolds. Biomaterials. 2014;35:1845-56.

[23] Shin S, Park JY, Lee JY, Park H, Park YD, Lee KB, et al. "On the fly" continuous generation of alginate fibers using a microfluidic device. Langmuir. 2007;23:9104-8.

[24] Vunjak-Novakovic G, Altman G, Horan R, Kaplan DL. Tissue engineering of ligaments. Annual Review of Biomedical Engineering. 2004;6:131-56.

[25] Khademhosseini A, Langer R, Borenstein J, Vacanti JP. Microscale technologies for tissue engineering and biology. Proceedings of the National Academy of Sciences of the United States of America. 2006;103:2480-7.

[26] Hasani-Sadrabadi MM, VanDersarl JJ, Dashtimoghadam E, Bahlakeh G, Majedi FS, Mokarram N, et al. A microfluidic approach to synthesizing high-performance microfibers with tunable anhydrous proton conductivity. Lab on a Chip. 2013;13:4549-53.

[27] Kang E, Jeong GS, Choi YY, Lee KH, Khademhosseini A, Lee SH. Digitally tunable physicochemical coding of material composition and topography in continuous microfibres. Nature Materials. 2011;10:877-83.

[28] Choi CH, Yi H, Hwang S, Weitz DA, Lee CS. Microfluidic fabrication of complex-shaped microfibers by liquid template-aided multiphase microflow. Lab on a Chip. 2011;11:1477-83.

[29] Boyd DA, Shields AR, Howell PB, Ligler FS. Design and fabrication of uniquely shaped thiol-ene microfibers using a two-stage hydrodynamic focusing design. Lab on a Chip. 2013;13:3105-10.

[30] Cho S, Shim TS, Yang SM. High-throughput optofluidic platforms for mosaicked microfibers toward multiplex analysis of biomolecules. Lab on a Chip. 2012;12:3676-9.

[31] Daniele MA, Boyd DA, Adams AA, Ligler FS. Microfluidic Strategies for Design and Assembly of Microfibers and Nanofibers with Tissue Engineering and Regenerative Medicine Applications. Advanced Healthcare Materials. 2015;4:11-28.

[32] Jun Y, Kang E, Chae S, Lee SH. Microfluidic spinning of micro- and nano-scale fibers for tissue engineering. Lab on a Chip. 2014;14:2145-60.

[33] Hwang DK, Dendukuri D, Doyle PS. Microfluidic-based synthesis of non-spherical magnetic hydrogel microparticles. Lab on a Chip. 2008;8:1640-7.

[34] Panda P, Ali S, Lo E, Chung BG, Hatton TA, Khademhosseini A, et al. Stop-flow lithography to generate cell-laden microgel particles. Lab on a Chip. 2008;8:1056-61.

[35] Thangawng AL, Howell PB, Richards JJ, Erickson JS, Ligler FS. A simple sheath-flow microfluidic device for micro/nanomanufacturing: fabrication of hydrodynamically shaped polymer fibers. Lab on a Chip. 2009;9:3126-30.

[36] Li Y-F, Rubert M, Aslan H, Yu Y, Howard KA, Dong M, et al. Ultraporous interweaving electrospun microfibers from PCL-PEO binary blends and their inflammatory responses. Nanoscale. 2014;6:3392-402.

[37] Soliman S, Pagliari S, Rinaldi A, Forte G, Fiaccavento R, Pagliari F, et al. Multiscale three-dimensional scaffolds for soft tissue engineering via multimodal electrospinning. Acta Biomaterialia. 2010;6:1227-37.

[38] Acar H, Çınar S, Thunga M, Kessler MR, Hashemi N, Montazami R. Study of Physically Transient Insulating Materials as a Potential Platform for Transient Electronics and Bioelectronics. Advanced Functional Materials. 2014;24:4135-43.

[39] Sung HJ, Meredith C, Johnson C, Galis ZS. The effect of scaffold degradation rate on three-dimensional cell growth and angiogenesis. Biomaterials. 2004;25:5735-42.

[40] Hong SG, Kim GH. Mechanically improved electrospun PCL biocomposites reinforced with a collagen coating process: preparation, physical properties, and cellular activity. Bioprocess Biosyst Eng. 2013;36:205-14.

[41] Hashemi N, Howell JPB, Erickson JS, Golden JP, Ligler FS. Dynamic reversibility of hydrodynamic focusing for recycling sheath fluid. Lab on a Chip. 2010;10:1952-9.

[42] Hashemi N, Erickson JS, Golden JP, Jackson KM, Ligler FS. Microflow Cytometer for optical analysis of phytoplankton. Biosensors and Bioelectronics. 2011;26:4263-9.

[43] Hashemi N, Erickson JS, Golden JP, Ligler FS. Optofluidic characterization of marine algae using a microflow cytometer. Biomicrofluidics. 2011;5:032009.

[44] Asrar P, Sucur M, Hashemi N. Multi-Pixel Photon Counters for Optofluidic Characterization of Particles and Microalgae. Biosensors. 2015;5:308-18.

[45] Zarrin F, Dovichi NJ. Sub-picoliter detection with the sheath flow cuvette. Analytical Chemistry. 1985;57:2690-2.

[46] Croisier F, Duwez AS, Jérôme C, Léonard AF, van der Werf KO, Dijkstra PJ, et al. Mechanical testing of electrospun PCL fibers. Acta Biomaterialia. 2012;8:218-24.

[47] Duling RR, Dupaix RB, Katsube N, Lannutti J. Mechanical characterization of electrospun polycaprolactone (PCL): A potential scaffold for tissue engineering. Journal of Biomechanical Engineering-Transactions of the Asme. 2008;130:13.

[48] Ghasemi-Mobarakeh L, Prabhakaran MP, Morshed M, Nasr-Esfahani M-H, Ramakrishna S. Electrospun poly(epsilon-caprolactone)/gelatin nanofibrous scaffolds for nerve tissue engineering. Biomaterials. 2008;29:4532-9.

[49] Baker SR, Banerjee S, Bonin K, Guthold M. Determining the mechanical properties of electrospun poly-ε-caprolactone (PCL) nanofibers using AFM and a novel fiber anchoring technique. Materials Science and Engineering: C. 2016;59:203-12.

CHAPTER 4

POLYCAPROLACTONE MICROFIBROUS SCAFFOLDS TO NAVIGATE NEURAL STEM CELLS [1]

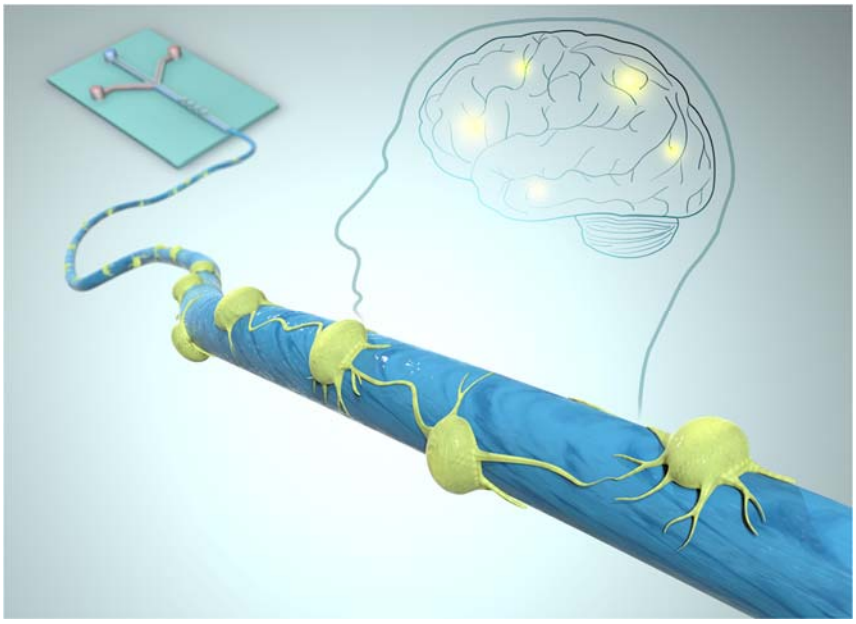

ABSTRACT

Fibrous scaffolds have shown promise in tissue engineering due to their ability to improve cell alignment and migration. In this paper, poly(ε-caprolactone) (PCL) fibers are fabricated in different sizes using a microfluidic platform. By using this approach, we demonstrated considerable flexibility in ability to control the size of the fibers. It was shown that the average diameter of the fibers was obtained in the range of 2.6–36.5 μm by selecting the PCL solution flow rate from 1 to 5 μL min^{-1} and the sheath flow rate from 20 to 400 μL min^{-1} in the microfluidic channel. The microfibers were used to create 3D microenvironments in order to investigate growth and differentiation of adult hippocampal stem/progenitor cells (AHPCs) in

[1] **F. Sharifi**, B. Patel, A. Dzuilko, R. Montazami, D.S. Sakaguchi, and N. Hashemi, "Polycaprolactone Microfibrous Scaffolds to Navigate Neural Stem Cells", Biomacromolecules, 17, 3287-3297 (2016).

vitro. The results indicated that the 3D topography of the PCL substrates, along with chemical (extracellular matrix) guidance cues supported the adhesion, survival, and differentiation of the AHPCs. Additionally, it was found that the cell deviation angle for 44–66% of cells on different types of fibers was less than 10°. This reveals the functionality of PCL fibrous scaffolds for cell alignment important in applications such as reconnecting serious nerve injuries and guiding the direction of axon growth as well as regenerating blood vessels, tendons, and muscle tissue. Moreover, the PCL fibers with different sizes and shapes (straight and wavy), were used to quantitatively analyze the cell adhesion, proliferation, and differentiation. Our first replicate showed that 5 μm had the most cell adhesion, 5 μm, straight 20 μm, and wavy 35 μm provided significantly better condition for the glial differentiation compared to control. More cell proliferation was observed on the wavy 35 μm fibers when compared to straight 35 μm fibers, showing that fiber morphology may have an effect on cell proliferation. However, this study goals to perform two more replicates in order to have more reliable results.

4.1 Introduction

Tissue engineering is an interdisciplinary area that combines engineering and biology in order to improve or replace biological functions [1, 2]. This area can be equipped by microfabrication methods, which are powerful tools with extremely high potential to handle some of the obstacles in tissue engineering [3]. In most applications, scaffolds are made of biomaterials and applied in order to provide a suitable 3D environment with intentions toward controlling cell behavior, such as adhesion, proliferation, differentiation, migration, alignment, and in providing efficient nutrient transport as well as sufficient mechanical properties [4, 5]. However, there are some challenges in tissue engineering; the biomaterial must be compatible

with the cells in question in order to sustain reasonably normal behaviors. As such, it is essential to gain a better understanding of the microenvironmental conditions required to regulate the cells fate. Additionally, tissue engineering suffers from a lack of biomaterials with desirable biological, chemical, and mechanical properties [4]. To meet this need, enormous efforts have been made to discover new biomaterials and to study the biocompatibility and biodegradability of different materials [6, 7].

A prominent area of tissue engineering is related to regenerative medicine and neurorepair. The discovery of effective therapeutic interventions targeted toward neurodegenerative conditions and nerve injuries has proven challenging. Scientists and engineers have been drawn into the field of neural tissue engineering due to its importance for development of novel therapeutic strategies. For example, peripheral nerve regeneration is a complicated phenomenon which is often successful as long as the injuries are small. With more severe nerve injuries such as a nerve gap, however, interposition of a nerve graft or nerve regeneration conduit is usually required. Complexity in spinal cord injury is more serious since, for the most part, regeneration is prohibited. Fortunately, neural tissue engineering provides extraordinary promise to combat this central nervous system (CNS) injury [8]. For example, Hurtado et al. demonstrated axonal regeneration within a spinal cord injury using aligned poly-L-lactic acid microfibers [9]. Microfibers may provide a supportive environment for a recovering nervous system due to the combination of physical and biological cues.

Microfibers have been fabricated for neural tissue engineering using different approaches such as microfluidics, electrospinning, and wet spinning [10]. Agarwal et al. reported some of the studies in electrospinning fiber fabrication technique for biomedical applications such as tissue engineering and drug delivery [11, 12]. Polycaprolactone (PCL) is one of the

biocompatible and biodegradable polymers applied for the fibers fabricated in this technique [12-16]. Schnell et al. showed that using electrospun PCL and collagen/PCL fibers can significantly improve the attachment, migration, and neurite orientation of Schwann cells [12]. In addition to PCL, other biocompatible polymers have been used in nerve tissue engineering such as gelatin and polylactic acid (PLA) [17, 18]. However, accurately aligning the fibers in electrospinning method is difficult [13, 17, 19]. This method is not functional for cell encapsulating purposes due to the fact that the size of the fibers are mostly limited to nanoscales. Furthermore, high voltages (5–50 kV) need to be applied for pulling the charged solution, which might damage sensitive biological materials. Wet spinning method has been employed in nerve tissue engineering as well. Siriwardane et al. fabricated collagen fibers and treated them by cross-linkers glutaraldehyde and genipin in order to improve the mechanical properties and decrease swelling [20]. In wetspinning, the sample is exposed to chemicals and osmotic gradients for a relatively long time, which can have detrimental effects on the cells [21, 22]. Additionally, the cross section of the fibers made by electrospinning and wetspinning are mostly round due to the surface tension in the two-phase systems of liquid/air and immiscible liquid/liquid, respectively [23].

Microfluidics is an interdisciplinary field that has received much attention, mostly because of its wide applications from energy systems to biomedical areas [24-29]. Microfluidic fiber fabrication, which is the newest approach, retains most advantages of other fiber fabrication approaches and minimizes some of their shortcomings. One of the important features of using microfluidic fiber fabrication is the compatibility with cells, proteins, drugs, and peptides as well as versatility, cost-effectiveness, and simplicity [5, 28, 30, 31]. In this method, there is no need to apply high temperature, high pressure, and high voltages [5, 23, 25, 30, 32, 33]. This approach

makes it feasible to fabricate fibers with different shapes of solid [23, 34-38], tubular [39, 40], hybrid [41], and flat [42-44] dimensions for divergent applications such as cell encapsulation, alignment, and immobilization.

In terms of material, there are both synthetic and natural biodegradable and biocompatible polymers. We used PCL, a synthetic polymer, in this study. Synthetic polymers have some advantages over the natural materials. For example, the polymer composition can be accurately controlled such that a wide range of properties is obtainable for the synthetic polymers. In addition, they are more uniform with sufficient source of raw materials [45, 46]. Comparing with other synthetic polymers, such as PLGA, PCL has slower degradation rate, which makes it less acidic during degradation and desirable for long-term implantable devices. Although some studies focused on using the PCL electrospun fibrous scaffolds in nerve tissue engineering, there is no report on employing hydrodynamic focusing (microfluidic approach) and solvent extraction to fabricate biocompatible PCL fibers in nerve regeneration tissue engineering [47, 48].

In this paper, we show that microfluidic fiber fabrication may be used as a scalable and widely accessible alternative technique to fabricate PCL fibrous scaffolds with tuned characteristics to enhance the growth and differentiation of neural stem cells as well as neurite orientation. We cultured green fluorescent protein-expressing (GFP) adult hippocampal stem/progenitor cells (AHPCs) on PCL microfibers and investigated their ability to adhere, survive, proliferate and differentiate. AHPCs were used because of their ability to differentiate into the fundamental cells of the CNS. In order to study CNS regeneration therapies, it is important to consider the population of cells needed for repair of a damaged nervous system. The AHPCs were maintained in medium supplemented with bFGF and upon growth factor

withdrawal, these multipotent AHPCs differentiated into neurons and glial cells [49, 50]. Neurons are able to transmit information and are the key cells of the nervous system, whereas glial cells serve as the support cells of the CNS. The microfluidic microfabrication platform was able to create a biocompatible scaffold out of fibers to provide a desirable growth environment for the neural stem cells. We showed that the cells attach to and align themselves on the microfiber substrates. In this study, cell death was minimal, and cell proliferation was affected by changing the features of the fibrous scaffold. Ideally, as the scaffold is degraded a more natural microenvironment is created by the cells and the production of their extracellular matrix (ECM), thus resulting in a bioengineered 3D network that mimics the native tissue.

4.2 Experimental Section

4.2.1 Materials

Poly(ε-caprolactone) (PCL) (M_n = 80 000), polyethylene glycol (PEG) (M_n = 20 000), and ethanol were purchased from Sigma-Aldrich (St. Louis, MO). 2,2,2-Trifluoroethanol (TFE), which is the solvent for PCL, was obtained from Oakwood Chemical (West Columbia, SC).

4.2.2 Microfluidic channel

A SU8 photoresist-patterned silicon wafer was applied as a mold and the channel was made using soft lithography. We used two silicon wafers in order to create the pattern of the microchannel and the chevron grooves extended from two sides of the channel. The dimensions of the microchannel are 130 μm × 390 μm (height × width). The microchannel has four diagonal grooves with dimensions of 130 μm × 100 μm (height × width) and are spaced 200 μm apart. Polydimethylsiloxane (PDMS), which is a biocompatible and transparent elastomer, was made

from the mixture of Sylgard 184 elastomer base and cross-linker agents in a 10:1 ratio. Then, the mixture was poured onto the mold, and cured with the temperature of 85 °C for 25 min. After that, the PDMS layer on the silicon wafers were peeled off and the layers were bonded together using plasma treatment.

4.2.3 Microfluidic fiber fabrication

The 5 wt % PCL solution (core fluid) was obtained by mixing 1 g of PCL in 20 mL TFE at room temperature. The sheath solution was prepared by adding 1 g of PEG in 20 mL mixture of ethanol and deionized (DI) water with a volume ratio of 1:1 to prepare 5 wt % PEG solution. These two solutions were introduced into the microchannel via a double syringe pump (Cole-Parmer, Veron Hillss, IL) with different flow rate ranges of 2–5 μL min^{-1} and 10–120 μL min^{-1} for the core and sheath solution, respectively. Using this method, the fibers remain aligned after fabrication. The microchannel was vertically positioned into a water bath, and the resulting fibers were gathered around a paper frame in an aligned manner.

4.2.4 Cell culture

Adult hippocampal progenitor cells (AHPCs) were originally isolated from adult Fischer 344 rats and infected with a retrovirus to express green fluorescence protein (GFP) as described previously and were a generous gift from F. H. Gage (Salk Institute for Biological Sciences, La Jolla, CA) [51]. Cells were grown in flasks coated with poly-L-ornithine (10 μg mL^{-1}; Sigma-Aldrich) and purified mouse laminin (5 μg mL^{-1}; R&D Systems) in Earle's balanced salt solution (EBSS). Maintenance media (MM) included Dulbecco's modified Eagle's medium/Ham's F-12 (DMEM/F-12, 1:1; Omega Scientific), supplemented with 2.5 mM L-glutamine, N2 supplement

(Gibco BRL), and 20 ng mL^{-1} basic fibroblast growth factor (human recombinant bFGF; Promega Corporation). The AHPCs were detached from flasks using 0.05% trypsin–EDTA (Gibco BRL) and harvested by centrifugation at 800 rpm for 5 min. A hemocytometer was used to perform a Trypan Blue viable cell count, and AHPCs were plated at a density of 10 000 cells/cm^2 on PCL-microfiber substrates (see below). Cells were maintained at 37 °C in a 5% CO_2/95% humidified air atmosphere. For cell differentiation, AHPCs were cultured in growth medium lacking bFGF (referred to as differentiation medium, DM) for 7 days. Half of the media was changed every other day.

4.2.5 Substrate preparation

Glass coverslips (12 mm, Fisher Scientific) were cleaned using RBS 35 (Thermo Scientific) detergent diluted (1:50) in deionized water and boiled for 15 min. Coverslips were then rinsed in DI water, air-dried and ultraviolet light was used for sterilization. The microfibers were then attached to the coverslips using medical adhesive. Small droplets of medical adhesive were placed at opposite sides of the coverglass and a parallel array of microfibers placed across the coverglass and attached to the medical adhesive droplets. Small chip of coverglass were then used to secure the microfibers to the coverglass. The microfibers were fixed at opposite ends and loose across the middle of the coverglass. The coverglass and PCL-microfiber substrates were sterilized by incubation in 70% ethanol for 20 min and rinsed with Earle's balanced salt solution (EBSS; Invitrogen). After 10 min of air-drying, the microfiber substrates were incubated at 4 °C overnight with Entactin-Collagen IV-Laminin (ECL; Millipore) at 10 μg mL^{-1} in DMEM/F-12 to facilitate cell attachment. The next day, the ECL was removed, samples were rinsed with EBSS, and cells plated.

4.2.6 Immunocytochemistry

After 7 days of culturing in DM, the cells were rinsed with 0.1 M phosphate ($P0_4$) buffer and immediately fixed with 4% paraformaldehyde (PFA) in 0.1 M $P0_4$ buffer for 20 min at room temperature. PFA was removed and rinsed with phosphate buffer saline (PBS; Invitrogen) and incubated in blocker solution (PBS supplemented with 5% normal donkey serum (Jackson ImmunoResearch), 5% normal goat serum (Jackson ImmunoResearch), 0.4% bovine albumin serum (Sigma), and 0.2% Triton X-100 (Fisher Scientific)) at room temperature for 1 h. Primary antibodies were diluted in blocker solution and samples incubated at 4 °C overnight. On the following day, antibodies were removed and samples were rinsed with PBS. Secondary antibodies, donkey anti-rabbit Cy3 and donkey anti-mouse Cy3 (Jackson ImmunoResearch), were diluted in blocking solution at a dilution of 1:500 along with the nuclear stain, DAPI (1:50, Invitrogen). Samples were incubated in secondary antibody/DAPI solution for 90 min at room temperature. Samples were then mounted on microscope slides using DAPI Fluoromount-G (Southern Biotech) mounting media and stored at 4 °C until imaging.

4.2.7 Propidium Iodide staining

Propidium iodide (PI) was used to measure cell death/survival at 7 days in vitro. Propidium iodide stain solution was prepared at a concentration of 1.5 μM in culture medium. Half of the samples served as the positive, reagent control for the PI stain and subjected to 70% ethanol for 5 min to induce cell death. The ethanol and MM were removed from all samples and the culture media containing PI was added for 20 min at 37 °C in a 5% CO_2 incubator. The samples were then rinsed with 0.1 M $P0_4$ buffer, fixed with 4% PFA, and rinsed again with PBS.

Samples were then incubated with DAPI (1:50) diluted in blocker solution for 1 h at room temperature. Following PBS rinses, samples were mounted on microscope slides using DAPI Fluoromount-G mounting media and stored at 4 °C until imaging.

4.2.8 Imaging and measuring the alignment angles

Fluorescent images were conducted using a fluorescence microscope (Nikon Microphot FXA, Nikon, Inc.), equipped with a Retiga 2000R digital camera controlled by QCapture software (QImaging). Images were pseudocolored using Adobe Photoshop CC. Scanning electron microscopy (SEM; JCM-6000 NeoScope Benchtop scanning electron microscope) was applied to study the size, morphology, and deviation angle of the fibers and cells. In order to acquire high quality SEM images, the substrates were made conductive using gold sputter-coating. The coating thickness of the samples was around 50 nm. The cell and fiber deviation angles were measured using the SEM images and ImageJ, which is an imaging analysis software. For the fiber size and deviation angle, around 30 fibers were studied, whereas the positions of around 100 cells were evaluated relative to the fiber direction in each type of fiber.

4.3 Results and Discussions

Two fluids, i.e., the core and sheath fluids, are introduced into the microchannel and diffusion occurs only at the core/sheath fluid interface due to the laminar flow regime. In order to have a continuous fiber fabrication process, a core/sheath flow profile is required [5].

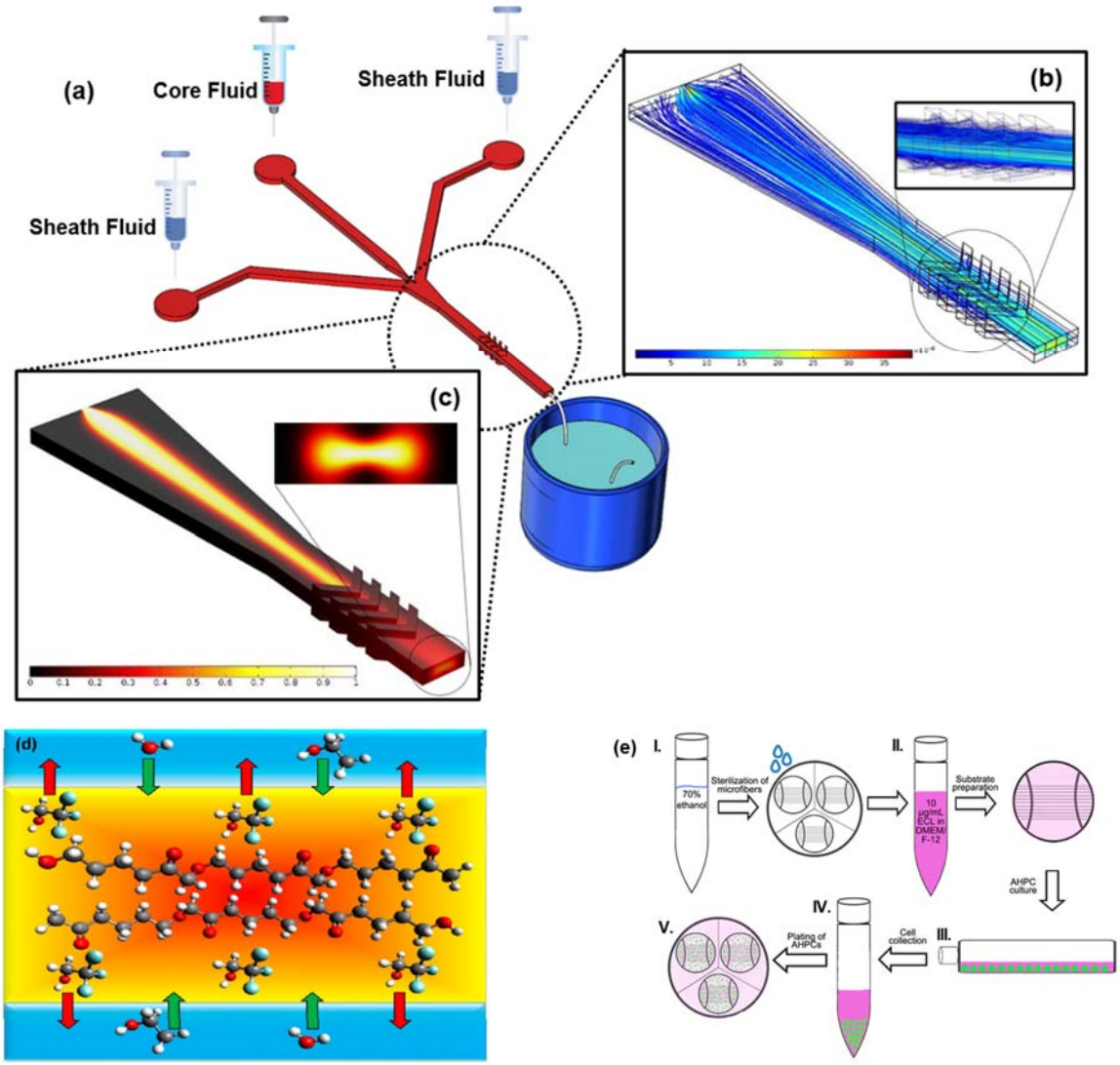

Figure 4.1 *(a) Schematic of the microfluidic fiber fabrication. (b) Streamline and velocity (m s–1) of the fluids along the channel. (c) Illustration of concentration profile (mol m^{-3}): the dark and bright colors represent the sheath and core fluids, respectively. (d) Phase inversion process: the TFE molecules are replaced with the molecules of the sheath fluid, which results in PCL solidification. (e) Cell culture procedure: (I) Sterilization of microfibers on coverslips using 70% ethanol for 20 min; (II) diluted ECM substrate (ECL) in DMEM/F-12 to a final concentration of 10 µg mL^{-1}; (III) culture AHPCs in T-75 flask until 80% confluent; (IV) apply trypsin to cells for collection; and (V) culture cells on ECL-coated microfibers in differentiation media for 7 days.*

Figure 4.1 (a) provides a schematic picture of the microfluidic fiber fabrication. The sheath fluid focuses the core fluid laterally after the two fluids are introduced at the upstream of the channel and changes the shape of the core fluid to a thin vertical strip. Chevron grooves in the downstream of the channel decrease the hydrodynamic resistance perpendicular to the flow direction. The sheath flow rate is higher than the core flow rate in order to provide the force needed to keep the core fluid at the center of the microchannel. Because the hydrodynamic resistance is inversely proportional to flow rate, the sheath fluid fills the grooves, wraps around the core fluid, and pushes it to the center of the channel [52-54]. The streamline and velocity distribution of the fluids along the channel are provided in **Figure 4.1** (b). **Figure 4.1** (c) demonstrates the concentration profile through the channel. The dark and bright colors show the sheath and core fluids, respectively. These figures clearly illustrate the role of the sheath fluid and chevron grooves to exert the lateral and vertical hydrodynamic focusing forces on the core fluid. The lateral and vertical hydrodynamic focusing forces, which are originated from the shear force between the core and sheath fluids, play a pivotal role to keep the core fluid at the center, align the polymer chain, and change the shape of the microfibers.

The hydrodynamic force depends on the viscosity and relative velocity of the core and sheath fluids. By adding polyethylene glycol (PEG) to the sheath fluid, the viscosity of core and sheath solutions match and there is no need to use high relative velocities to focus the core fluid when fabricating the fibers. Additionally, there is a possibility of flow instability in the channel at high relative velocities that results in changing the flow regime to transient from laminar. Phase inversion (solvent extraction) strategy was used to solidify PCL and fabricate microfibers. In this process, 2,2,2-trifluoroethanol (TFE) in the core fluid is replaced by the ethanol and water in the sheath fluid at the interface between the sheath and core solution (**Figure 4.1** (d)). This

exchange results in PCL solidification because the sheath fluid is miscible to TFE, but not solvent to PCL. **Figure 4.1** (e) describes the sterilization and cell culture protocol for AHPCs. Following the plating of AHPCs, cells are incubated for 7 days in differentiation media, and subsequently fixed and immunolabeled for further analysis.

Figure 4.2 shows the SEM images of the fibers fabricated using the flow rate ranges of 1–5 μL min^{-1} and 20–400 μL min^{-1} corresponding to the core and sheath fluids, respectively. The concentration of the PCL in TFE and PEG in the water/ethanol were kept at a constant value of 5%. In the phase inversion solidification process, used to solidify the PCL fibers, the molecules of TFE are replaced by the molecules of the sheath fluid. Due to this diffusion at the fluid/fluid interface, the surface of the PCL fibers are not smooth, which could provide a better environment for the cells to adhere to the surface of the fibers. Additionally, this figure shows consistency with the theory of hydrodynamic focusing meaning that when the flow rate ratio between the core and sheath fluids decreases, the shear force at the interface exerted from the sheath fluid to the core fluid weakens. Therefore, the core fluid extends in the channel and the size of the resulting fiber increases.

This figure also demonstrates that once the flow rate ratio exceeds 50, the fibers will not be smooth anymore. This condition continues until the wavy fibers connect with each other and create a chain, that could be considered as a self-assembly structure (**Figure 4.2** (e)). This was expected because when the flow rate ratio between the fluids increases, the sharp velocity gradient at the fluid/fluid interface intensifies the shear force, which decreases the flow stability and the regime starts to lie in the transition region [25].

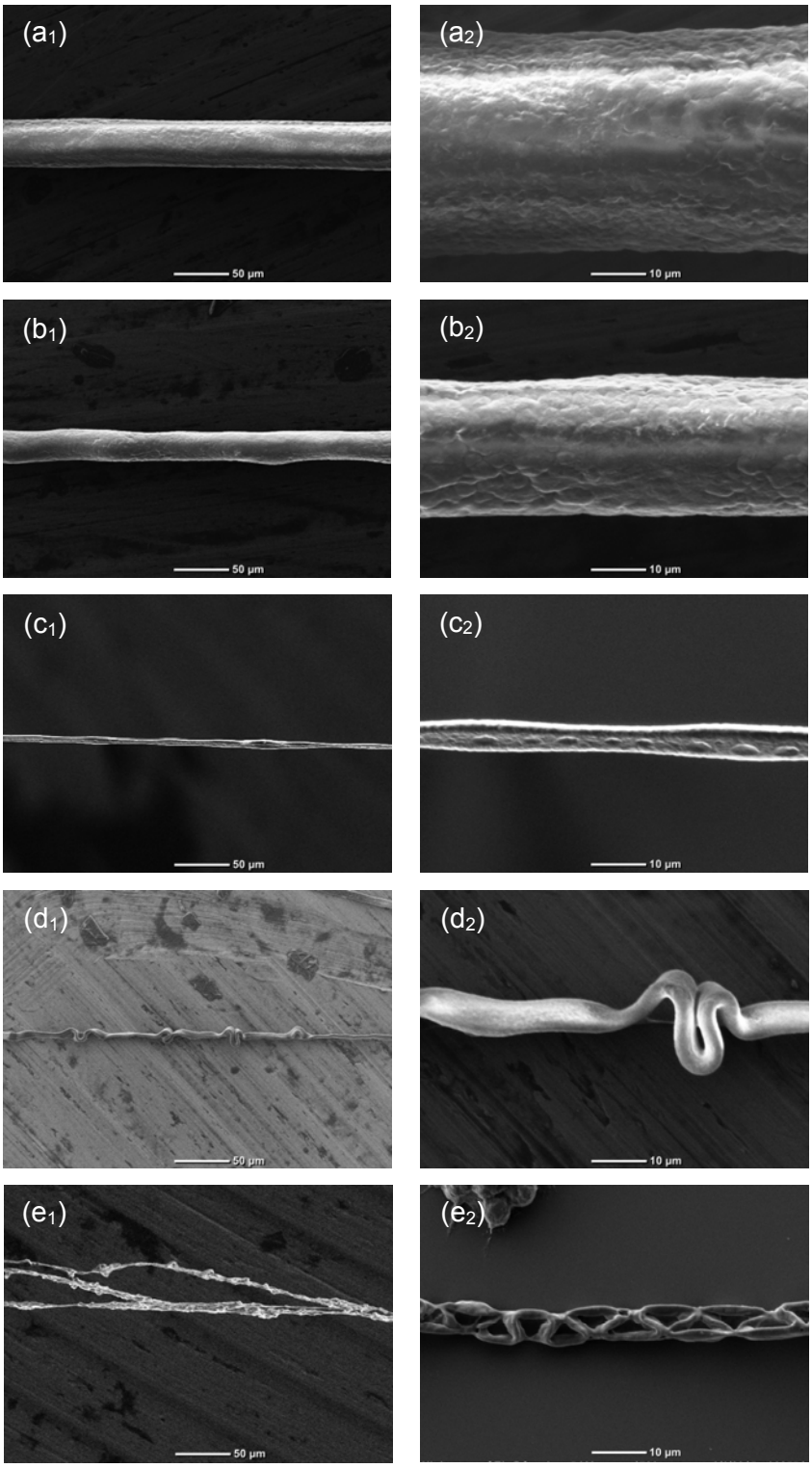

Figure 4.2 *SEM images of the microfluidic spun PCL microfibers at different sheath-to-core flow rates of (a) 20:5, (b) 60:5, (c) 200:4, (d) 300:2, and (e) 400:1. The concentrations of the PCL and PEG are 5% in TFE and water/ethanol, respectively.*

The average size and production rate of the fibers (mean ± standard error) are shown in **Figure 4.3** (a) and (b), respectively. The results show that the diameters of the fibers lie in the range of 2.6–36.5 μm, which can be obtained by changing the sheath-to-core flow rate of 400:1–20:5, respectively. This figure demonstrates the capability of the microfluidic fiber fabrication in tuning the size of the fibers by simply changing the flow rate ratio between the sheath and core fluids. As expected, the production rate of the fiber directly depends on the sheath and core flow rates. The maximum production rate was 37 mm s^{-1} for the sheath-to-core flow rates of 400:1, and it decreases to 6.5 mm s^{-1} when the sheath-to-core flow rate of 60:5 is used. However, it does not mean that the range of the production rate in microfluidic approach is limited. We can increase the production rate by increasing the sheath and core flow rates. However, in this study, we mostly focused on studying the alignment of the AHPCs on fibers with different sizes. The small error bars reveal the uniformity of the size and production rate of the fibers made by this method. **Figure 4.3** (c) illustrates the alignment of different types of fibers by presenting the percentage of fiber deviation angle, i.e., the angle between each one of the fibers and a reference. This figure shows that the percentage of the fibers with fiber deviation angle larger than 10° are 5.55%, 0%, 0%, 2.38%, and 6.1% for the sheath-to-core flow rates of 20:5, 60:5, 200:4, 300:2, and 400:1, respectively. This shows one of the advantages of microfluidic approach over common fiber fabrication methods, which is the feasibility of this method to simply fabricate the aligned fibers.

*K*i-67 immunolabeling was used to evaluate whether the PCL microfibers would support proliferation of the AHPCs. Expression of the *K*i-67 antigen occurs during the cell cycle (not detected in cells in the resting phase) and therefore is commonly used as a cellular marker for cell proliferation. *K*i-67 immunolabeled cells were present on all microfibers examined.

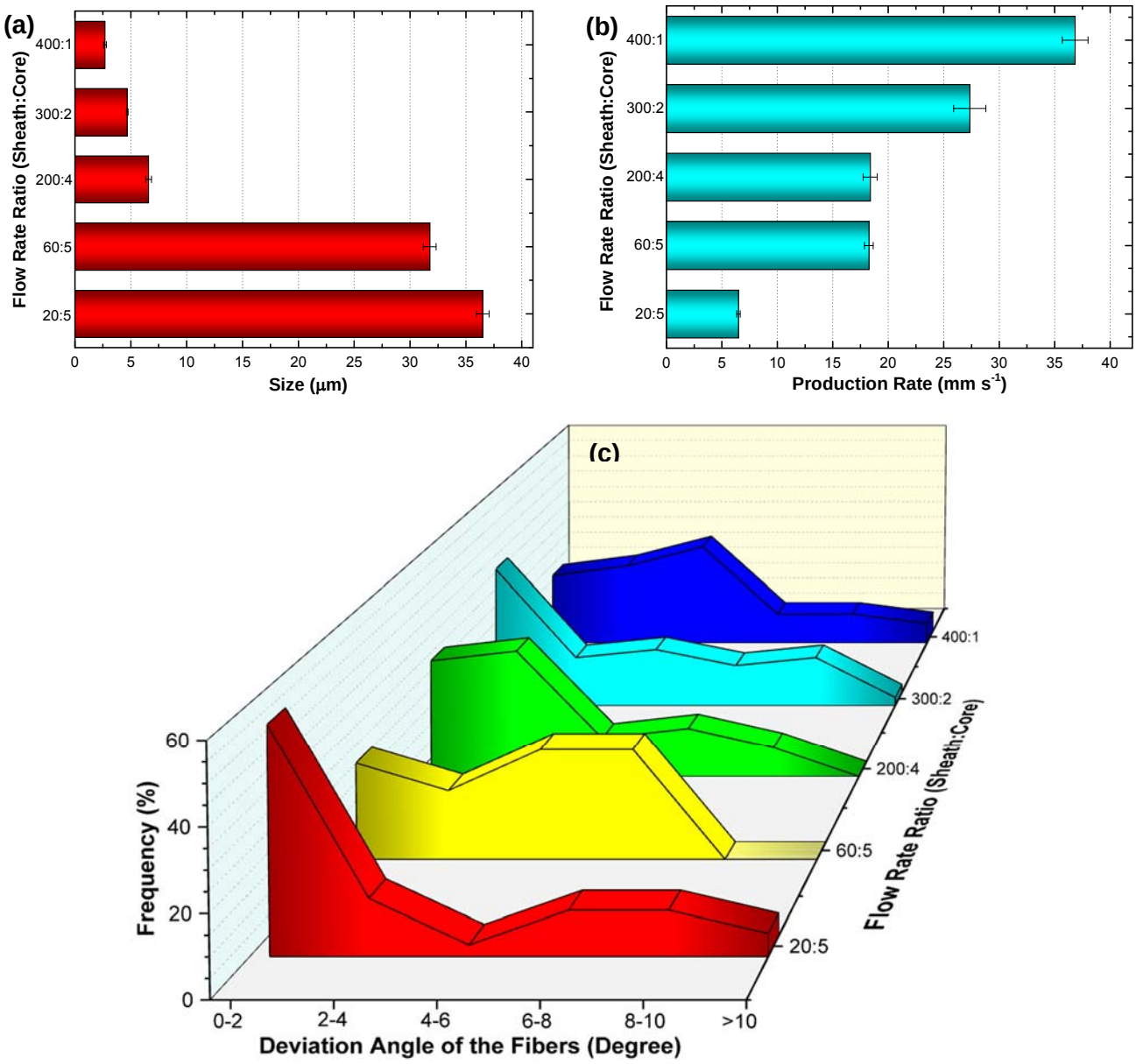

Figure 4.3 *Characteristics of the PCL microfibers: (a) size, (b) production rate, and (c) alignment of the fibers fabricated using different sheath-to-core flow rate ratios.*

Figure 4.4 (A-C) illustrates an example of *K*i-67 immunolabeled cells growing on microfluidic spun PCL microfibers at a sheath-to-core flow rate of 60:5. Propidium iodide staining was used to evaluate survival of AHPCs growing on the microfibers (**Figure 4.4** (D-I)). Propidium iodide is a fluorescent nuclear and chromosome counterstain that is membrane impermeant and commonly used to identify dead cells in a population.

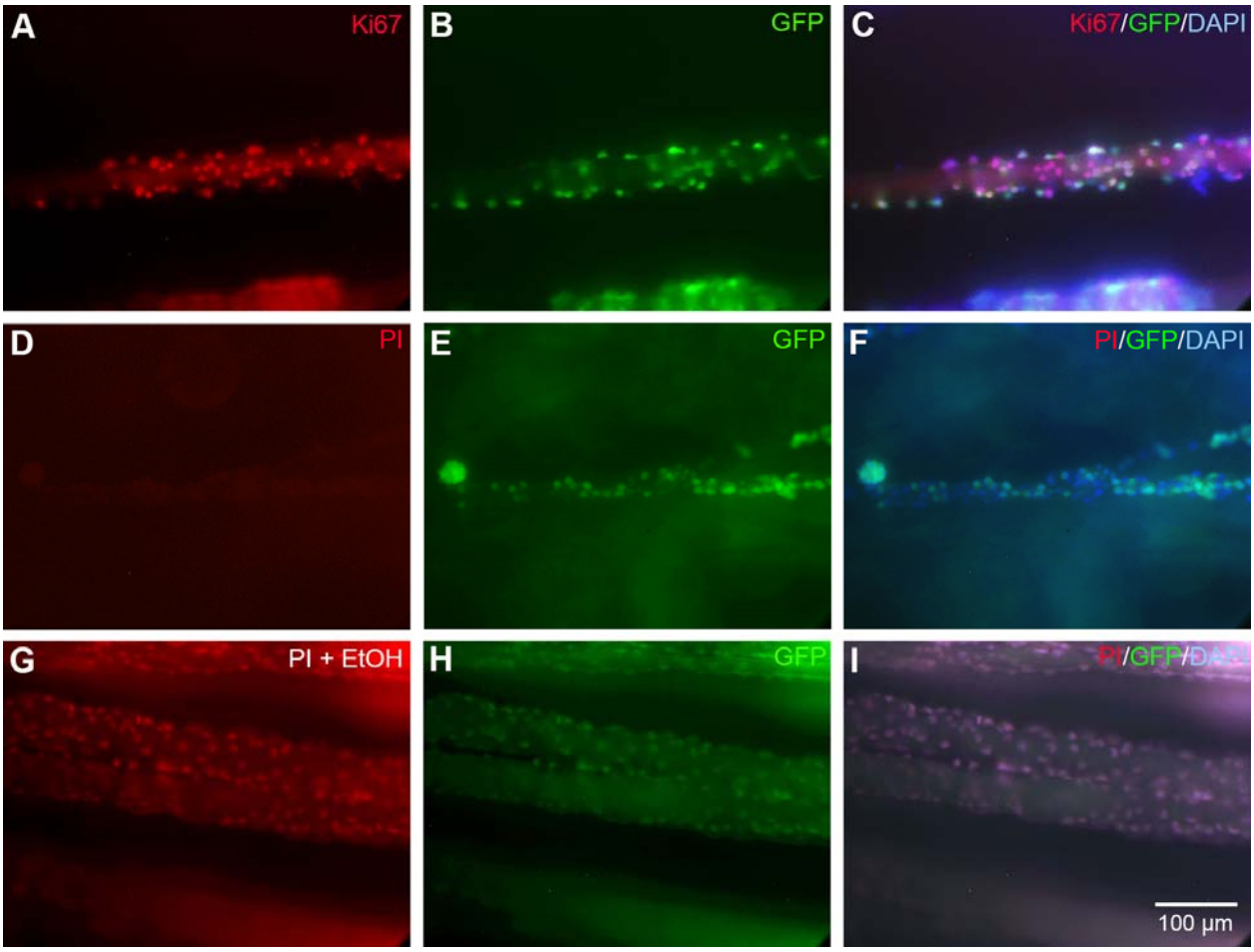

Figure 4.4 *Proliferation and survival of AHPCs cultured on PCL microfibers. Fluorescence images of AHPCs immunolabeled for Ki-67, cell proliferation marker (A−C) or propidium iodide (PI) staining. Middle column of images illustrate GFP-expressing AHPCs (B, E, and H). As a control for the PI staining reagents, samples were subjected to ethanol (EtOH) treatment that causes most cells to die resulting in extensive PI staining (G, H, and I). Merged images (C, F, and I) of antibody labeling or PI-staining (red) with GFP-expression (green) and DAPI nuclei counterstaining (blue). Scale bar = 100 µm.*

Figure 4.4 (D-F) shows that very few PI-positive cells were detected in the microfiber cultures. In contrast, as a positive control for the PI reagents, some samples were subjected to 70% ethanol, a condition that kills most cells, resulting in the majority of cells PI-labeled (**Figure 4.4** (G-I)). It is notable that the cells remained attached following the 70% ethanol

treatment. This is likely due in part to the immediate fixation in paraformaldehyde. Furthermore, the ECL substrate absorption onto the PCL microfibers facilitates cell attachment. Taken together, the *K*i-67 immunolabeling and Propidium Iodide staining results indicate that the different PCL microfibers produced by the different sheath-to-core flow rates all supported adhesion and cell proliferation, and did not dramatically affect cell viability.

AHPCs growing on the different PCL microfibers were characterized morphologically and immunocytochemically using a panel of cell-type specific antibodies. The AHPCs are a multipotent population of adult neural stem cells and have the capacity to differentiate into neurons, oligodendrocytes and astrocytes [50]. The phenotypes of AHPCs growing on the microfibers were assessed using antibodies directed against nestin, an intermediate filament protein present in neural stem/progenitor cells; class III β-tubulin (TuJ1), a protein characteristic of early neurons; microtubule-associated protein 2ab (MAP2ab), characteristic of maturing neurons; and the glial markers, receptor interacting protein (RIP) and glial fibrillary acidic protein (GFAP), for oligodendrocytes and astrocytes, respectively. AHPCs were identified in culture based on green fluorescent protein GFP-expression and counterstaining with DAPI allowed visualization of the cell nuclei. Many of the AHPCs were immunolabeled with the nestin, TuJ1 and MAP2ab antibodies (**Figure 4.5**), fewer cells were immunoreactive for the glial markers RIP and GFAP.

Figure 4.5 (A-I) illustrates examples of AHPCs growing on microfluidic spun PCL microfibers at a sheath-to-core flow rate of 300:2 that were immunolabeled with the nestin (**Figure 4.5** (A-C)), TuJ1 (**Figure 4.5** (D-F)) or MAP2ab (**Figure 4.5** (G-I)) antibodies.

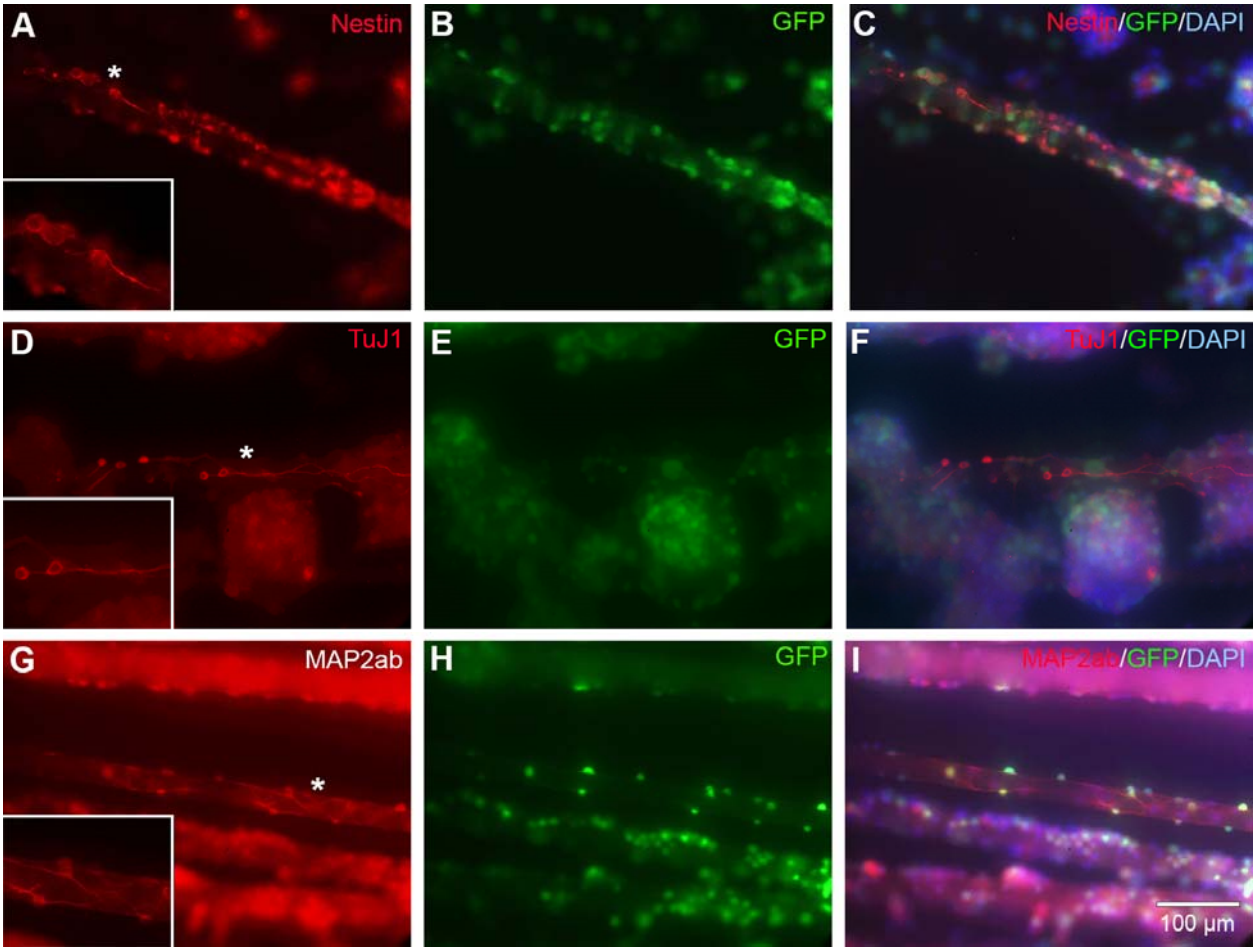

Figure 4.5 *Attachment and differentiation of AHPCs cultured on PCL microfibers. Fluorescence images of AHPCs immunolabeled for nestin (A–C), TuJ1 (D–F), and MAP2ab (G–I). Middle column of images illustrate GFP-expressing AHPCs (B, E, and H). Merged images (C, F, and I) of antibody labeling (Cy3, red) with GFP-expression (green) and DAPI nuclei counterstaining (blue). Asterisks indicate the location of the higher magnification inset images in (A), (D), and (G). Attachment of cells is seen through immunolabeling of processes around microfibers. Scale bar = 100 µm (200 µm for insets).*

Nestin, a marker for multipotent neural stem cells, has important functions in the survival and self-renewal of NSCs. AHPCs immunolabeled for nestin indicates that many of the cells growing on the PCL microfibers retained their progenitor-like status. Under differentiation conditions (initiated by growth factor withdrawal) AHPCs begin differentiating and many cells

were immunolabeled with the neuronal markers TuJ1 and MAP2ab. Immunolabeled cells displayed neuronal morphologies, often exhibiting longer neurites of various lengths on the microfiber surface. Though all three antibody markers (nestin, TuJ1, and MAP2ab) label different cytoskeletal elements, all are expressed within the cytoskeleton of the neurite processes as was clearly evident in the fluorescent images (**Figure 4.5**). It was noted that some of the AHPCs undergo a decrease in expression of GFP during the course of cell culture, indicating a down regulation of the GFP transgene during the course of establishment of stable cell populations that allow long-term culture. However, these low GFP expressing AHPCs continued to survive, proliferate, and differentiate in a normal fashion.

The SEM images of AHPCs on the PCL microfibers are shown in **Figure 4.6**. This figure illustrates that most of the cells can be aligned to the longitudinal direction of the fibers with different sizes. This reveals the role of the fibers as scaffolds to be applied for supporting the proliferation and differentiation of AHPCs. However, the fibers with larger sizes can physically support more cells on their surfaces compared to smaller ones. The SEM images with higher magnifications are provided in **Figure 4.7** (a-e).

In terms of the size of the aligned PCL fibers, this figure shows that while the predominant alignment of the cells is in the axial direction of the fibers, the cells on fibers with the average size of 4–7 μm on occasion bridged from one fiber to another one (**Figure 4.7** (d)). The likely reason for such behavior is that the distance between the thinner fibers is shorter and that bundles of fibers have been created. As a result, the cell can bridge between two fibers. However, **Figure 4.7** (e) demonstrates that this behavior is not observed for the thinnest fiber. That is because the fibers are wavy (**Figure 4.2** (e)) due to the large velocity difference between the core and sheath fluids and resulting instability.

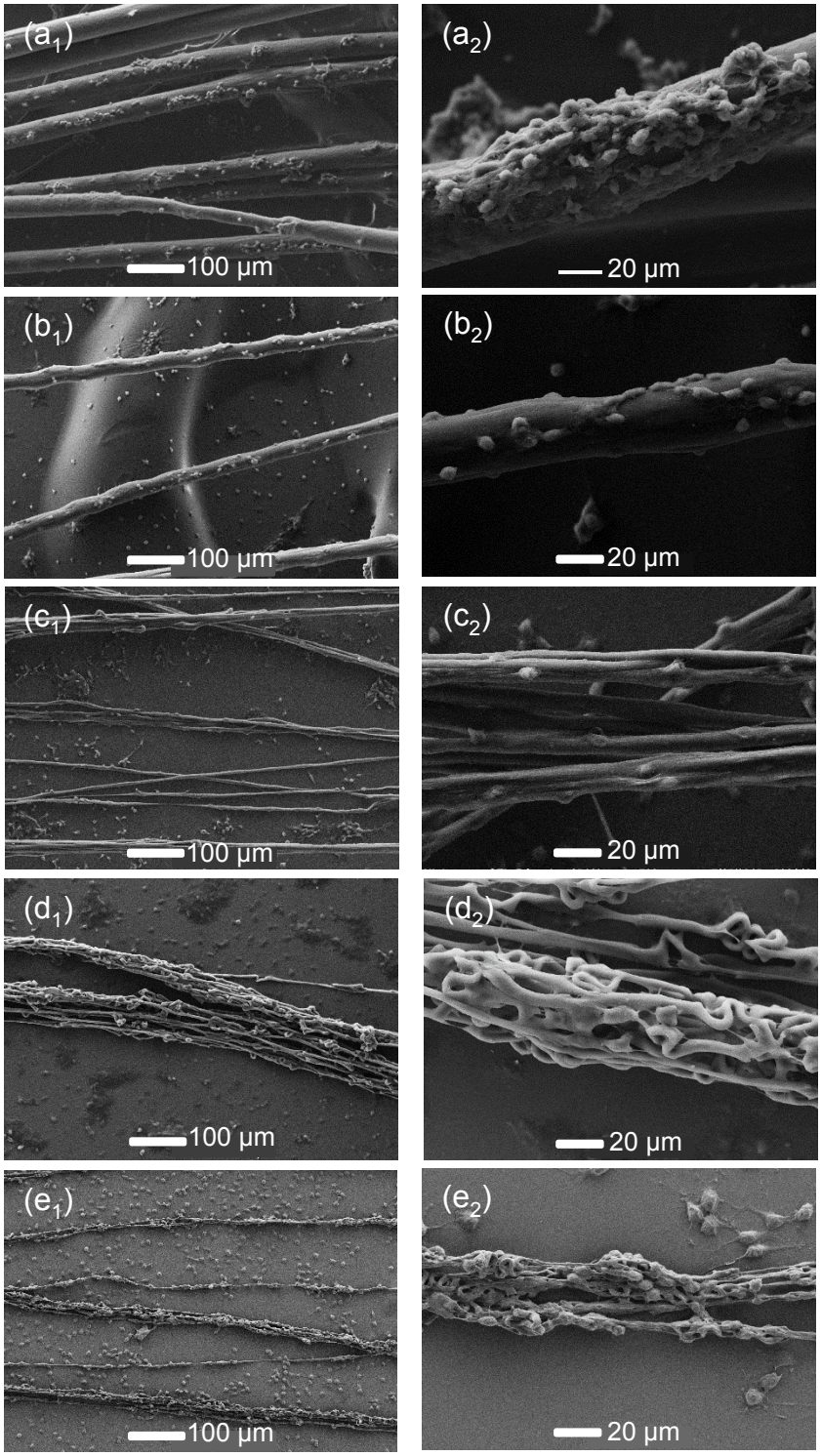

Figure 4.6 *SEM images of the AHPCs growing on PCL microfibrous scaffolds fabricated by using different sheath-to-core flow rates of (a) 20:5, (b) 60:5, (c) 200:4, and (d) 300:2. PCL and PEG concentrations are 5% in TFE and water/ethanol, respectively.*

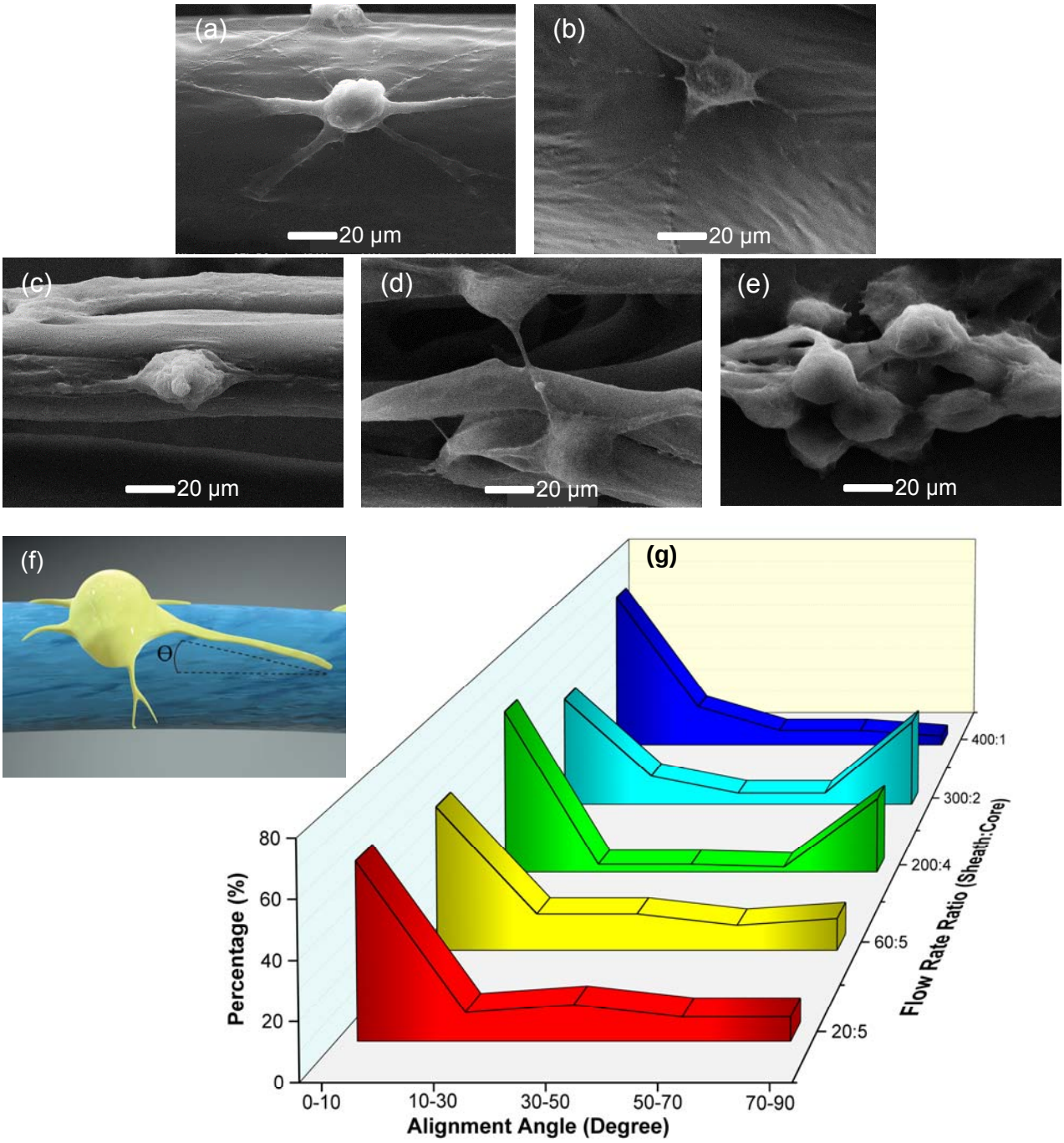

Figure 4.7 *(a–e) SEM images of the AHPCs cultured on the PCL microfibers. (f) Illustration of cell deviation angle. (g) Quantification of the neurite orientation on the fibers.*

It is possible that when placed in cell culture, the fibers become braided such that it is more difficult to separate the fibers from each other. When the fibers with the flow rate ratio of 400:1 are braided, a uniform bundle is created which allows more cells to attach on the surface due to increase surface area. Additionally, the empty space between the fibers may mimic a 3D microenvironment for the cells in order to allow nutrients to be exchanged to increase survival of cells. It can be observed that although this type of fiber is wavy and develop in different directions, the ultimate direction of all of the fibers are in the same direction. However, it was reported that the mechanical properties of the PCL fibers decrease with increasing flow rate ratio [25]. Therefore, if high mechanical properties are required, larger fibers are better choices for the PCL fibrous scaffolds that provide enough strength as well as a desirable microenvironment for aligning the cells. The neurite orientation on the fibers was analyzed quantitatively based on SEM images by measuring the cell deviation angle, which is the angle between the main axis of the cells and the fibers (**Figure 4.7** (f)). The results of measuring the cell deviation angle are shown in **Figure 4.7** (g). This figure demonstrates that the cell deviation angle is mostly less than 10° for fibers with different sizes, which reflects that the PCL microfibers were able to align the AHPCs efficiently along their axial directions. The percentage of the cells with deviation angle lower than 10° is 61%, 53%, 63%, 44%, and 66% for the fibers fabricated using the sheath-to-core flow rate ratio of 20:5, 60:5, 200:4, 300:2, and 400:1, respectively. The percentage of the cells with deviation angle larger than 10° decreases significantly. However, number of the cells with the cell deviation angle in the range of 70–90° increases to the maximum values of 29% and 35% on the fibers made by the sheath-to-core flow rate of 200:4 and 300:2, respectively due to cells bridging within the bundles of microfibers.

We continued this work to study the cell adhesion, survival, proliferation, and differentiation quantitatively. For this study, we fabricated fibers with different sizes (5 µm, 20 µm, and 35 µm) and shapes (straight and wavy). **Table 4.1** shows the PCL concentration and flow rate ratio between the core and sheath fluids, used to fabricate fibers with different characteristics.

Table 4.1 *PCL fibers with different characteristics.*

PCL concentration (%)	Sheath-to core flow rate ratio (µL/min)	Diameter (µm)	Shape
5	200:2	5	Chain shape
2	150:10	20	Straight
5	150:5	20	Wavy
5	50:10	35	Straight
5	90:5	35	Wavy

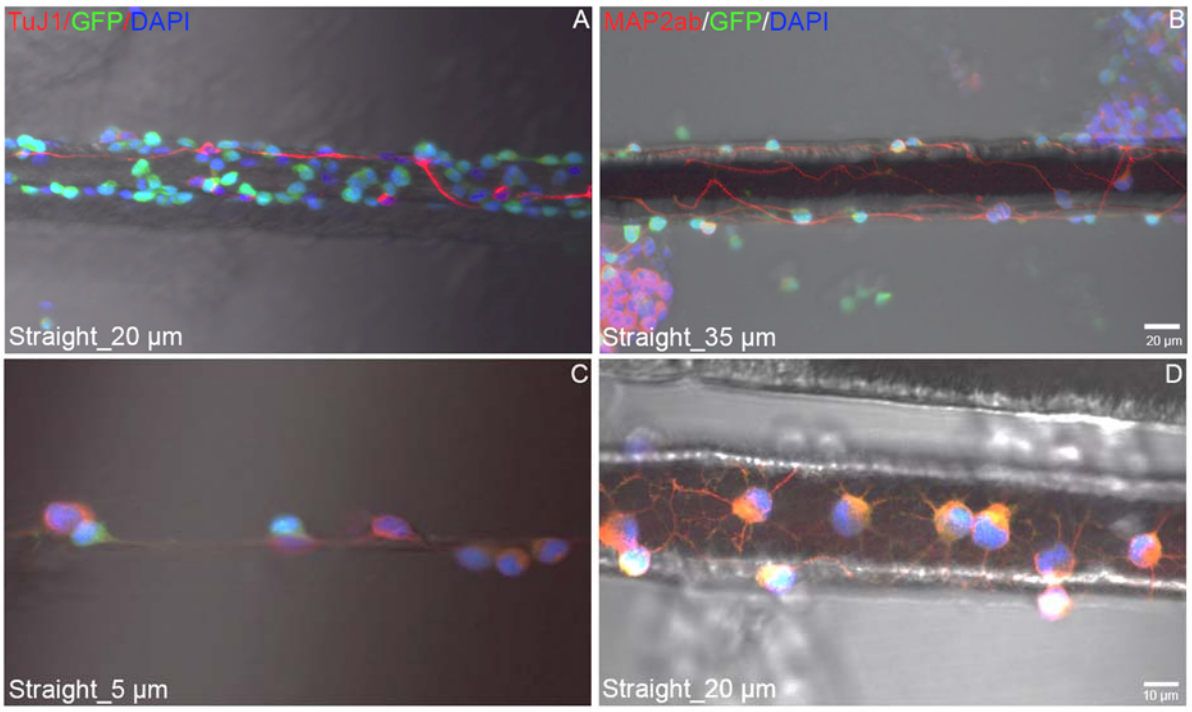

Figure 4.8 *AHPC's growing on PCL microfiber. (A,C) cultures were stained for TuJ1 (red), GFP (green) and DAPI (cell nuclei, blue) all merged with DIC. (B,D) cultures were stained for MAP2ab (red), GFP (green) and DAPI (cell nuclei, blue) all merged with DIC. Top row: 20 µm scale bar. Bottom row: 10 µm scale bar.*

Proliferating cells were immunolabeled with Ki67 antibody, neural progenitor/stem cells detected with Nestin antibody, neuronal cell differentiation characterized by TuJ1 and MAP2ab antibodies, and glial cell differentiation characterized by GFAP and RIP antibodies. **Figure 4.8** and **4.9** are microscopic images that indicate in more detail that the PCL microfibers support cell adhesion, survival, proliferation and differentiation of the AHPCs.

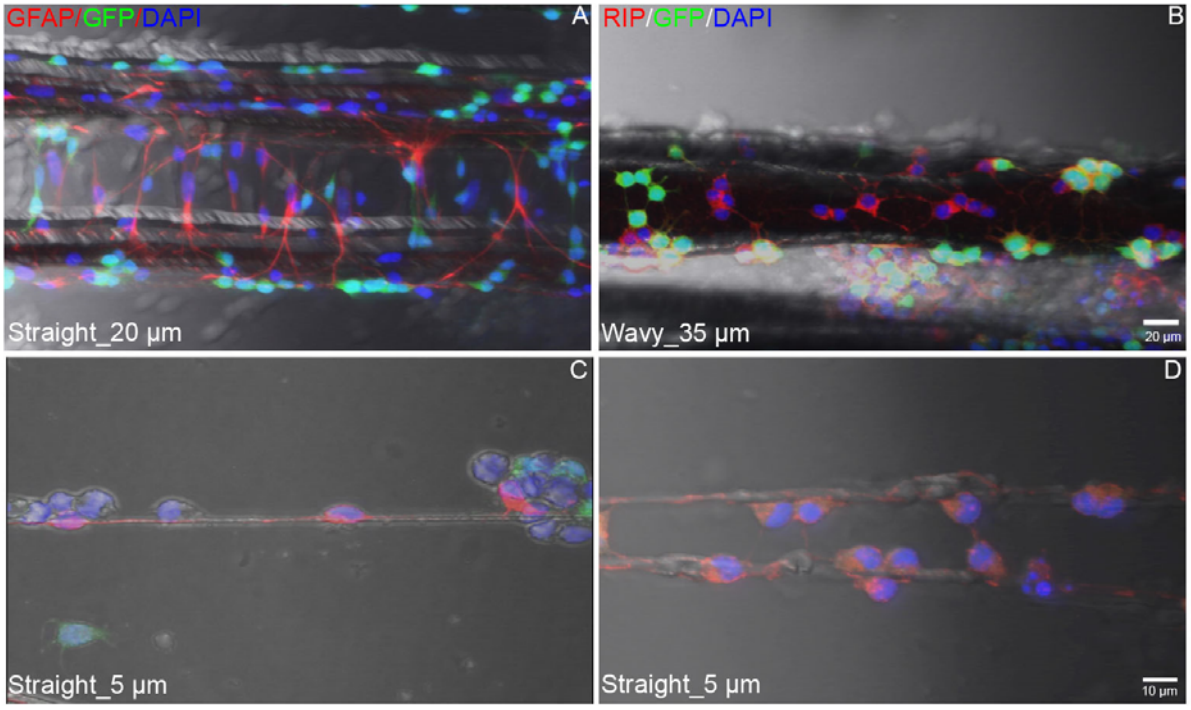

Figure 4.9 *AHPC's growing on PCL microfiber. (A,C) cultures were stained for GFAP (red), GFP (green) and DAPI (cell nuclei, blue) all merged with DIC. (B,D) cultures were stained for RIP (red), GFP (green) and DAPI (cell nuclei, blue) all merged with DIC. Top row: 20 µm scale bar. Bottom row: 10 µm scale bar.*

Figure 4.10-4-12, show the quantitative results of cell adhesion, proliferation, and differentiation, respectively on PCL microfluidic-spun fibers for one replicate. It should be mentioned that this study aims to determine the most biocompatible PCL fiber by performing

three individual replicates. For the quantification, five different sites were imaged and analyzed. The results show that the 5 µm has the most cell adhesion. Wavy 35 µm shows more proliferation when compared to straight 35 µm fibers indicating fiber morphology may have an effect on cell proliferation. For glial differentiation, 5 µm, straight 20 µm, and wavy 35 µm are statistically significant compared to control.

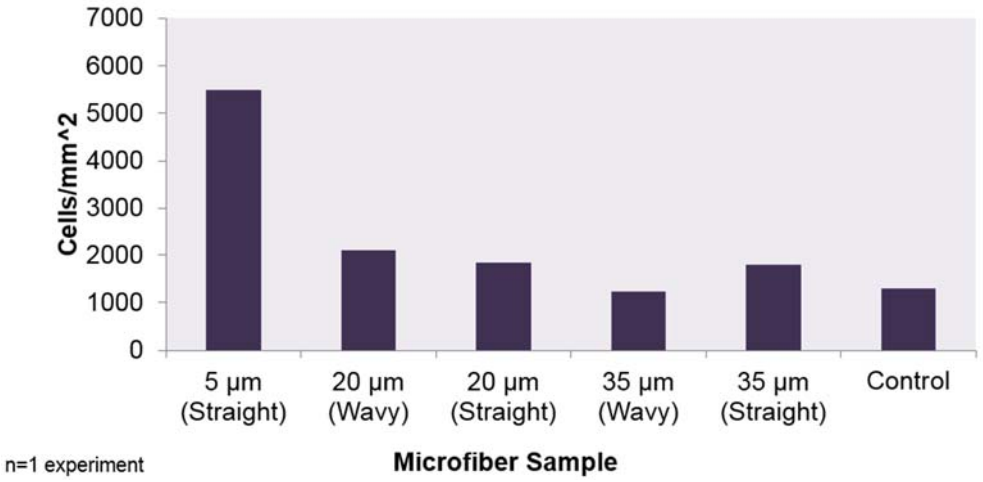

Figure 4.10 *Number of cells per mm^2 adhered to microfiber samples.*

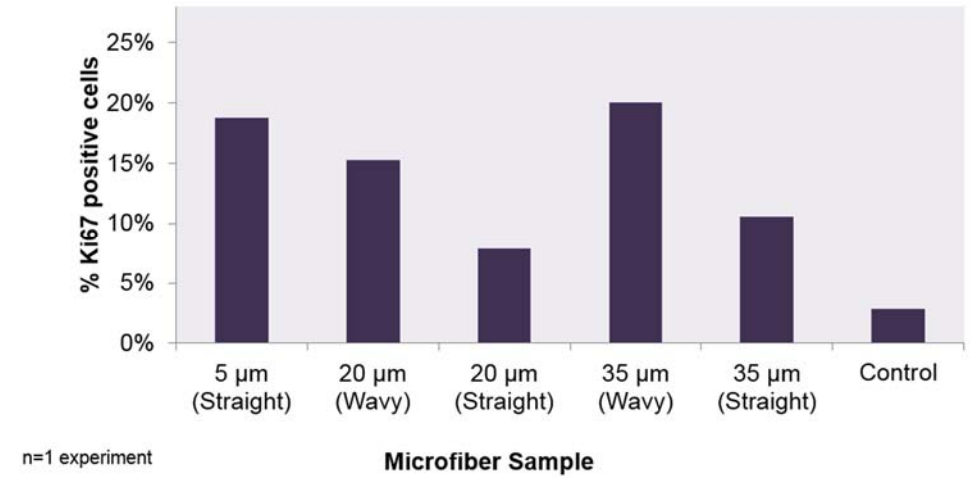

Figure 4.11 *Percentage of cells stained positive for Ki67 on PCL microfibers.*

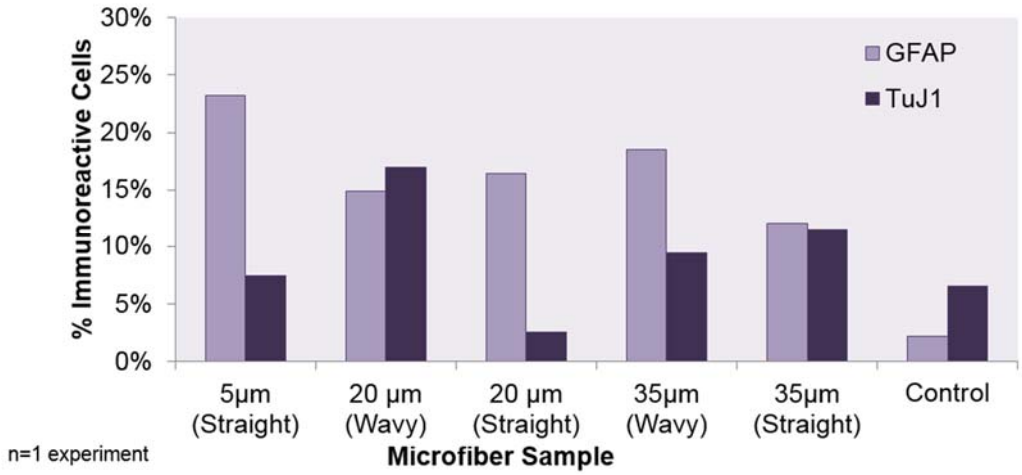

Figure 4.12 *Percentage of cells stained positive for neuronal marker (TuJ1) and glial marker (GFAP) on PCL fibers.*

4.4 Conclusions

Aligned PCL microfibers with different features were fabricated in this study using microfluidic fiber fabrication. The mean diameter of the fabricated fibers ranged from 2.6 to 36.5 µm by selecting the sheath-to-core flow rate ratio from 400:1 to 20:5. The mean deviation angles (±standard error) were found 3.95 ± 0.70, 4.64 ± 0.51, 3.84 ± 0.50, 4.39 ± 0.54, and 4.88 ± 0.62 for the sheath-to-core flow rates of 20:5, 60:5, 200:4, 300:2, and 400:1, respectively. The fibers were coated with a complex extracellular matrix substrate via physical absorption to facilitate cell attachment and for guiding the direction of AHPC growth in vitro. The results showed that the PCL fiber can be used as a fibrous scaffold which is not cytotoxic to the AHPCs, and supports cell adhesion, differentiation, and proliferation. Additionally, it was shown that the clusters of these adult neural stem cells can be aligned using the PCL microfibers. The quantitative analysis demonstrated that the cell deviation angle for most of the cells guided by

different types of fibers was less than 10°. On average, 58% of the cells in all types of the fibers had a cell deviation angle less than 10°, revealing the functionality and potential of the PCL microfibers for guiding nerve regeneration within the central (CNS) and peripheral nervous system (PNS) and may facilitate repair of spinal cord injuries (SCI) and peripheral nerve injuries (PNI). This integration of multiple cues within a 3D context is important for gaining a better understanding in regulating neural stem cell differentiation and in designing scaffolds for neural tissue engineering. Additionally, the PCL fibers with different sizes and shapes (straight and wavy), were used to quantitatively analyze the cell adhesion, proliferation, and differentiation. Our first replicate showed that 5 μm had the most cell adhesion; the 5 μm, straight 20 μm, and wavy 35 μm provided significantly better condition for the glial differentiation compared to control. More cell proliferation was observed on the wavy 35 μm fibers when compared to straight 35 μm fibers, showing that fiber morphology may have an effect on cell proliferation. However, this study goals to do two more replicates in order to have more reliable results.

In addition, we are currently implanting bundles of PCL microfibers into conduits, and the preliminary results suggest that this approach may aid in regeneration of severed nerve injuries. By mimicking the microenvironment of the nervous system, regeneration can be enhanced due to biological and chemical cues in the environment. Using conduits with PCL microfiber bundles can be investigated for various regeneration strategies including central nervous system diseases in order to repair a damaged system. In addition, the PCL fibers can be applied in regeneration of other tissues such as muscle, tendons, and blood vessels.

REFERENCES

[1] Langer R, Vacanti J. Tissue engineering. Science. 1993;260:920-6.

[2] Caplin JD, Granados NG, James MR, Montazami R, Hashemi N. Microfluidic Organ-on-a-Chip Technology for Advancement of Drug Development and Toxicology. Advanced Healthcare Materials. 2015;4:1426-50.

[3] Andersson H, Berg Avd. Microfabrication and microfluidics for tissue engineering: state of the art and future opportunities. Lab on a Chip. 2004;4:98-103.

[4] Khademhosseini A, Langer R, Borenstein J, Vacanti JP. Microscale technologies for tissue engineering and biology. Proceedings of the National Academy of Sciences of the United States of America. 2006;103:2480-7.

[5] Daniele MA, Boyd DA, Adams AA, Ligler FS. Microfluidic Strategies for Design and Assembly of Microfibers and Nanofibers with Tissue Engineering and Regenerative Medicine Applications. Advanced Healthcare Materials. 2015;4.

[6] Deshayes S, Kasko AM. Polymeric biomaterials with engineered degradation. Journal of Polymer Science Part a-Polymer Chemistry. 2013;51:3531-66.

[7] Acar H, Çınar S, Thunga M, Kessler MR, Hashemi N, Montazami R. Study of Physically Transient Insulating Materials as a Potential Platform for Transient Electronics and Bioelectronics. Advanced Functional Materials. 2014;24:4135-43.

[8] Schmidt CE, Leach JB. Neural Tissue Engineering: Strategies for Repair and Regeneration. Annual Review of Biomedical Engineering. 2003;5:293-347.

[9] Hurtado A, Cregg JM, Wang HB, Wendell DF, Oudega M, Gilbert RJ, et al. Robust CNS regeneration after complete spinal cord transection using aligned poly-l-lactic acid microfibers. Biomaterials. 2011;32:6068-79.

[10] Song HJ, Stevens CF, Gage FH. Neural stem cells from adult hippocampus develop essential properties of functional CNS neurons. Nature Neuroscience. 2002;5:438-45.

[11] Agarwal S, Wendorff JH, Greiner A. Use of electrospinning technique for biomedical applications. Polymer. 2008;49:5603-21.

[12] Schnell E, Klinkhammer K, Balzer S, Brook G, Klee D, Dalton P, et al. Guidance of glial cell migration and axonal growth on electrospun nanofibers of poly-ε-caprolactone and a collagen/poly-ε-caprolactone blend. Biomaterials. 2007;28:3012-25.

[13] Ghasemi-Mobarakeh L, Prabhakaran MP, Morshed M, Nasr-Esfahani MH, Ramakrishna S. Electrospun poly(epsilon-caprolactone)/gelatin nanofibrous scaffolds for nerve tissue engineering. Biomaterials. 2008;29:4532-9.

[14] Cooper A, Bhattarai N, Zhang M. Fabrication and cellular compatibility of aligned chitosan–PCL fibers for nerve tissue regeneration. Carbohydrate Polymers. 2011;85:149-56.

[15] Nisbet DR, Yu LMY, Zahir T, Forsythe JS, Shoichet MS. Characterization of neural stem cells on electrospun poly(ε-caprolactone) submicron scaffolds: evaluating their potential in neural tissue engineering. Journal of Biomaterials Science, Polymer Edition. 2008;19:623-34.

[16] Daud MFB, Pawar KC, Claeyssens F, Ryan AJ, Haycock JW. An aligned 3D neuronal-glial co-culture model for peripheral nerve studies. Biomaterials. 2012;33:5901-13.

[17] Gnavi S, Fomasari BE, Tonda-Turo C, Ciardelli G, Zanetti M, Geuna S, et al. The influence of electrospun fibre size on Schwann cell behaviour and axonal outgrowth. Materials Science & Engineering C-Materials for Biological Applications. 2015;48:620-31.

[18] Kador KE, Montero RB, Venugopalan P, Hertz J, Zindell AN, Valenzuela DA, et al. Tissue engineering the retinal ganglion cell nerve fiber layer. Biomaterials. 2013;34:4242-50.

[19] Jung JH, Choi CH, Chung S, Chung YM, Lee CS. Microfluidic synthesis of a cell adhesive Janus polyurethane microfiber. Lab on a Chip. 2009;9:2596-602.

[20] Siriwardane ML, DeRosa K, Collins G, Pfister BJ. Controlled formation of cross-linked collagen fibers for neural tissue engineering applications. Biofabrication. 2014;6.

[21] Han L-H, Yu S, Wang T, Behn AW, Yang F. Microribbon-Like Elastomers for Fabricating Macroporous and Highly Flexible Scaffolds that Support Cell Proliferation in 3D. Advanced Functional Materials. 2013;23:346-58.

[22] Leonor IB, Rodrigues MT, Gomes ME, Reis RL. In situ functionalization of wet-spun fibre meshes for bone tissue engineering. Journal of Tissue Engineering and Regenerative Medicine. 2011;5:104-11.

[23] Bai Z, Reyes JMM, Montazami R, Hashemi N. On-chip development of hydrogel microfibers from round to square/ribbon shape. Journal of Materials Chemistry A. 2014;2:4878-84.

[24] Hashemi N, Lackore JM, Sharifi F, Goodrich PJ, Winchell ML, Hashemi N. A paper-based microbial fuel cell operating under continuous flow condition. TECHNOLOGY. 2016;04:98-103.

[25] Sharifi F, Kurteshi D, Hashemi N. Designing highly structured polycaprolactone fibers using microfluidics. Journal of the Mechanical Behavior of Biomedical Materials. 2016;61:530-40.

[26] Sharifi F, Bai Z, Montazami R, Hashemi N. Mechanical and physical properties of poly(vinyl alcohol) microfibers fabricated by a microfluidic approach. RSC Advances. 2016;6:55343-53.

[27] Sharifi F, Patel BB, Dzuilko AK, Montazami R, Sakaguchi DS, Hashemi N. Polycaprolactone Microfibrous Scaffolds to Navigate Neural Stem Cells. Biomacromolecules. 2016.

[28] Goodrich PJ, Sharifi F, Hashemi N. Rapid prototyping of microchannels with surface patterns for fabrication of polymer fibers. RSC Advances. 2015;5:71203-9.

[29] Sharifi F, Ghobadian S, Cavalcanti FR, Hashemi N. Paper-based devices for energy applications. Renewable and Sustainable Energy Reviews. 2015;52:1453-72.

[30] Shi X, Ostrovidov S, Zhao Y, Liang X, Kasuya M, Kurihara K, et al. Microfluidic Spinning of Cell-Responsive Grooved Microfibers. Advanced Functional Materials. 2015;25:2250-9.

[31] Daniele MA, Adams AA, Naciri J, North SH, Ligler FS. Interpenetrating networks based on gelatin methacrylamide and PEG formed using concurrent thiol click chemistries for hydrogel tissue engineering scaffolds. Biomaterials. 2014;35:1845-56.

[32] Jun Y, Kang E, Chae S, Lee SH. Microfluidic spinning of micro- and nano-scale fibers for tissue engineering. Lab on a Chip. 2014;14:2145-60.

[33] Daniele MA, Radom K, Ligler FS, Adams AA. Microfluidic fabrication of multiaxial microvessels via hydrodynamic shaping. Rsc Advances. 2014;4:23440-6.

[34] Hwang CM, Khademhosseini A, Park Y, Sun K, Lee S-H. Microfluidic Chip-Based Fabrication of PLGA Microfiber Scaffolds for Tissue Engineering. Langmuir. 2008;24:6845-51.

[35] Daniele MA, North SH, Naciri J, Howell PB, Foulger SH, Ligler FS, et al. Rapid and Continuous Hydrodynamically Controlled Fabrication of Biohybrid Microfibers. Advanced Functional Materials. 2013;23:698-704.

[36] Lin YS, Huang KS, Yang CH, Wang CY, Yang YS, Hsu HC, et al. Microfluidic Synthesis of Microfibers for Magnetic-Responsive Controlled Drug Release and Cell Culture. Plos One. 2012;7:8.

[37] Hasani-Sadrabadi MM, VanDersarl JJ, Dashtimoghadam E, Bahlakeh G, Majedi FS, Mokarram N, et al. A microfluidic approach to synthesizing high-performance microfibers with tunable anhydrous proton conductivity. Lab on a Chip. 2013;13:4549-53.

[38] Raof NA, Padgen MR, Gracias AR, Bergkvist M, Xie YB. One-dimensional self-assembly of mouse embryonic stem cells using an array of hydrogel microstrands. Biomaterials. 2011;32:4498-505.

[39] Kang E, Jeong GS, Choi YY, Lee KH, Khademhosseini A, Lee SH. Digitally tunable physicochemical coding of material composition and topography in continuous microfibres. Nature Materials. 2011;10:877-83.

[40] Choi CH, Yi H, Hwang S, Weitz DA, Lee CS. Microfluidic fabrication of complex-shaped microfibers by liquid template-aided multiphase microflow. Lab on a Chip. 2011;11:1477-83.

[41] Jung J-H, Choi C-H, Chung S, Chung Y-M, Lee C-S. Microfluidic synthesis of a cell adhesive Janus polyurethane microfiber. Lab on a Chip. 2009;9:2596-602.

[42] Boyd DA, Shields AR, Howell PB, Ligler FS. Design and fabrication of uniquely shaped thiol-ene microfibers using a two-stage hydrodynamic focusing design. Lab on a Chip. 2013;13:3105-10.

[43] Cho S, Shim TS, Yang SM. High-throughput optofluidic platforms for mosaicked microfibers toward multiplex analysis of biomolecules. Lab on a Chip. 2012;12:3676-9.

[44] Kang E, Choi YY, Chae S-K, Moon J-H, Chang J-Y, Lee S-H. Microfluidic Spinning of Flat Alginate Fibers with Grooves for Cell-Aligning Scaffolds. Adv Mater. 2012;24:4271-7.

[45] Patenaude M, Hoare T. Injectable, Mixed Natural-Synthetic Polymer Hydrogels with Modular Properties. Biomacromolecules. 2012;13:369-78.

[46] Middleton JC, Tipton AJ. Synthetic biodegradable polymers as orthopedic devices. Biomaterials. 2000;21:2335-46.

[47] Mahapatro A, Singh DK. Biodegradable nanoparticles are excellent vehicle for site directed in-vivo delivery of drugs and vaccines. Journal of Nanobiotechnology. 2011;9:1-11.

[48] Woodruff MA, Hutmacher DW. The return of a forgotten polymer—Polycaprolactone in the 21st century. Progress in Polymer Science. 2010;35:1217-56.

[49] Recknor JB, Sakaguchi DS, Mallapragada SK. Directed growth and selective differentiation of neural progenitor cells on micropatterned polymer substrates. Biomaterials. 2006;27:4098-108.

[50] Oh J, Daniels GJ, Chiou LS, Ye E-A, Jeong Y-S, Sakaguchi DS. Multipotent adult hippocampal progenitor cells maintained as neurospheres favor differentiation toward glial lineages. Biotechnology Journal. 2014;9:921-33.

[51] Gage FH, Coates PW, Palmer TD, Kuhn HG, Fisher LJ, Suhonen JO, et al. Survival and differentiation of adult neuronal progenitor cells transplanted to the adult brain. Proceedings of the National Academy of Sciences of the United States of America. 1995;92:11879-83.

[52] Hashemi N, Erickson JS, Golden JP, Jackson KM, Ligler FS. Microflow Cytometer for optical analysis of phytoplankton. Biosensors and Bioelectronics. 2011;26:4263-9.

[53] Hashemi N, Erickson JS, Golden JP, Ligler FS. Optofluidic characterization of marine algae using a microflow cytometer. Biomicrofluidics. 2011;5:032009.

[54] Hashemi N, Howell JPB, Erickson JS, Golden JP, Ligler FS. Dynamic reversibility of hydrodynamic focusing for recycling sheath fluid. Lab on a Chip. 2010;10:1952-9.

CHAPTER 5

DEVELOPMENT OF PHOTO-CROSS-LINKED POLY(ETHYLENE GLYCOL) DIACRYLATE HYDROGEL FROM SPHERICAL MICROPARTICLES TO BOW TIE-SHAPED MICROFIBERS VIA MICROFLUIDIC APPROACH

ABSTRACT

Poly(ethylene glycol) (PEGDA) hydrogel was photo-polymerized in a wide range of shapes via a microfluidic approach. In this work, we showed that with immiscible and miscible fluids, spherical microparticles and bow tie-shaped fibers can be fabricated using PEGDA. The flow rate ratio between the core and sheath fluids is found to be an important parameter in accurately tuning the diameter of the particles as well as cross-section and size of the fibers. Glucose, sucrose, collagen, gelatin, PEG, and PVA were incorporated into the PEGDA fibers to study the porosity of the resulting fibers. It was found that sucrose and PVA can create porosity on the surface of the fibers after soaking the fibers in water for 6 days at 37 °C. The tensile properties of the PEGDA fibers with different characteristics were tested. It was found that when the core flow rate increases, the resulting fibers become more stiff and brittle, which might be due to the increase of the cross-linking density. The mechanical properties of the PEGDA/collagen drop due to the low strength of the collagen, which is a natural polymer. On the other hand, the incorporation of glucose could improve the tensile properties of PEGDA fibers. In addition, we encapsulated the AHPCs into the PEGDA fibers in order to create a cell-laden fiber. Propidium Iodide (PI) was used for the cell viability, and the results showed that the cells could not survive.

We believe that another hydrogel or the same polymer with higher molecular weight needs to be used in order to increase the cell survival into the hydrogel network.

5.1 Introduction

Hydrogels are insoluble three-dimensional cross-linked networks made from hydrophilic polymer chains that swell in aqueous solutions [1, 2]. They can be used in a wide range of biomedical applications such as cell encapsulation [3-5], tissue engineering [6-8], wound dressing [9, 10], and drug delivery [11-13] due to their high biocompatibility and versatile mechanical properties. Additionally, the transport of oxygen, nutrients and other water-soluble metabolites is efficient through the hydrogel network, which diminishes buildup of acid products in the hydrogels and makes them good candidates to be used as scaffolds in tissue engineering [14, 15].

There are various methods for synthesizing physical and chemical hydrogels [16]. Photopolymerization is a biocompatible strategy used for creating chemical hydrogels because they can be formed *in situ*, and a minimum invasive environment is created [17]. There is no need for high or low temperatures, which can be important when the biological micro-molecules such as cells, bacteria, and enzymes are incorporated into the prepolymer solution [18, 19]. In this process, liquid monomers or macromeres can be photopolymerized in the presence of photoinitiators via visible or ultraviolet (UV) light both *in vivo* and *in vitro*.

Microfluidics is an emerging area in both science and technology since it uses small amounts of material and can play astounding roles in a wide range of areas such as biomedical areas, optics, and energy systems [20-27]. This approach can be used to fabricate polymeric materials with various shapes such as particles and fibers [19, 28-33]. The microfluidic

particle/fiber fabrication is a cost-effective, simple, and highly biocompatible platform. Change in environmental condition such as temperature or pressure is not needed in this method. Additionally, the other advantage of this approach is its versatility, which makes it feasible to accurately obtain different sizes, microstructures, and morphologies and tune the mechanical properties within a desirable range [22, 23, 34, 35]. One of the solidification strategies used in microfluidic particle/fiber fabrication is the aforementioned photopolymerization. The advantage of this approach is that the polymerization happens in a fraction of a second, which could be useful for the conditions in which microsctructures with accurate patterns are desirable [33].

Poly(ethylene glycol) diacrylate (PEGDA) is used in various biomedical applications due to its high biocompatibility. It is one of the derivatives of PEG that contains acrylate group in its chain, which makes it possible to form chemical hydrogel via crosslinking reaction. PEGDA has been used in microfluidic particle/fiber fabrication [33, 36, 37]. In this work, we apply the microfluidic approach to fabricate both PEGDA spherical particles and ribbon shaped fibers using immiscible and miscible fluids, respectively. The bow tie shaped fibers have been fabricated using the microfluidic platform [34, 38-40]. However, the application of this type of fiber has been kept unclear. We encapsulated Adult hippocampal progenitor cells (AHPCs) into the PEGDA fibers, but the cells did not survive in the hydrogel network. We believe that the grooves embedded on the surface of the fibers can play a significant role in aligning the cells in one direction, which has applications in nerve tissue engineering. Additionally, we could be able to obtain a wide range of mechanical properties by changing the flow rate ratio between the core and sheath fluid as well as incorporating different contents of glucose and alginate into the core fluid.

5.2 Experimental Section

5.2.1 Materials

Poly(ethylene glycol) diacrylate (PEGDA) (Mn=575), polyethylene glycol (PEG) (M_n = 20 000) were purchased from Sigma-Aldrich (St. Louis, MO). Irgacure 2959 was obtained from Hidley & Peto Company.

5.2.2 Microfluidic channel

A SU8 photoresist-patterned silicon wafer was applied as a mold and the channel was made using soft lithography. We used two silicon wafers in order to create the pattern of the microchannel and the chevron grooves extended from two sides of the channel. The dimensions of the microchannel are 130 μm × 390 μm (height × width). The microchannel has four diagonal grooves with dimensions of 130 μm × 100 μm (height × width) and are spaced 200 μm apart. Polydimethylsiloxane (PDMS), which is a biocompatible and transparent elastomer, was made from the mixture of Sylgard 184 elastomer base and cross-linker agents in a 10:1 ratio. Then, the mixture was poured onto the mold, and cured with the temperature of 85 °C for 25 min. After that, the PDMS layer on the silicon wafers were peeled off and the layers were bonded together using plasma treatment.

5.2.3 Microfluidic particle/fiber fabrication

The core fluid was made by mixing different concentrations of PEGDA and Irgacure 2959 (PI) with deionized (DI) water and ethanol at room temperature. For the particle fabrication, the core fluid consists of 60 v% PEGDA, 40 v% ethanol, and 8 w% Irgacure 2959. We used mineral

oil for the sheath and bath, which is immiscible to the core fluid. On the other hand, miscible fluids were used for fiber fabrication. For the core fluid, we used 30 v% PEGDA, 40 v% DI water, and 2 w% Irgacure 2959. We used 5 w% PEG solution (PEG in DI water) for the sheath fluid and DI water for the bath. The solutions were introduced into the microchannel via a double syringe pump (Cole-Parmer, Veron Hillss, IL) with different flow rates. The microchannel was vertically positioned into a water bath.

5.2.4 Characterization and imaging

Fluorescent images were conducted using a fluorescence microscope (Nikon Microphot FXA, Nikon, Inc.), equipped with a Retiga 2000R digital camera controlled by QCapture software (QImaging). Images were pseudocolored using Adobe Photoshop CC. Scanning electron microscopy (SEM; JCM-6000 NeoScope Benchtop scanning electron microscope) was applied to study the size and morphology of the particles and fibers. In order to acquire high quality SEM images, the substrates were made conductive using gold sputter-coating. The coating thickness of the samples was around 50 nm. The cross sections of the ribbon shaped fibers were measured using the SEM images and ImageJ, which is an imaging analysis software. For measuring the stress–strain behavior of the fibers, single fiber was tested using Instron Universal Testing machine (Model 5569, Instron Engineering Corp., Canton, MA). For each type of the fibers, 10 samples were tested and the average values for each type were reported. Since the PCL fibers have high ductility, we used a 10 N load cell to get enough resolution, and the extension rate was set to 20 mm/min. In this test, the samples were prepared by attaching them on a paper frame in order to be gripped properly by the Instron machine. After mounting the sample on the machine, we cut two sides of the frame to get the mechanical properties of PCL fiber. The length of the samples for

this test was 15 mm. The results were found using Bluehill software. A video file is provided in supplementary materials, that shows high ductility of the fiber during the tensile test. The stress–strain curves were fitted with linear line for the elastic region. Second order polynomial equation was used for the plastic region because its coefficient of determination (R-Square) was better compared to the linear line for all of the data.

5.2.5 Cell culture

Adult hippocampal progenitor cells (AHPCs) were originally isolated from adult Fischer 344 rats and infected with a retrovirus to express green fluorescence protein (GFP) as described previously and were a generous gift from F. H. Gage (Salk Institute for Biological Sciences, La Jolla, CA) [41]. Cells were grown in flasks coated with poly-L-ornithine (10 μg mL^{-1}; Sigma-Aldrich) and purified mouse laminin (5 μg mL^{-1}; R&D Systems) in Earle's balanced salt solution (EBSS). Maintenance media (MM) included Dulbecco's modified Eagle's medium/Ham's F-12 (DMEM/F-12, 1:1; Omega Scientific), supplemented with 2.5 mM L-glutamine, N2 supplement (Gibco BRL), and 20 ng mL^{-1} basic fibroblast growth factor (human recombinant bFGF; Promega Corporation). The AHPCs were detached from flasks using 0.05% trypsin–EDTA (Gibco BRL) and harvested by centrifugation at 800 rpm for 5 min. A hemocytometer was used to perform a Trypan Blue viable cell count, and AHPCs were plated at a density of 10 000 cells/cm^2 on PCL-microfiber substrates (see below). Cells were maintained at 37 °C in a 5% CO_2/95% humidified air atmosphere. For cell differentiation, AHPCs were cultured in growth medium lacking bFGF (referred to as differentiation medium, DM) for 7 days. Half of the media was changed every other day.

5.3 Results and Discussions

A schematic of the microfluidic particle/fiber fabrication is shown in **Figure 5.1** (a). We introduced both of the core and sheath fluid into the 3 inlet microchannel. The flow regime is laminar and the diffusion takes place at the interface. The microchannel consists of two main regions: the nozzle (upstream) and four chevrons (downstream), and the polymerization occurs at the outlet of the channel. **Figure 5.1** (b) demonstrates the photo-polymerization process of PEGDA hydrogel. The photoinitiator absorbs UV light and creates free radicals, which react with PEGDA macromers and break the carbon-carbon bond. Then, the reactive PEGDA macromers connect with each other and form a large molecule. For the particle fabrication, sheath fluid is wrapped around the core fluid at the beginning of the chevron area due to the high hydrophobicity of the mineral oil. On the other hands, the fiber fabrication process has some differences due to the fact that miscible fluids are used. In this process, the sheath fluid focuses the core fluid laterally. The focusing force is originated from the shear force that arises from velocity gradient at the interface between the core and sheath fluid. At the end of nozzle region, the core fluid changes to a vertical thin strip. Then, the sheath fluid fills the chevron areas and exerts vertical force on the core fluid. In the chevron region, the hydrodynamic resistance perpendicular to the flow direction decreases. The reason that the sheath fluid goes into the chevron areas is that the hydrodynamic resistance is inversely dependent on the flow rate. Because the sheath fluid has a higher flow rate in this experiment, it will experience less resistance compared to the core fluid. This means that the sheath fluid fills the top and bottom of the channel and wraps around the core fluid, and exerts vertical force as well as lateral force, such that the core fluid is placed at the center of the channel.

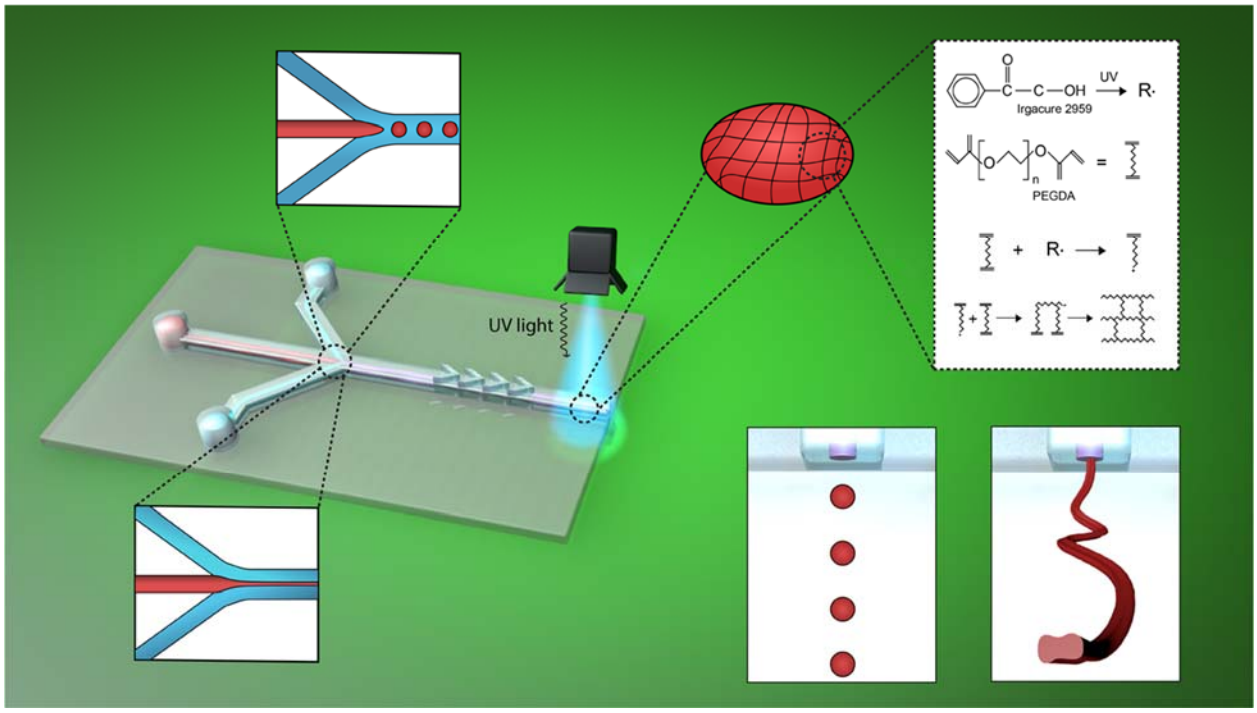

Figure 5.1 *(a) Schematic of the microfluidic particle/fiber fabrication using photopolymerization strategy. (b) The photopolymerization process of PEGDA hydrogels.*

5.3.1 Microfluidic PEGDA particle fabrication

The experimental set-up for the fabrication of spherical particles is shown in **Figure 5.2** (a). The microchannel is vertically positioned and the UV light with the intensity of 340 mW is irradiating at the outlet of the channel. The SEM images of one of the particles, which is depicted in **Figure 5.2** (b), shows the symmetric shape of the spherical particles. The effect of flow rate ratio on the diameter (±standard error) of the particles is demonstrated in **Figure 5.2** (c). This figure shows that a wide range of diameter could be created simply by changing the flow rate ratio between the two fluids. When the shear-to-core flow rate ratio decreases from 50:2 to 100:8, the diameter of the particles increases by a factor of 4.6. Additionally, the low standard errors demonstrates the uniformity of the particles.

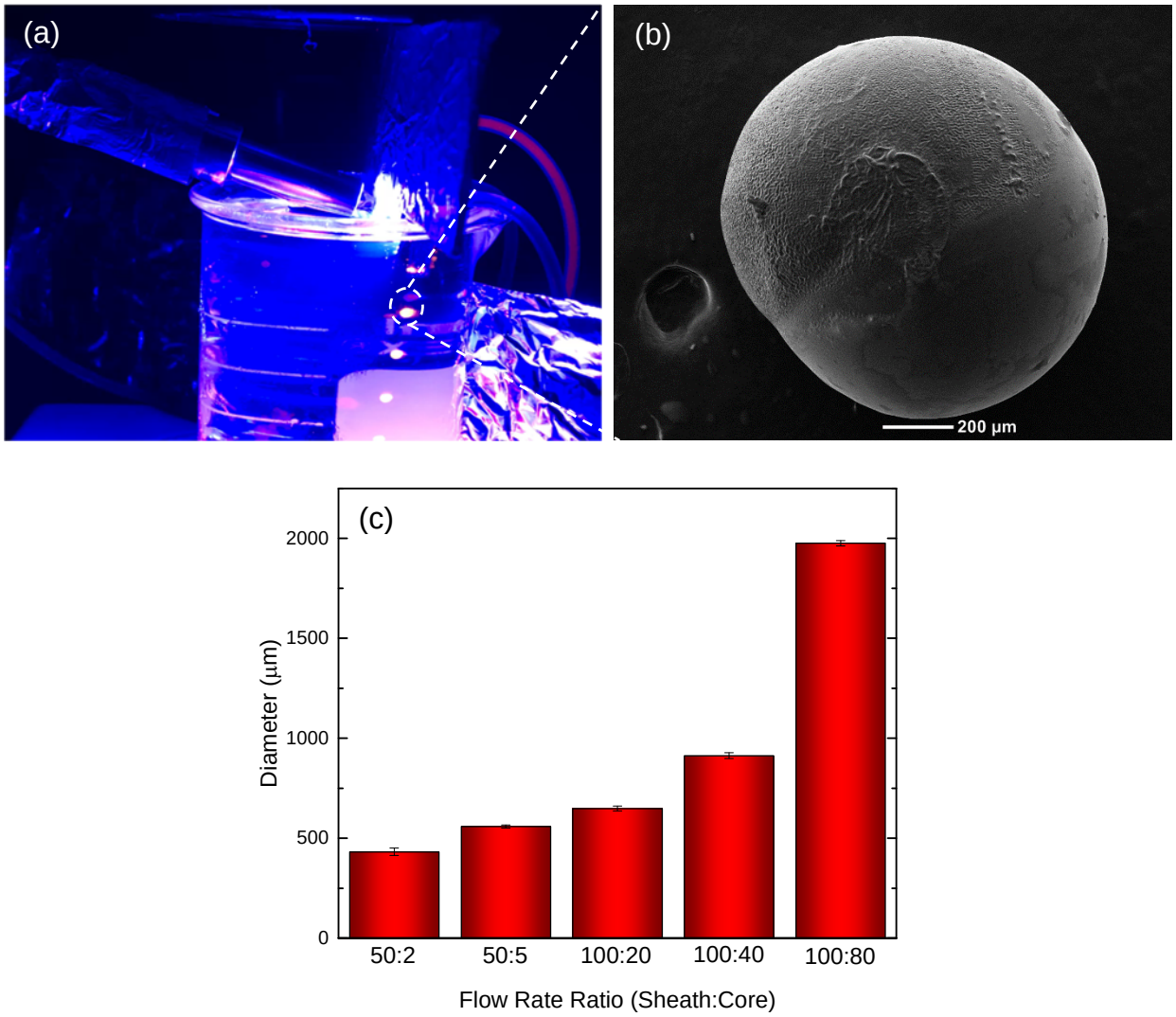

Figure 5.2 *Microfluidic spherical PEGDA particle fabrication. (a) Experimental set-up: the microchannel is vertically positioned and the UV light is irradiating at the outlet of the channel. (b) SEM image of a particle made by the sheath-to-core flow rate of 100:40. (c) The diameter of the particles made by different flow rate ratios.*

5.3.2 Microfluidic PEGDA fiber fabrication

Miscible fluids were applied in order to create a continuous core flow, which can be polymerized as the microfibers. **Figure 5.3** (a) shows the experimental set-up and the continuity of the PEGDA microfiber fabrication. One of the advantages of using ultraviolet light is the rapid

polymerization that help design and fix fibers with various noncircular cross-sections. On the other hand, in other solidification methods such as phase inversion or chemical cross-linking, the cross-section of the fibers are affected by the surface tension in the two-phase systems due to their slow solidification rates. The SEM image of the PEGDA fibers with longitudinal view is shown in **Figure 5.3** (b). This figure demonstrates that there is no shape gradient across the length of the fiber. The SEM images of the cross-section of the fibers fabricated with different flow rate ratios are depicted in **Figure 5.3** ($c_{1,2}$-$f_{1,2}$). In these figures, the effect of hydrodynamic focusing force from the sheath fluid to the core fluid in both lateral and vertical directions can be clearly observed. The roughness of the fibers made by different flow rates are negligible due to the rapid polymerization process, which minimizes the diffusion at the fluid/fluid interface.

The results of quantitative analysis on the size of the PEGDA fibers are demonstrated in **Figure 5.3** (g). This figure shows that the width of the fiber increases as the sheath-to-core flow rate ratio decreases from 100:40 to 100:100. That was expected, because when the flow rate ratio reduces, the velocity gradient at the interface decreases, which results in the weakening of the lateral shear force exerted on the core fluid from the sheath fluid. Consequently, the core fluid expands laterally in the channel, which results in the fabrication of fibers with higher width. When the flow rate ratio decreases from 2.5 to 1, for instance, the width of the PEGDA fiber increases by 42%. However, the height of the fibers does not change significantly due to the fact that the height of the fiber is dependent on the vertical force on the core fluid from the sheath fluid. The vertical hydrodynamic force is mostly dependent on the number of the chevrons, which were kept constant in this study [42]. Additionally, the microfluidic fiber fabrication process was simulated using COMSOL Multiphysics. Both of the Stoke's and Fick's equations were solved in order to obtain concentration distributions of the core and sheath fluid along the channel. **Figure 5.3** (c_3-f_3) shows

the concentration distribution of the core and sheath fluids at the outlet of the channel. The red and blue colors represent the core and sheath fluids, respectively. The results demonstrated the same behavior as the experimental result, which reflects consistency between the numerical and experimental results.

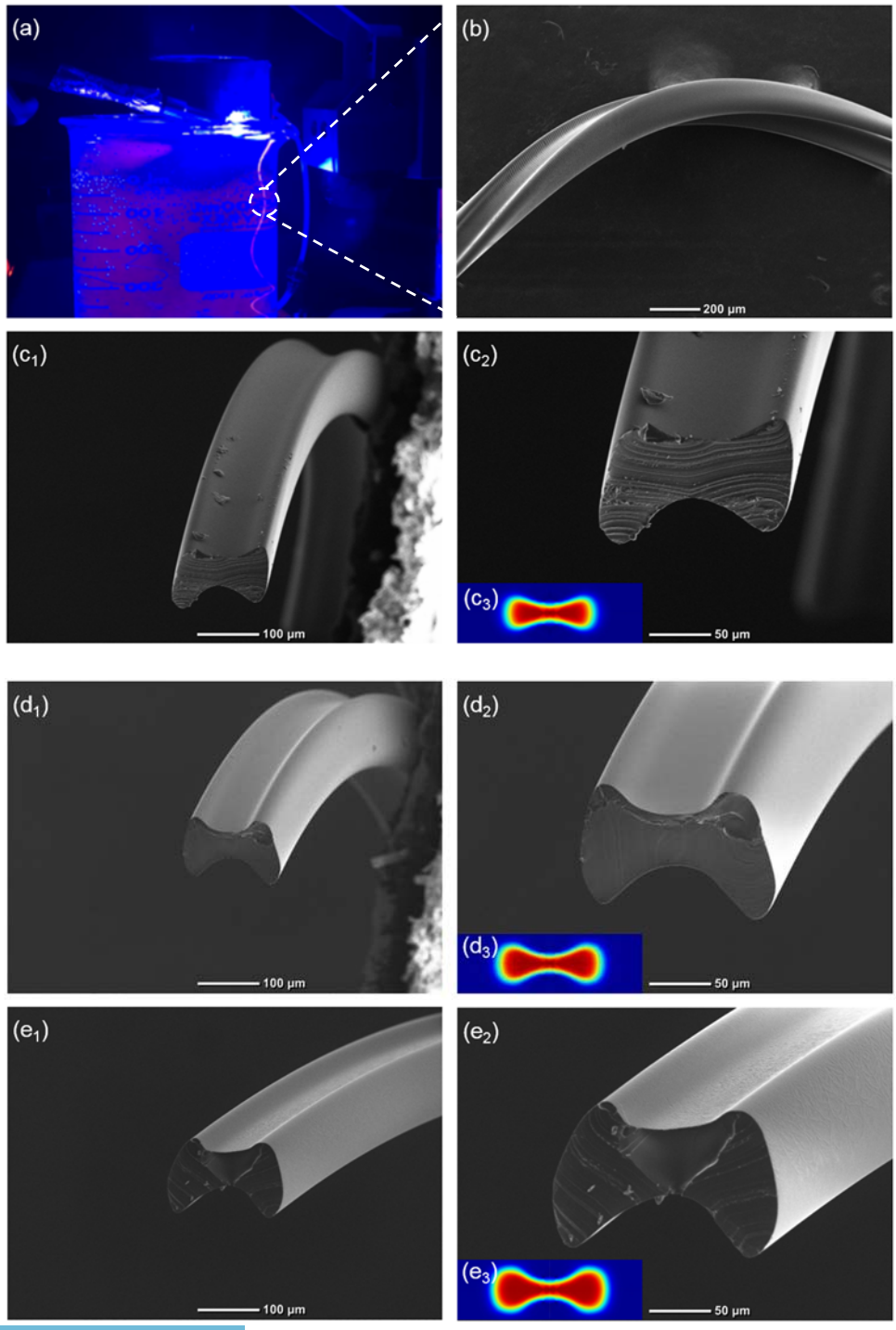

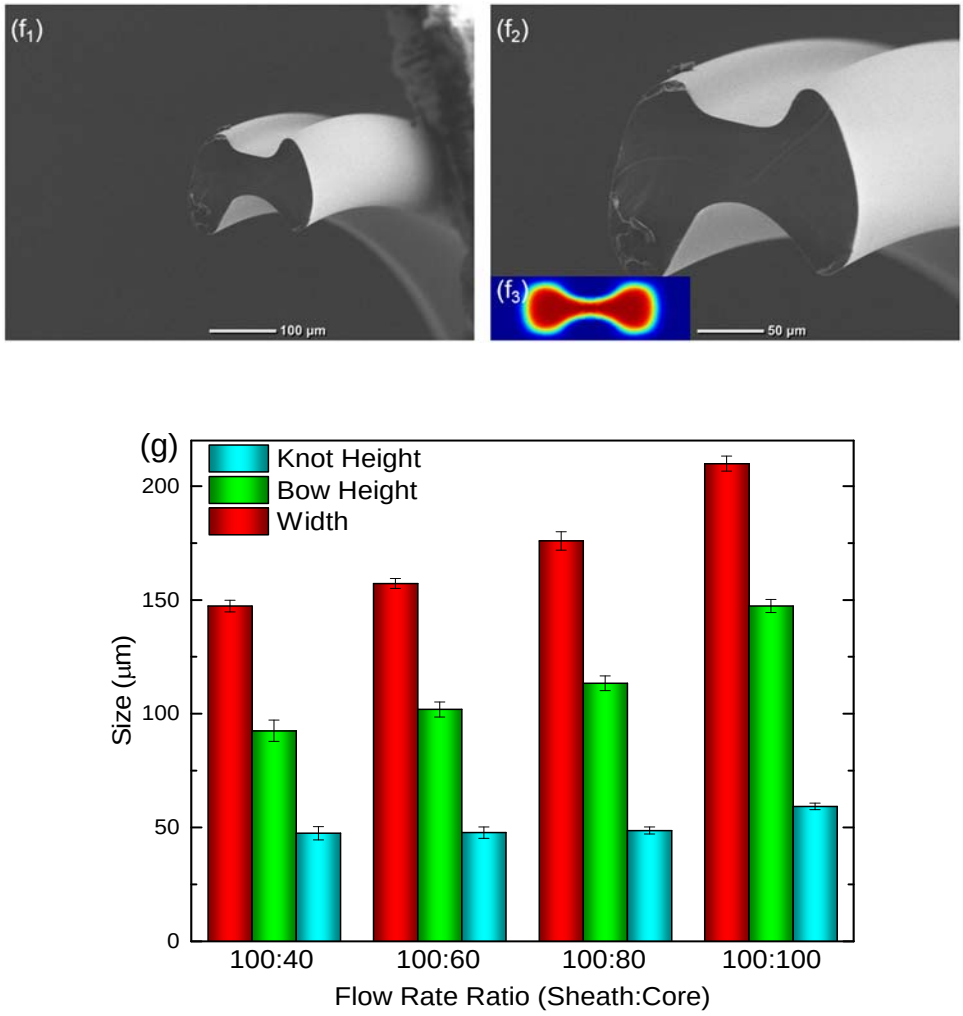

Figure 5.3 *Microfluidic PEGDA fiber fabrication. (a) The experimental set-up, which is similar to the set-up used for particle fabrication. (b) The longitudinal SEM image of the PEGDA fibers made by the sheath-to-core flow rate of 100:100 μL/min. ($c_{1,2}$-$f_{1,2}$) The cross-section SEM images of the fibers made by different flow rates of 100:40 μL/min to 100:100 μL/min, respectively. (c_3-f_3) The numerical results made by simulating the microfluidic fiber fabrication. (g) Dimensions of the PEGDA fibers made by different sheath-to-core flow rate ratios.*

Because fibers have a higher surface to volume ratio than the spherical particles, they can play more effective roles in biomedical applications like tissue engineering. In addition, lower UV intensity is needed to polymerize the microfibers compared to the spherical particles, which is

an advantage when biological molecules, such as cells or bacteria, are incorporated into the process.

5.3.3 Mechanical properties of the PEGDA microfibers

The mechanical properties of the PEGDA microfibers with different characteristics were studied in this work. The effect of flow rate ratio between the core and sheath fluids on the mechanical properties were investigated. Additionally, we incorporated collagen and glucose into the PEGDA fibers to study their influence on the tensile properties of the resulting fibers. Collagen is a natural polymer that could improve the biocomatibility of the resulting fibers. **Figure 5.4** (a and b) shows the tensile properties of the PEGDA fibers with different characteristics.

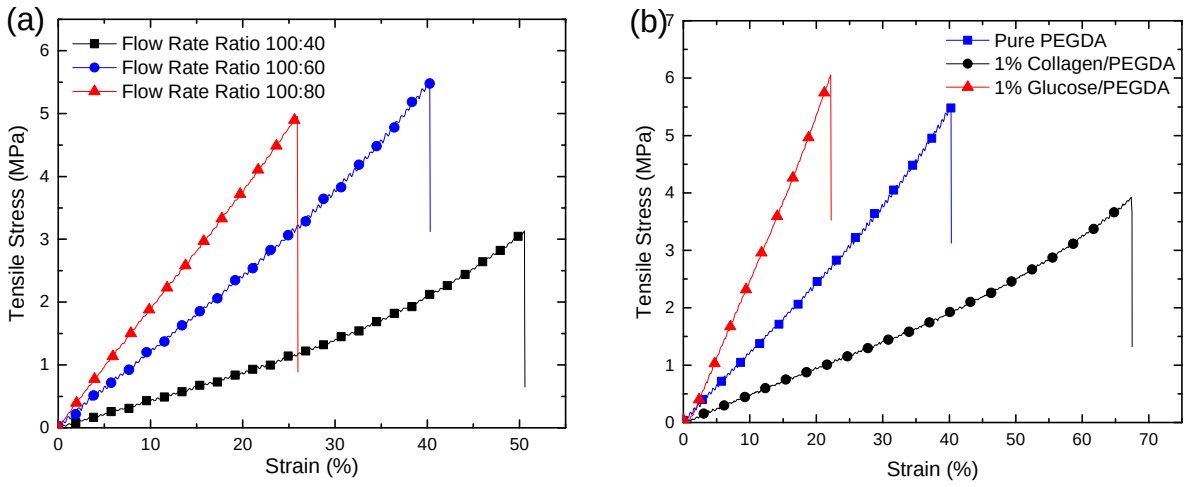

Figure 5.4 *Tensile properties of the PEGDA fibers with different characteristics. (a) Pure PEGDA fibers fabricated with different flow rate ratios between the core and sheath fluids. (b) The effect of incorporation of collagen and glucose on the mechanical properties of the fibers. The flow rate ratio was kept constant at 100:60 μL/min. The concentrations of PEGDA and PI were 30 % and 2%, respectively, for all of the fibers.*

Stress at break (MPa), Strain at break (%), and Young's modulus (MPa) of different types of PEGDA fibers were averaged and listed in **Table 5.1** as well. The stress-strain curves of the PEGDA fibers demonstrate that all of the fibers made in this study are brittle, which might be due to the chemical cross-linking of PEGDA during the fiber fabrication process. When the core flow rate increases from 40 μL/min to 80 μL/min, the strain at break (%) decreases by a factor of 1.3, whereas the stress at break (MPA) and Young's modulus (MPa) become 1.3 and 1.6 times. That was expected because when the core flow rate increases, the cross-linking density increases, which results in the formation of more brittle structures.

Table 5.1 *Mechanical properties of the PEGDA fibers.*

Sample	Flow Rate Ratio (Sheath:Core)	Stress at Break (MPa)	Strain at Break (%)	Young's Modulus (MPa)
30% PEGDA	100:40	5.6 ± 1.1	43.6 ± 5.0	10.3 ± 1.1
30% PEGDA	100:60	5.9 ± 0.6	39.7 ± 2.7	14.1 ± 1.4
30% PEGDA	100:80	7.4 ± 2.1	34.2 ± 7.1	16.8 ± 1.2
1% Collagen/30% PEGDA	100:60	3.7 ± 1.0	42.5 ±7.2	6.7 ± 0.4
1% Glucose/30% PEGDA	100:60	6.5 ± 1.0	33.9 ± 3.9	19.0 ± 1.3

Apart from changing the flow rate ratio, collagen and glucose were incorporated into the PEGDA fibers to investigate their effects on the mechanical properties of the PEGDA fibers. It was found that when 1 v% collagen is added to the core solution, the stress at break (MPa) and Young's modulus (MPa) drops by 38% and 53%, respectively, whereas the strain at break (%) increases by a factor of 1.07. The reason for increasing the strain at break (%) can be due the fact that the collagen molecules do not react with UV light and the photoinitiator. As a result, they hinder part of the cross-linking binding, which makes the network less brittle. Additionally, it was expected to obtain lower stress at break and Young's modulus because the mechanical properties of the natural polymers are lower than those of the synthetic polymers. Therefore, by blending

PEGDA, which is a synthetic polymer, with collagen, the resulting mixture will have lower mechanical properties. In addition, the results show that the both elastic modulus and stress at break of the fibers increase by a factor of 1.1 and 1.34, respectively, when the PEGDA fibers include 1% glucose. That might be due to the high mechanical properties of the PEGDA fibers.

5.3.4 Surface study of the PEGDA fibers

The PEGDA microfluidic-spun fibers fabricated in this study have the potential to be used in biomedical applications such as cell delivery, drug delivery, and tissue engineering. We incorporated different materials, such as glucose, sucrose, gelatin, collagen, PEG, and PVA, into the PEGDA fibers and soaked the resulting fibers in water for 6 days at 37 °C.

It was found that adding the glucose, gelatin, and PEG do not create a significant porosity on the surface of the fiber (data not shown). However, PEGDA fibers with porous surfaces were created by incorporating sucrose and PVA into the fiber. **Figure 5.5** shows the SEM images from the longitudinal view of the fibers made by PEGDA/sucrose, PEGDA/PVA, and PEGDA/collagen. The results show that incorporating PVA into the PEGDA fibers (**Figure 5.5** (a_1, a_2)) results in formation of porosity at the groove areas of the fibers, whereas sucrose can create porosity in all parts of the fibers (**Figure 5.5** (b_1, b_2)). Although collagen does create porosity on the surface of the fiber, it increases the roughness, which could be desirable for a specific applications (**Figure 5.5** (c_1, c_2)). Additionally, incorporation of a natural polymer into a synthetic polymer increases the biocompatibility of the network due to the fact that biological characteristics such as cell adhesion will be enhanced.

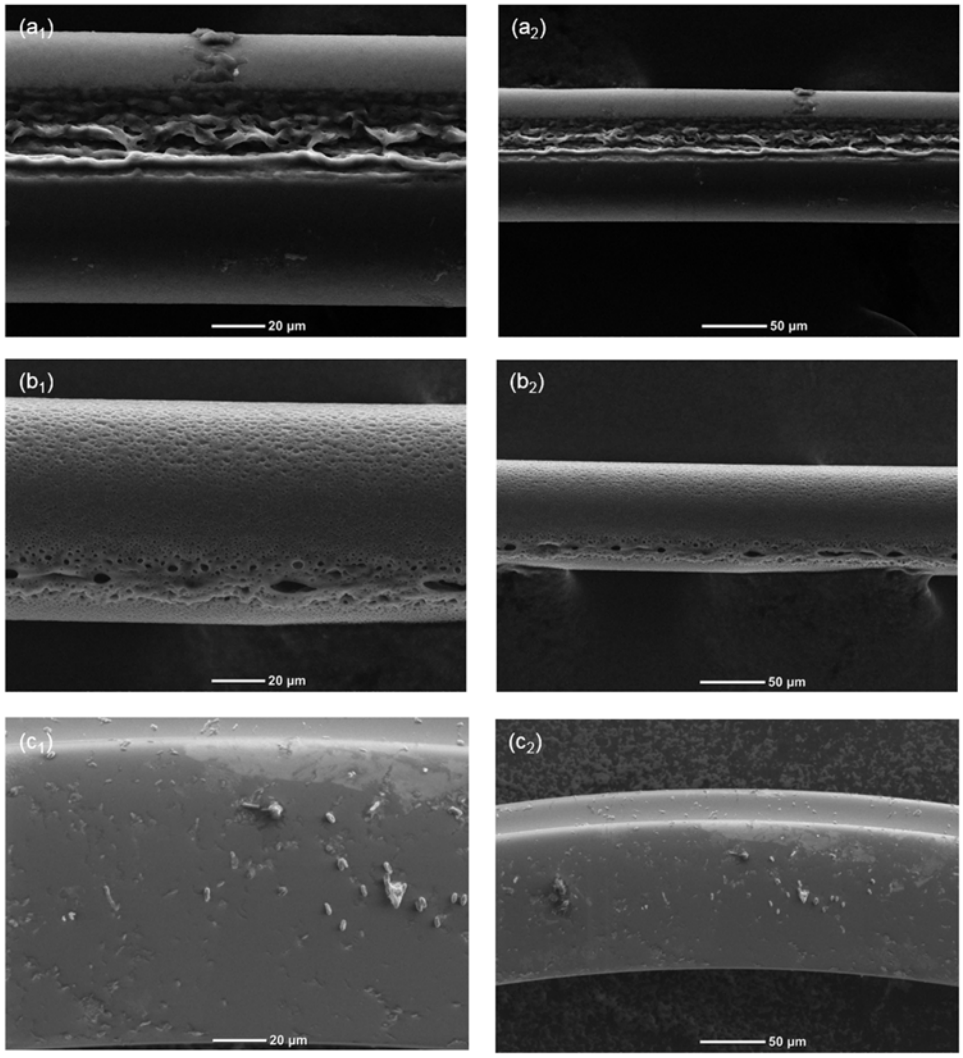

Figure 5.5 *SEM images of the (a) 30%PEGDA/2% PVA, (b) 30% PEGDA/10% sucrose, and (c) 30% PEGDA/1% collagen after soaking them in water for 6 days at 37 °C.*

5.3.5 Cell encapsulating in PEGDA fibers

We encapsulated adult hippocampal progenitor cells (AHPCs) into the PEGDA fibers by mixing a cell suspension solution with hydrogel pre-polymer solution containing a photoinitiatior to polymerize the PEGDA. We performed the cell viability assay by means of Propidium Iodide (PI) after 6 hours and no cells survived this experiment. We thought about different possibilities that may resulted in dying the cells inside of the PEGDA network. In order to increase the cell

survival, we did not use photoinitiator, UV light, and the microfluidic fiber fabrication channel. Rat bone marrow derived mesenchymal stem cells (uMSCs) were also used for the cell viability because they are more resilient to environmental changes compared to AHPCs. Additionally, a very low concentration of PEGDA (5% and 10%) was used as the pre-polymer solution. These solutions were mixed with the cell suspension and incubated at room temperature for 20 minutes on a rotator. After 20 minutes, cells were centrifuged at 800 rpm for 5 min in order to remove the PEGDA solution from the cells. Cells were then plated onto coated poly-L-ornithine (10 μg mL^{-1}; Sigma-Aldrich) and purified mouse laminin glass coverslips. The cell viability results for both of the AHPCs and uMSCs were shown in **Figure 5.6** and **Figure 5.7**, respectively. The figures demonstrate that the AHPCs control samples containing no PEGDA solutions, had processes and were phase bright, whereas those in the PEGDA solutions were dark, no processes and had vacuoles forming around cells indicating possible cell death. uMSC controls were all adherent after 24 hours and had very little floating cells. uMSCs exposed to PEGDA solutions were more rounded cells and did not flatten out. These cells also had vacuoles forming indicating cell death. Additionally, both AHPCs and uMSCs did not survive the experiment as indicated through the positive propidium iodide labeling. Based on the cell viability results, we concluded that the PEGDA (M_n=575) is not ideal for cell encapsulation. For the future work, we can consider other hydrogels, which provide a biocompatible environment for the cells. Additionally, using PEGDA with higher molecular weight could be another solution, but PEGDA with high molecular weights are very expensive, which is not consistent with the cost effective aspect of microfluidic approach. Nevertheless, the bow tie shaped PEGDA fibers could be useful for aligning the neural cells. Compared to round fibers, the bow tie shaped fibers can catch more cells in their groove regios, which makes the tissue regeneration process more efficient.

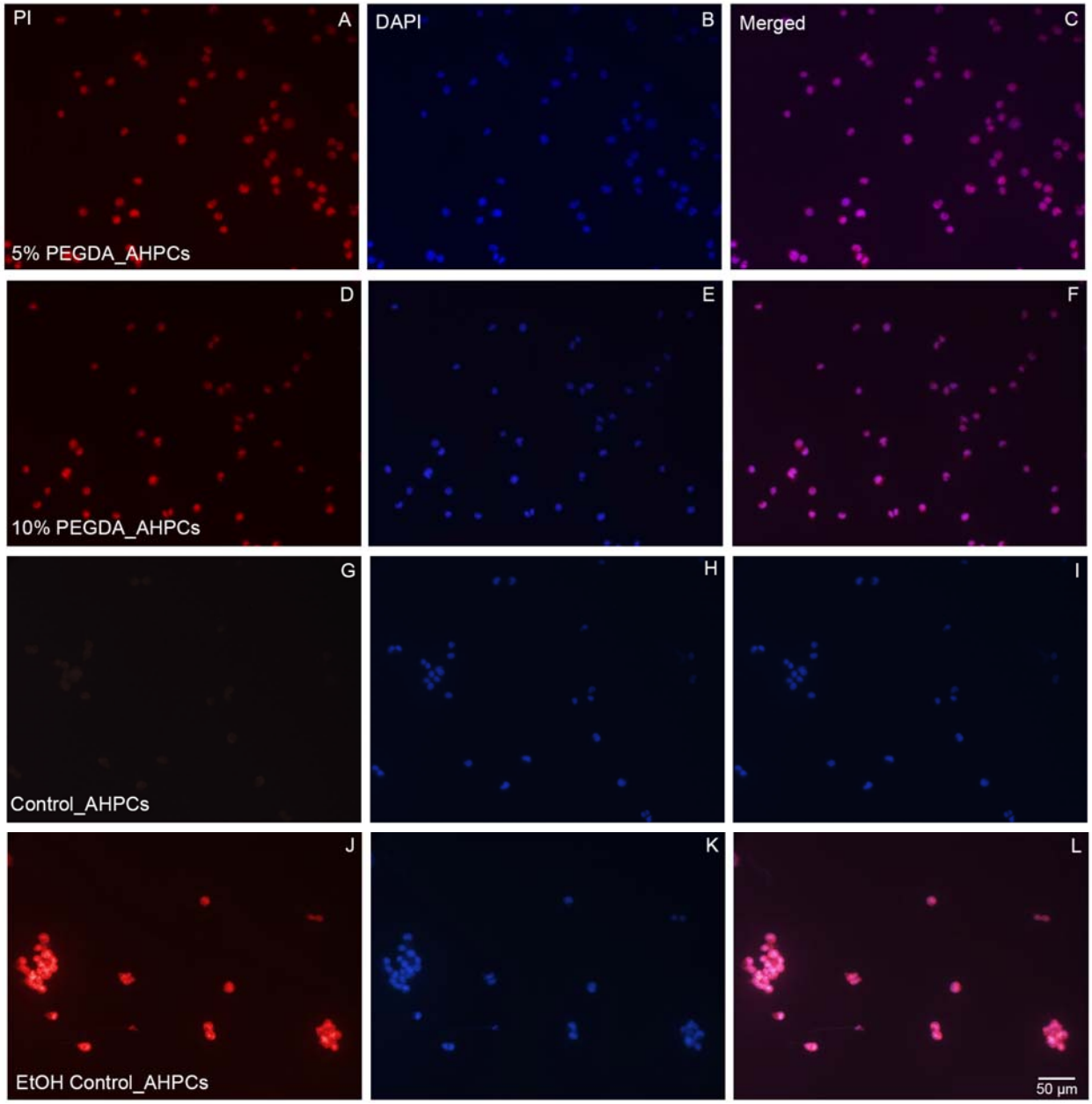

Figure 5.6 *Propidium Iodide assay for AHPCs after 1 DIV. (A,D,G,J) shows Cy3 labeling in red. (B, E, H, K) shows DAPI staining in blue. (C, F, I, L) shows merged image of Cy3 and DAPI. (J) serves as a positive reagent control. Cells were exposed to 70% ethanol to purposefully kill cells in order to test if propidium iodide reagent was working properly. All dead cells would take up the propidium iodide and fluoresce red.*

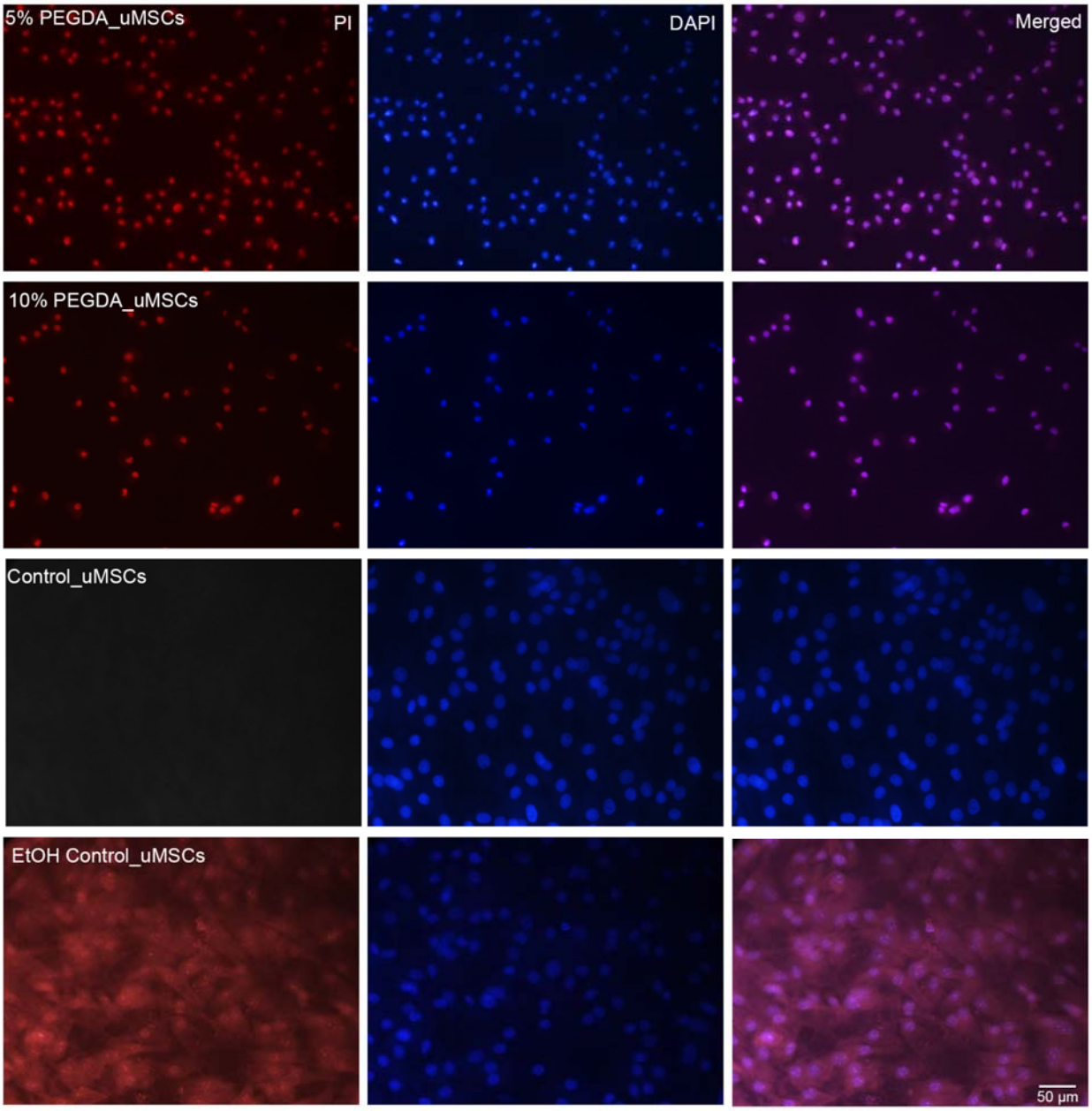

Figure 5.7 *Propidium Iodide assay for uMSCs after 1 DIV. (A,D,G,J) shows Cy3 labeling in red. (B, E, H, K) shows DAPI staining in blue. (C, F, I, L) shows merged image of Cy3 and DAPI. (J) serves a positive reagent control. Cells were exposed to 70% ethanol to purposefully kill cells in order to test if propidium iodide reagent is working properly. All dead cells would take up the propidium iodide and fluoresce red.*

5.4 Conclusions

We used microfluidic approach and photopolymerization strategy to fabricate PEGDA spherical particles as well as bow tie shaped fibers. The effect of the flow rate ratio between the core and sheath fluid on the size of the particles and fibers were investigated. It was found that the decrease of the flow rate ratio between the fluids increases the diameter and width of the particles and fibers, respectively. The tensile properties of the PEGDA fibers were studied as well. It was found that when the core flow rate increases, the cross-linking density increases, which results in the fabrication of more stiff and brittle fibers. Collagen and glucose were incorporated into the PEGDA fibers and their effects on the tensile properties were studied. The results showed that the mechanical properties of the PEGDA/collagen mixture drops due to the low strength of the collagen, which is a natural polymer. On the other hand, it was found that the presence of glucose in the PEGDA/glucose network can improve the mechanical properties. We studied the effect of adding different materials such as glucose, sucrose, gelatin, collagen, PVA, and PEG into the PEGDA network. Based on the SEM images, it was observed that the porosity of the fiber can be tuned by incorporating sucrose and PVA into the PEGDA fibers. In addition, we encapsulated AHPCs into the PEGDA fibers in order to create a cell-laden fiber. Propidium Iodide (PI) was used to examine cell viability, and the results showed that the cells could not survive. We provided a more biocompatible condition by mixing the cell suspension solution with low concentrated PEGDA (M_n=575) solution for 20 minutes in the absence of photoinitiator, UV light, and microfluidic fiber fabrication process, but the cells still did not survive. We believe that another polymer or the same polymer with higher molecular weight needs to be used in order to increase the cell survival into the hydrogel network.

REFERENCES

[1] Yeh J, Ling Y, Karp JM, Gantz J, Chandawarkar A, Eng G, et al. Micromolding of shape-controlled, harvestable cell-laden hydrogels. Biomaterials. 2006;27:5391-8.

[2] Peppas NA, Hilt JZ, Khademhosseini A, Langer R. Hydrogels in biology and medicine: From molecular principles to bionanotechnology. Adv Mater. 2006;18:1345-60.

[3] Cao Y, Lee BH, Peled HB, Venkatraman SS. Synthesis of stiffness-tunable and cell-responsive Gelatin–poly(ethylene glycol) hydrogel for three-dimensional cell encapsulation. Journal of Biomedical Materials Research Part A. 2016;104:2401-11.

[4] Yoshino T, Tanaka T, Nakamura S, Negishi R, Hosokawa M, Matsunaga T. Manipulation of a Single Circulating Tumor Cell Using Visualization of Hydrogel Encapsulation toward Single-Cell Whole-Genome Amplification. Analytical Chemistry. 2016;88:7230-7.

[5] Davey SK, Aung A, Agrawal G, Lim HL, Kar M, Varghese S. Embedded 3D Photopatterning of Hydrogels with Diverse and Complex Architectures for Tissue Engineering and Disease Models. Tissue Engineering Part C: Methods. 2015;21:1188-96.

[6] Munoz-Pinto DJ, Jimenez-Vergara AC, Gharat TP, Hahn MS. Characterization of sequential collagen-poly(ethylene glycol) diacrylate interpenetrating networks and initial assessment of their potential for vascular tissue engineering. Biomaterials. 2015;40:32-42.

[7] Zhang X, Xu B, Puperi DS, Yonezawa AL, Wu Y, Tseng H, et al. Integrating valve-inspired design features into poly(ethylene glycol) hydrogel scaffolds for heart valve tissue engineering. Acta Biomaterialia. 2015;14:11-21.

[8] Zhang H, Wang L, Song L, Niu G, Cao H, Wang G, et al. Controllable properties and microstructure of hydrogels based on crosslinked poly(ethylene glycol) diacrylates with different molecular weights. Journal of Applied Polymer Science. 2011;121:531-40.

[9] Xie Z, Aphale NV, Kadapure TD, Wadajkar AS, Orr S, Gyawali D, et al. Design of antimicrobial peptides conjugated biodegradable citric acid derived hydrogels for wound healing. Journal of Biomedical Materials Research Part A. 2015;103:3907-18.

[10] McMahon S, Kennedy R, Duffy P, Vasquez JM, Wall JG, Tai H, et al. Poly(ethylene glycol)-Based Hyperbranched Polymer from RAFT and Its Application as a Silver-Sulfadiazine-Loaded Antibacterial Hydrogel in Wound Care. ACS Applied Materials & Interfaces. 2016.

[11] Anselmo AC, Mitragotri S. Impact of particle elasticity on particle-based drug delivery systems. Advanced Drug Delivery Reviews.

[12] Hao L, Gwangjun G, Seong Yong K, Jong-Oh P, Sukho P. Magnetic actuated pH-responsive hydrogel-based soft micro-robot for targeted drug delivery. Smart Materials and Structures. 2016;25:027001.

[13] Chen Y-T, Goudar VS, Wu R-G, Hsieh H-Y, Yang C-S, Chang H-Y, et al. A UV-sensitive hydrogel based combinatory drug delivery chip (UV gel-Drug Chip) for cancer cocktail drug screening. RSC Advances. 2016;6:44425-34.

[14] Cavallo A, Madaghiele M, Masullo U, Lionetto MG, Sannino A. Photo-crosslinked poly(ethylene glycol) diacrylate (PEGDA) hydrogels from low molecular weight prepolymer: Swelling and permeation studies. Journal of Applied Polymer Science. 2016:n/a-n/a.

[15] Martino C, Vigolo D, Solvas XCi, Stavrakis S, deMello AJ. Real-Time PEGDA-Based Microgel Generation and Encapsulation in Microdroplets. Advanced Materials Technologies. 2016;1:1600028-n/a.

[16] Hoffman AS. Hydrogels for biomedical applications. Advanced Drug Delivery Reviews. 2012;64, Supplement:18-23.

[17] Nguyen KT, West JL. Photopolymerizable hydrogels for tissue engineering applications. Biomaterials. 2002;23:4307-14.

[18] de Groot JH, van Beijma FJ, Haitjema HJ, Dillingham KA, Hodd KA, Koopmans SA, et al. Injectable Intraocular Lens Materials Based upon Hydrogels. Biomacromolecules. 2001;2:628-34.

[19] Daniele MA, Boyd DA, Adams AA, Ligler FS. Microfluidic Strategies for Design and Assembly of Microfibers and Nanofibers with Tissue Engineering and Regenerative Medicine Applications. Advanced Healthcare Materials. 2015;4:11-28.

[20] Whitesides GM. The origins and the future of microfluidics. Nature. 2006;442:368-73.

[21] Sharifi F, Patel BB, Dzuilko AK, Montazami R, Sakaguchi DS, Hashemi N. Polycaprolactone Microfibrous Scaffolds to Navigate Neural Stem Cells. Biomacromolecules. 2016.

[22] Sharifi F, Kurteshi D, Hashemi N. Designing highly structured polycaprolactone fibers using microfluidics. Journal of the Mechanical Behavior of Biomedical Materials. 2016;61:530-40.

[23] Sharifi F, Bai Z, Montazami R, Hashemi N. Mechanical and physical properties of poly(vinyl alcohol) microfibers fabricated by a microfluidic approach. RSC Advances. 2016;6:55343-53.

[24] Goodrich PJ, Sharifi F, Hashemi N. Rapid prototyping of microchannels with surface patterns for fabrication of polymer fibers. RSC Advances. 2015;5:71203-9.

[25] Sharifi F, Ghobadian S, Cavalcanti FR, Hashemi N. Paper-based devices for energy applications. Renewable and Sustainable Energy Reviews. 2015;52:1453-72.

[26] Hashemi N, Lackore JM, Sharifi F, Goodrich PJ, Winchell ML, Hashemi N. A paper-based microbial fuel cell operating under continuous flow condition. TECHNOLOGY. 2016;04:98-103.

[27] Stone HA, Kim S. Microfluidics: Basic issues, applications, and challenges. AIChE Journal. 2001;47:1250-4.

[28] Chung BG, Lee KH, Khademhosseini A, Lee SH. Microfluidic fabrication of microengineered hydrogels and their application in tissue engineering. Lab on a Chip. 2012;12:45-59.

[29] Krutkramelis K, Xia B, Oakey J. Monodisperse polyethylene glycol diacrylate hydrogel microsphere formation by oxygen-controlled photopolymerization in a microfluidic device. Lab on a Chip. 2016;16:1457-65.

[30] Celetti G, Natale CD, Causa F, Battista E, Netti PA. Functionalized poly(ethylene glycol) diacrylate microgels by microfluidics: In situ peptide encapsulation for in serum selective protein detection. Colloids and Surfaces B: Biointerfaces. 2016;145:21-9.

[31] Tamayol A, Akbari M, Zilberman Y, Comotto M, Lesha E, Serex L, et al. pH-Sensing Hydrogel Fibers: Flexible pH-Sensing Hydrogel Fibers for Epidermal Applications (Adv. Healthcare Mater. 6/2016). Advanced Healthcare Materials. 2016;5:624-.

[32] Akbari M, Tamayol A, Laforte V, Annabi N, Najafabadi AH, Khademhosseini A, et al. Composite Living Fibers for Creating Tissue Constructs Using Textile Techniques. Advanced Functional Materials. 2014;24:4060-7.

[33] Choi CH, Yi H, Hwang S, Weitz DA, Lee CS. Microfluidic fabrication of complex-shaped microfibers by liquid template-aided multiphase microflow. Lab on a Chip. 2011;11:1477-83.

[34] Bai ZH, Reyes JMM, Montazami R, Hashemi N. On-chip development of hydrogel microfibers from round to square/ribbon shape. Journal of Materials Chemistry A. 2014;2:4878-84.

[35] Haynl C, Hofmann E, Pawar K, Förster S, Scheibel T. Microfluidics-Produced Collagen Fibers Show Extraordinary Mechanical Properties. Nano Letters. 2016;16:5917-22.

[36] Nunes JK, Wu C-Y, Amini H, Owsley K, Di Carlo D, Stone HA. Fabricating Shaped Microfibers with Inertial Microfluidics. Adv Mater. 2014;26:3712-7.

[37] Dendukuri D, Gu SS, Pregibon DC, Hatton TA, Doyle PS. Stop-flow lithography in a microfluidic device. Lab on a Chip. 2007;7:818-28.

[38] Thangawng AL, Howell PB, Richards JJ, Erickson JS, Ligler FS. A simple sheath-flow microfluidic device for micro/nanomanufacturing: fabrication of hydrodynamically shaped polymer fibers. Lab on a Chip. 2009;9:3126-30.

[39] Boyd DA, Shields AR, Howell PB, Ligler FS. Design and fabrication of uniquely shaped thiol-ene microfibers using a two-stage hydrodynamic focusing design. Lab on a Chip. 2013;13:3105-10.

[40] Shields AR, Spillmann CM, Naciri J, Howell PB, Thangawng AL, Ligler FS. Hydrodynamically directed multiscale assembly of shaped polymer fibers. Soft Matter. 2012;8:6656-60.

[41] Gage FH, Coates PW, Palmer TD, Kuhn HG, Fisher LJ, Suhonen JO, et al. Survival and differentiation of adult neuronal progenitor cells transplanted to the adult brain. Proceedings of the National Academy of Sciences of the United States of America. 1995;92:11879-83.

[42] Howell Jr PB, Golden JP, Hilliard LR, Erickson JS, Mott DR, Ligler FS. Two simple and rugged designs for creating microfluidic sheath flow. Lab on a Chip. 2008;8:1097-103.

CHAPTER 6

FUTURE WORK

It was found that the microfluidic fiber fabrication approach is a functional device that could be utilized in biomedical applications such as tissue engineering, cell delivery, and drug delivery.

As mentioned in chapter 4, we plan to have three replicates of cell seeding on the PCL fibers, each made with different characteristics, to investigate quantitatively which one can provide the best conditions in terms of cell adhesion, proliferation, and differentiation. One of the replicates was finished and the results were provided in chapter 4. Two more replicates are needed in order to obtain more reliable results about cell behavior on different types of fibers.

The PCL fibers can be embedded inside of the conduits in order to create a 3D environment for the cell culture that could be more effective in terms of nerve tissue regeneration, which makes it one step closer to the application of the PCL fibers in tissue engineering.

As mentioned in chapter 5, we tried to encapsulate different types of cells into the PEGDA hydrogel networks to create a cell-laden fiber. However, the cells did not survive even after removing photoinitiator and UV light. In order to resolve this problem, we can use another polymer with high biocompatibility or we can change our solidification strategy to chemical cross-linking. Nevertheless, the bow tie-shaped fibers have a groove on their surfaces, which could be useful for aligning cells. We believe that the grooves embedded on the surface of the PEGDA fibers can make the tissue regeneration process more effective since they are able to provide a 3D environment for the cells. In addition, the cell adhesion on this type of fibers will be significantly higher compared to the round shaped fibers.

As mentioned in chapter 1, the microfluidic spun microfibers could have applications in drug delivery devices. In this area, we can use blend of polymers or different concentrations of cross-linking agents to design flexible microfiber-based for *in-vivo* drug release according to the requirements of different medications.

Luminescent nanospecies could be incorporated into the microfibers using a microfluidic platform, which may have application for bio-imaging or bio-markers for wound dressing, tissue engineering, and drug delivery.

The mechanical properties of the cells could be measured by the microfluidic spun fibers by measuring the mechanical properties of the fibers both with and without the cells, and calculating the difference. However, it is predicted that there might be some challenges in terms of the accuracy and resolution of the equipment used that need to be considered during this study.